12-14-2015

Viruses and Metals in Ocean Food Webs: Top-Down and Bottom-Up Effects of Marine Viruses and Trace Elements on Marine Picophytoplankton

Brady Robert Cunningham
University of South Carolina - Columbia

VIRUSES AND METALS IN OCEAN FOOD WEBS: TOP-DOWN AND BOTTOM-UP EFFECTS OF MARINE VIRUSES AND TRACE ELEMENTS ON MARINE PICOPHYTOPLANKTON

by

Brady Robert Cunningham

Bachelor of Science
University of Maryland, 2011

Submitted in Partial Fulfillment of the Requirements

For the Degree of Doctor of Philosophy in

Marine Science

College of Arts and Sciences

University of South Carolina

2015

Accepted by:

Seth John, Co-Major Professor

Tammi Richardson, Co-Major Professor

Ryan Rykaczewski, Committee Member

Matthew Sullivan, Committee Member

Lacy Ford, Senior Vice Provost and Dean of Graduate Studies

DEDICATION

"Sentiment without action is the ruin of the soul."

-Edward Abbey

I dedicate this dissertation work to my mother, Diane, who has always supported me no-matter what life has thrown my way. I wouldn't have made it this far without you. And to my father, Robert, who first sparked my love of science and ecology during summer weekends when we spent hours cleaning a creek in my backyard.

ACKNOWLEDGEMENTS

I would like to acknowledge my funding source, the Gordon and Betty Moore Foundation, for supplying the monetary means to complete my dissertation. I would also like to thank the University of South Carolina Graduate School for awarding me with both the Presidential Fellowship and the Dean's Dissertation Fellowship. Finally, I would like to thank my committee and my lab mates for all their help throughout this degree process.

ABSTRACT

Viruses are the most numerous biological entities in the ocean, playing a key role in microbial ecology and biogeochemical cycling. In order to replicate, viruses must first infect a host and then use the host's cellular machinery to produce new viral particles. Some of the most abundant viral hosts in the subtropical open ocean are picophytoplankton. However, picophytoplankton growth is typically constrained by nutrient availability. In many regions of the ocean, iron (Fe) is only available in very low concentrations causing growth-limitation of picophytoplankton. Interestingly, the interactions between Fe-limitation and viral infection of picophytoplankton have not been extensively studied. This dissertation adds to the field by producing novel interdisciplinary research between chemical oceanography and viral ecology. The first project in this dissertation describes a new method to count DNA-stained viruses, which is drastically less expensive than commonly used methods. The new method uses epifluorescence microscopy to enumerate fluorescently stained viruses. The virus sample is combined with a known concentration of silica beads and wet mounted directly onto a slide. Viral concentration is then determined by the relative abundance of viruses and silica beads in the sample. The second project describes one-step growth curves of viruses Syn9, S-SM1, and S-PM2 infecting host *Synechococcus* WH7803 grown under both nutrient-replete and Fe-limited conditions. The results indicate that for these virus strains, decreased host growth rate from Fe-limitation seems to have no effect on viral reproduction. The third project presents data on the internal cellular concentrations of

nutrients and trace elements when picophytoplankton are grown under varying conditions. Determining internal cellular concentrations are important when attempting to understand what nutrients are absorbed and then released by the host during viral infection and lysis. We find that Fe-limitation of cyanobacteria cells elicits a similar response to that of P-limitation, causing an overall decrease in cellular P concentration under both conditions. Overall, this dissertation provides a more complete understanding of differences in viral and cellular production of Fe-limited hosts and suggests a possible role for Fe in the efficiency of the marine microbial loop, carbon, and nitrogen cycle.

.

TABLE OF CONTENTS

DEDICATION iii

ACKNOWLEDGEMENTS iv

ABSTRACT v

LIST OF TABLES ix

LIST OF FIGURES x

CHAPTER 1: INTRODUCTION 1

1.1: BOTTOM-UP CONTROL: TRACE ELEMENT LIMITATION OF CELLS 2

1.2: TOP-DOWN CONTROL: VIRAL PREDATION AND INFECTION 4

1.3: BOTTOM-UP AND TOP-DOWN EFFECTS 6

CHAPTER 2: AN INEXPENSIVE, ACCURATE AND PRECISE WET-MOUNT METHOD FOR ENUMERATING AQUATIC VIRUSES 11

2.1: ABSTRACT 12

2.2: INTRODUCTION 13

2.3: MATERIALS AND METHODS 14

2.4: RESULTS AND DISCUSSION 18

2.5: CONCLUSION 22

CHAPTER 3: PHAGE GROWTH KINETICS OF 3 CYANOPHAGES PROPAGATED ON FE-LIMITED HOST *SYNECHOCOCCUS* WH7803 31

3.1: ABSTRACT 31

3.2: INTRODUCTION 32

3.3: MATERIALS AND METHODS 34

3.4: Results and Discussion 38

3.5: Conclusion 41

Chapter 4: Changes in elemental stoichiometry of picophytoplankton grown under Fe-limitation and infection 44

4.1: Abstract 44

4.2: Introduction 45

4.3: Materials and methods 49

4.4: Results and Discussion 54

4.5: Conclusion 66

Chapter 5: Conclusions and climate change 81

5.1: Fe-limitation during climate change 81

5.2: Climate change and viral infection of Fe-limited cyanobacteria 84

5.3: Climate change and extended elemental stoichiometry of Fe-limited picophytoplankton 85

5.4: Future directions 86

References 88

Appendix A – Permission to reprint 102

LIST OF TABLES

Table 2.1 Reagent preparation for wet-mount virus enumeration protocol.....23

Table 2.2 Wet-mount protocol for virus enumeration 24

Table 2.3 Description of samples used for comparison of the wet-mount and filter-mount virus enumeration methods.....25

Table 3.1 Physiological measurements of host and phage production 42

Table 4.1 Average growth rates of picophytoplankton cells 67

Table 4.2 Comparison of the combined average elemental stoichiometry.....68

Table 4.3 Comparison of the average elemental stoichiometry for each species 69

Table 4.4 Time course comparison of the average elemental stoichiometry.....70

LIST OF FIGURES

Figure 1.1 The biological pump in the subtropical open ocean 10

Figure 2.1 Overview of the wet-mount method for enumeration of aquatic viruses 27

Figure 2.2 Images of samples prepared using the filter-mount and wet-mount virus enumeration methods 28

Figure 2.3 Viral concentrations from natural samples and lysates obtained using the filter-mount and wet-mount enumeration methods 29

Figure 2.4 Storage of samples prepared using the wet-mount method 30

Figure 3.1 Comparison of external virus production and cell counts 43

Figure 4.1 Average cellular P concentration between species 71

Figure 4.2 Comparison of average elemental quotas 72

Figure 4.3 Average cellular Fe concentration between species 73

Figure 4.4 Comparison of flow cytometry data between species 74

Figure 4.5 Comparison of average elemental quotas of metal cofactors per species 75

Figure 4.6 Average growth rate of WH7803 post-infection 76

Figure 4.7 Change in WH7803 cellular P concentration post-infection 77

Figure 4.8 Changes in average elemental quotas of alkaline phosphatase cofactors post-infection 78

Figure 4.9 Changes in the average elemental quotas of macronutrients post-infection 79

Figure 4.10 Changes in the average elemental quotas of nutrient-like elements post-infection 80

CHAPTER 1

INTRODUCTION

Marine microbes are some of the major contributors to carbon fixation and biogeochemical cycling in the ocean. Two of the main groups of microbes, marine phytoplankton and viruses, are important due to their high abundance and combined effects on nutrient cycling and flux through the microbial loop and biological pump (Fuhrman 1999; Suttle 2005). Within the microbial loop, nutrients are cycled as heterotrophic bacteria take up dissolved organic matter (DOM) and then the bacteria become prey for grazers and viruses, leading to DOM release continuing the microbial loop (Figure 1.1) (Azam 1998). However, the microbial loop is not a closed system. The loop is part of a much larger system, the biological pump.

The biological pump is the biologically driven portion of the oceanic carbon cycle. Within the pump, phytoplankton take up CO_2 during the photosynthesis process, fixing the CO_2 and turning it into organic matter (Figure 1.1). In fact, phytoplankton are responsible for close to half of global carbon fixation (Field et al. 1998), fixing about 45 gigatons of carbon per year, with 16 gigatons exported to the ocean benthos (Falkowski et al. 1998). However, not all phytoplankton grow and assimilate nutrients at similar rates. Differences between phytoplankton are due to the variation in cell size ranging from 0.2 to 200 μm. One of the most abundant and cosmopolitan fractions of phytoplankton is the picophytoplankton. Picophytoplankton are the smallest fraction of phytoplankton, ranging in size from 0.2 to 2 μm. They inhabit both neritic (coastal ocean)

and pelagic (open-ocean) zones and are comprised of both prokaryotes and eukaryotes. Also, due to the small size of picophytoplankton, these cells also tend to have a competitive advantage in low nutrient regions, like open ocean environments. Picophytoplankton have a larger surface area to volume ratio compared to bigger phytoplankton cells. This difference provides a growth advantage since picophytoplankton take up less nutrients per cell compared to their larger counterparts (Azam et al. 1983; Chisholm and Morel 1991; Chisholm 1992; Azam 1998; Maranon et al. 2001). In this dissertation, I focus on the biological and chemical interactions between picophytoplankton, viruses, and trace nutrients in the subtropical open ocean environment. This environment is primarily inhabited by two broad categories of picophytoplankton, the cyanobacteria (*Synechococcus* and *Prochlorococcus*) and the picoeukaryotes (e.g. *Ostreococcus*).

1.1 BOTTOM-UP CONTROL: TRACE ELEMENT LIMITATION OF CELLS

Within the biological pump, one of the major controls of picophytoplankton growth is nutrient availability. In ecology, the availability of nutrients is typically referred to as a "bottom-up control" due to the direct influence that nutrient availability has on controlling picophytoplankton growth. Some of the earliest inquires into ocean plankton nutrient concentration and availability were performed by Albert Redfield. In 1934, Redfield published his discovery of an almost constant molar ratio of 106 carbon (C) to 16 nitrogen (N) to 1 phosphorus (P) in plankton biomass and dissolved nutrients in surface seawater (Redfield 1934). This ratio, commonly referred to as the Redfield Ratio, shows that phytoplankton require certain concentrations of macronutrients (N and P) to promote growth. Redfield's research provided the foundation leading to future studies on

nutrient limitation of phytoplankton. Initial nutrient limitation studies focused primarily on macronutrient limitation. Studies show that the macronutrients nitrogen and phosphorus can typically be limiting factors in marine and freshwater systems (Tilman et al. 1982; Hecky and Kilham 1988). However, researchers have identified ocean regions with high levels of macronutrients, but still observe slow growing phytoplankton cells.

Regions with high macronutrient concentrations, but low phytoplankton growth are termed high nutrient, low chlorophyll (HNLC) regions. HNLC regions make up 25% of the surface of the global ocean (Maldonado et al. 2001). Since one-quarter of the global ocean is considered HNLC, it is important to study the effect of growth-limiting nutrients other than nitrogen and phosphorus and examine the effect of micronutrient availability on phytoplankton growth. These nutrients are typically called trace elements due to their low surface seawater concentrations. Some of the most commonly studied trace elements include iron (Fe), zinc (Zn), nickel (Ni), cobalt (Co), cadmium (Cd), and copper (Cu). Early attempts at measuring these elements proved difficult, but the advent of trace element clean techniques has allowed researchers to prevent low-level elemental contamination and permit measurement of extremely low concentrations of elements (Morel et al., 1991). One of the first studies to investigate micronutrient limitation found that phytoplankton growth may be influenced by iron concentrations in culture media (Menzel and Ryther 1961). This study showed that Fe addition enhanced C uptake in cultured phytoplankton, indicating enhanced growth. To determine if this finding also occurs in the field, researchers fertilized HNLC regions with large quantities of Fe. The addition of Fe promoted phytoplankton growth and C uptake, leading to large blooms. This finding confirmed the importance of Fe as a micronutrient for phytoplankton growth

(Martin et al. 1994; Coale et al. 1996; Scharek et al. 1997; Boyd et al. 2000, 2007; Maldonado et al. 2001).

Fe is not the only important micronutrient for phytoplankton growth. Researchers have found that certain trace elements exhibit similar ocean depth profiles to that of macronutrient depth profiles. A typical nutrient depth profile relates element concentration to ocean depth. In the surface waters, if an element is used for cellular growth, concentrations are extremely low due to biological uptake. As depth increases and concentrations rates of primary production decreases, elemental concentrations increase and stay constant throughout deep water due to remineralization and lack of biological uptake (Boyle et al., 1976). The pattern of these trace element depth profiles shows that some trace elements can be used as nutrients for phytoplankton.

In this dissertation, I focus solely on the effects of Fe-limitation on picophytoplankton. I cultured two strains of cyanobacteria (*Synechococcus* WH7803 and *Prochlorococcus* MED4) and one picoeukaryote strain (*Ostreococcus lucimarinus*). Over the course of my experiments, I decreased the growth rates of the cultured picophytoplankton by lowering the concentration of Fe 100-fold in each metal-buffered media. Overall, the growth rates in the Fe-deplete medias declined on average by 50% compared to the nutrient-replete medias.

1.2 TOP-DOWN CONTROL: VIRAL PREDATION AND INFECTION

Many studies of ocean food web dynamics focus on zooplankton predation and impacts of grazing on phytoplankton communities (McCauley and Briand 1979; Lynch and Shapiro 1981). However, since the discovery of high abundances of viruses in aquatic habitats, scientists have begun to investigate how viruses affect phytoplankton growth

and nutrient cycling (Bergh et al. 1989; Proctor and Fuhrman 1990; Suttle and Chan 1994). One of the first studies of viral-phytoplankton interaction observed the effects of viral infection on the coccolithophore, *Emiliania huxleyi* (Bratbak et al. 1993). This study intended to investigate the effects of dissolved nutrient composition on phytoplankton dynamics. They found that viruses were responsible for 25-100% of the net mortality of *Emiliania huxleyi* during algal bloom decline under nutrient-replete or N-limited conditions. However, under P-limited conditions, they observed limited viral production throughout the decline of the algal bloom. Interestingly, this information led the researchers to propose that viruses play an important "side-in" role in phytoplankton bloom termination. In ecology, a "side-in" role is considered to be a counterpart to the "top-down" control that grazers impart on phytoplankton communities (Bratbak et al. 1993). This study posits that viruses only have partial influence on phytoplankton growth and decline, while grazers are the main phytoplankton population control. However, more recently, researchers have determined that viruses, much like zooplankton, actually have a top-down effect on phytoplankton communities (Bouvy et al. 2004, 2011; Deng et al. 2013). The viral predation effect creates a "viral shunt" that interrupts energy flow from phytoplankton to grazers and higher trophic levels. This shunt releases nutrients back into the surrounding media via viral lysis, stimulating the microbial loop (Wilhelm and Suttle 1999). Overall, this shows that viruses have a similar influence on phytoplankton growth and biogeochemical cycling when compared to grazing.

As noted above, one of the main reasons for the lack of studies investigating marine virus and phytoplankton ecology, compared to phytoplankton and zooplankton ecology, was due to the difficulty in determining marine viral abundance. Initially, the

enumeration of viruses in aquatic samples was accomplished by using transmission electron microscopy (Bergh et al. 1989). This piece of equipment was too large to bring on research cruises and therefore virus samples could not be immediately determined while in the field. Since then, methods have been developed using epifluorescence microscopy (Suttle and Fuhrman 2010) and flow cytometry making viral enumeration much simpler (Brussaard et al. 2010). While each of the above methods requires the use of relatively expensive laboratory equipment, the per-sample cost for the widely used filter-mount epifluorescence microscopy method has recently increased dramatically. To address this, chapter 2 of this dissertation describes a new, less costly 'wet-mount' epifluorescence microscopy method to enumerate aquatic viruses. Briefly, fluorescently stained samples are combined with a known concentration of silica microsphere beads and then wet-mounted directly onto a slide. Determination of viral concentration is based on the relative abundance of viruses and silica beads in the sample. This method was used throughout this dissertation to determine total marine virus concentration during each project.

1.3 BOTTOM-UP AND TOP-DOWN EFFECTS

There are few studies that combine bottom-up effects of nutrient limitation and top-down effects of viral infection on phytoplankton. One of the first pieces of research studying these combined effects compared the effect of phosphate abundance on viral infection of the cyanobacterium *Synechococcus* WH7803. This study found that under phosphate limitation the viral burst size (the number of viruses produced per infected host cell) was reduced by 80% and the latency period (the time from viral infection to lysis of host) increased compared to the host grown in phosphate-replete conditions (Wilson et al.

1996). Further examination of these systems reveals that there are specific host and virus genes relating to host phosphate acquisition. In this study, researchers found up-regulation of phosphate-binding protein gene (*pstS*) and alkaline phosphatase gene (*phoA*) in the host when viruses infected P starved cyanobacteria hosts compared to P-replete control hosts. This is the first finding to show regulation of genes by viral infection during host nutrient limitation (Zeng and Chisholm 2012). Aside from prokaryotes, studies of marine eukaryotic phytoplankton have also shown similar reduction in viral production under P-limitation. Under various conditions, P-limitation of hosts seems to reduce viral burst size and increase viral latency period (Bratbak et al. 1993, 1998; Maat et al. 2014). However, there was no observed difference in viral growth kinetics when an eukaryotic host was grown in the absence of metals Zn, Cd, or Co. Interestingly, the addition of Cu did reduce viral burst size and latency period, but this may be a result of Cu toxicity impacting host cellular functions, most likely leading to lower viral production (Gledhill et al. 2012). These few, but important, results from viral infection studies in nutrient-limited systems indicate that nutrient limitation plays an important role in the viral infection of host phytoplankton cells. This information may further illustrate how carbon is cycled in HNLC regions and shed light on the impacts which phytoplankton have on local and global processes including the subtropical open ocean biological pump.

In chapters 3 and 4, I performed experiments that combine bottom-up and top-down effects of cyanophage infection on Fe-limited phytoplankton cells and analyzed the nutrients within nutrient-replete and Fe-limited cells. In chapter 3, I performed phage growth kinetic experiments using three cyanophage strains and one *Synechococcus* host.

The host was grown in nutrient-replete and Fe-limited media to mimic optimal and open-ocean conditions, respectively. The original assumption was if I reduced host growth rate by growing cells in Fe-limited media, then I would observe a reduction in viral burst size and an increase in viral latency period. I was anticipating that the findings in viral growth kinetic experiments under P-limitation were a general effect of reduced cell growth rate rather than a specific effect due to solely P-limitation (Wilson et al. 1996; Bratbak et al. 1998; Zeng and Chisholm 2012; Maat et al. 2014). Following these experiments, I was interested in determining the relative concentration of nutrients within the host cells grown under various conditions. Understanding the concentration of cellular nutrients can help determine what is released from a cell after it has been infected and lysed. This information can be used to determine how host growth rate and lysis affects the biological pump. In chapter 4, I culture three strains of picophytoplankton in nutrient-replete and Fe-limited medias. These cells were harvested, processed, and the internal elemental cellular concentrations were determined using mass spectrometry. I predicted that Fe concentrations would decrease in phytoplankton grown in Fe-limited media, but other nutrient-like trace elements would increase due to cell scavenging to more nutrients to replace the scarce Fe availability. This phenomenon has been observed in several species of cyanobacteria, where cells can up-regulate specific genes while under Fe stress. This causes the cell to use or take up other nutrients vital to the production of these stress-reducing enzymes (Webb et al. 2001; Rivers et al. 2009). Finally, I also performed an experiment that tracked the change in nutrient concentration in infected and uninfected Fe-limited *Synechococcus* cells. It has previously been shown that viruses can regulate a host's genome when a host cell is P-limited to up-regulate P acquisition genes (Zeng and

Chisholm 2012). This up-regulation in acquisition genes could alter cellular elemental composition. However, I am currently unaware of any prior studies that have directly evaluated the changes in cellular elemental concentration during viral infection. Therefore, I predicted that viral infection of a Fe-limited host would cause an increase in P cellular concentration since the host is already Fe-limited but still needs an ample supply of P to produce viral particles.

* * *

This dissertation examines the effects of viruses and trace elements on picophytoplankton cells. I measure phytoplankton physiological data using flow cytometry and fluorometry, viral growth kinetics and concentration using qPCR and the wet-mount method, and internal cellular elemental composition using mass spectrometry on laboratory cultures of *Synechococcus*, *Prochlorococcus*, and *Ostreococcus*. This combination of approaches provides a more complete understanding of viral infection and Fe-limitation in various picophytoplankton species and could relate to the biological pump and carbon sequestration.

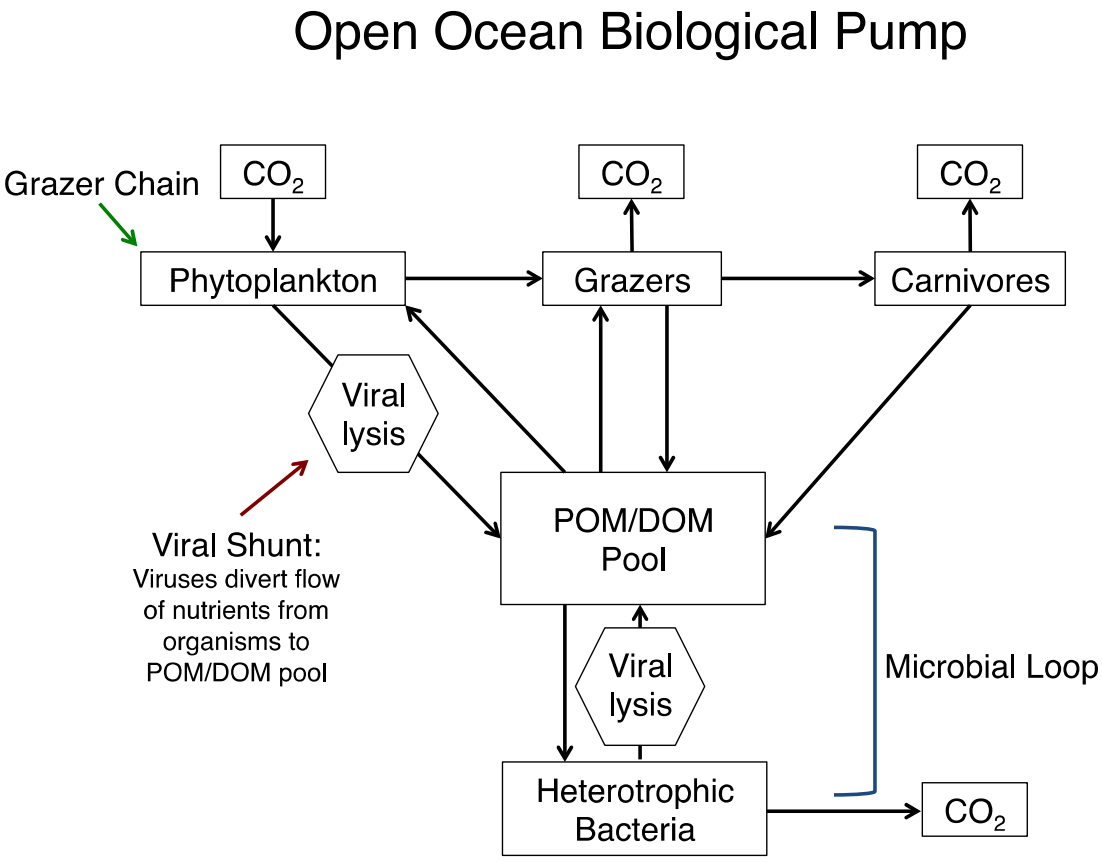

Figure 1.1. The biological pump in the subtropical open ocean is depicted in this box model showing the link between the grazer chain, viral shunt, and microbial loop. The green arrow is indicating the beginning of the grazer chain where energy flows from phytoplankton to grazers to carnivores. The red arrow is showing how viral lysis can transfer energy from the grazer chain to the microbial loop. The blue bracket is indicating the microbial loop portion of the tropic food web where heterotrophic bacteria and other microscopic organisms cycle energy in and out of the POM/DOM pool.

CHAPTER 2

AN INEXPENSIVE, ACCURATE AND PRECISE WET-MOUNT METHOD FOR ENUMERATING AQUATIC VIRUSES[1]

[1]Cunningham BR, Brum JR, Schwenck SM, Sullivan MB, John SG. 2015. An inexpensive, accurate and precise wet-mount method for enumerating aquatic viruses. Appl. Environ. Microbiol. 81:2995–3000.

Reprinted here with permission of publisher. (Appendix A)

2.1 ABSTRACT

Viruses affect biogeochemical cycling, microbial mortality, gene flow, and metabolic functions in diverse environments through infection and lysis of microorganisms. Fundamental to quantitatively investigating these roles is the determination of viral abundance in both field and laboratory samples. One current, widely-used method to accomplish this in aquatic samples is the 'filter-mount' method in which samples are filtered onto costly 0.02 μm-pore-size ceramic filters for enumeration of viruses with epifluorescence microscopy. Here we describe a cost-effective (ca. 500-fold lower materials cost) alternative virus enumeration method in which fluorescently-stained samples are wet-mounted directly onto slides, after optional chemical flocculation of viruses in samples with viral concentrations $<5\times10^7$ mL^{-1}. The concentration of viruses in the sample is then determined from the ratio of viruses to a known concentration of added microsphere beads via epifluorescence microscopy. Virus concentrations obtained using this wet-mount method, with and without chemical flocculation, were significantly correlated with, and had equivalent precision to, those from the filter-mount method across concentrations ranging from 2.17×10^6 to 1.37×10^8 viruses mL^{-1} when tested using cultivated viral isolates and natural samples from marine and freshwater environments. In summary, the wet-mount method is significantly less expensive than the filter-mount method, and is appropriate for rapid, precise and accurate enumeration of aquatic viruses over a wide range of viral concentrations ($\geq1\times10^6$ viruses mL^{-1}) encountered in field and laboratory samples.

2.2 INTRODUCTION

Viruses are the most abundant biological entities in aquatic systems and their infection of microorganisms has substantial influences on microbial ecology, biogeochemical cycling, and gene transfer in aquatic environments (e.g., reviewed by Suttle 2005; Breitbart 2012). An accurate method to quantify aquatic viruses is thus essential for use in field and laboratory studies to investigate the roles of viruses in aquatic environments. This enumeration of viruses in aquatic samples has previously been accomplished using transmission electron microscopy (TEM; Bergh et al. 1989), epifluorescence microscopy (reviewed by Suttle and Fuhrman 2010), and flow cytometry (reviewed by Brussaard et al. 2010).

While each of the above methods requires the use of relatively expensive laboratory equipment, the per-sample cost for the widely used epifluorescence microscopy method has recently increased dramatically. This method involves filtering the sample onto 0.02 μm-pore-size ceramic filters, staining viruses on the filters using one of several available nucleic acid dyes, mounting the filter onto a slide, and visually enumerating the deposited viruses by epifluorescence microscopy (reviewed by Suttle and Fuhrman 2010). However, the filters used in this 'filter-mount' method have risen in cost to ca. $10 each in the US (with increased costs in some other countries), creating a significant financial burden for researchers pursuing studies of environmental viruses. To address this, we have developed a new, less costly 'wet-mount' epifluorescence microscopy method to enumerate aquatic viruses in which fluorescently stained samples are wet-mounted directly onto a slide, with quantification of viral concentration based on the relative abundance of viruses and silica beads in the sample.

2.3 MATERIALS AND METHODS

2.3.1 COMPARISON OF THE WET-MOUNT AND FILTER-MOUNT METHODS FOR VIRUS ENUMERATION

The wet-mount method was tested by comparing viral concentrations obtained with the wet-mount and filter-mount methods in triplicate samples collected from a variety of marine and freshwater environments, as well as in cultivated viral lysates (described in Table 2.3). Briefly, field samples included a 6-depth profile (5–300m) from the Eastern Tropical North Pacific Ocean (using whole seawater samples), 8 surface ocean locations throughout the Pacific, Atlantic and Southern Oceans chosen for their range in chlorophyll concentrations (collected on the *Tara* Oceans Expedition (Karsenti et al. 2011); using 0.2 μm-filtered samples), and a freshwater location from South Carolina, USA. All field samples were preserved with glutaraldehyde (0.5% final concentration), flash-frozen in liquid nitrogen, and stored at -80°C until analysis. Lysate samples included the *Synechococcus* virus S-WHM1 (Millard et al. 2004), two dilutions of the *Synechococcus* virus S-SM1 (Sullivan et al. 2003), and the *Prochlorococcus* virus P-HM2 (Sullivan et al. 2010). Triplicate independent 1-mL samples were processed using each the filter-mount and wet-mount methods, as described below. Statistical comparison of viral concentrations obtained using each method was then performed using two-tailed t-tests and Pearson correlation (SigmaPlot v12.5, Systat Software Inc).

2.3.2 FILTER MOUNT SAMPLE PREPARATION AND ANALYSIS

The filter-mount method was performed according to Suttle and Fuhrman (Suttle and Fuhrman 2010). Briefly, samples were filtered onto 0.02 μm-pore-size ceramic filters (Whatman Anodisc), stained with SYBR Gold (Invitrogen) for 15 minutes, and mounted

on a glass slide with antifade solution (Acros Organics). Viruses were viewed under blue excitation using a Nikon TS100 inversion microscope or a Zeiss Axio Imager epifluorescence microscope at 1000× magnification. Viral concentration was determined using the average number of fluorescent viruses within a given area of the microscope reticle in 20 fields of view and the total volume of sample filtered through a measured area on the filter.

2.3.3 WET-MOUNT SAMPLE PREPARATION AND ANALYSIS

The wet-mount method for enumerating viruses involves an optional viral concentration step followed by combining a known volume of stained sample with a known volume and concentration of silica beads for relative enumeration of viruses and beads to calculate virus concentration in the sample (Figure 2.1). The reagents and protocol for assessing viral concentrations using the wet-mount method are fully described in Tables 2.1 and 2.2. A full, illustrated protocol describing this method is also available online for convenience (http://eebweb.arizona.edu/faculty/mbsulli/protocols/). For analysis of samples with $<5\times10^7$ viruses mL^{-1}, viruses must be concentrated with chemical flocculation using a method adapted from John *et al.* (John et al. 2011) to obtain a sufficient concentration of viruses for analysis (Figure 2.1A). Samples in this study with viral concentrations below that threshold were first concentrated 100-fold with this chemical flocculation method (step 1 in Table 2.2) before being stained with SYBR Gold for 15 minutes, then combined with silica beads and glycerol (added to create a more viscous solution and reduce clumping of beads; Figure 2.1B; steps 2-3 in Table 2.2). The silica bead size (2.34 μm) was selected due to the ease of visually counting the beads under white light. Due to the relatively large size of the beads (as compared to viruses),

the bead solution must be vortexed thoroughly prior to adding beads to the sample to ensure addition of an accurate concentration of beads. These concentrated samples did not require addition of an antifade solution since they were resuspended in a buffer containing ascorbic acid which reduces fading of the fluorescent signal (Patel et al. 2007). Samples were then pipetted directly onto an isopropanol-cleaned glass microscope slide and covered with a cleaned glass cover slip (step 4 in Table 2.2). Viruses and beads were enumerated in multiple fields of view on a Nikon TS100 inversion microscope or a Zeiss Axio Imager epifluorescence microscope at 1000× magnification until at least 100 each of viruses and beads were enumerated to calculate virus concentration (steps 5-6 in Table 2.2). For each field of view, the total number of fluorescent viruses was determined under blue excitation, after which the total number of beads within the same field of view was determined under white light (Figure 2.2).

For analysis of samples with $>5\times10^7$ viruses mL^{-1}, chemical flocculation of viruses prior to wet-mount sample preparation was not necessary to obtain a sufficient concentration of viruses for enumeration. These samples (S-SM1 lysates) were prepared by staining 10 μL of sample with SYBR Gold, followed by addition of an ascorbic acid solution (to act as an antifade), glycerol, and silica beads (Figure 2.1B; steps 2-3 in Table 2.2). These samples were then wet-mounted onto slides and enumerated exactly as the samples that had been concentrated with chemical flocculation. To compare the wet-mount method with the filter-mount method for these samples with high viral concentration, they were diluted 10-fold in PBS prior to filtering 1 mL of sample for the filter-mount method, as the undiluted sample would have resulted in excessive viral density on the filter, preventing analysis. We also note that while p-phenylenediamine is

a popular antifade chemical (Suttle and Fuhrman 2010), it reacted with glutaraldehyde to form a precipitate in these wet-mount samples and thus should not be used in the wet-mount method with fixed samples. determined under white light (Figure 2.2).

The minimum number of beads and viruses enumerated per sample is justified as follows. Counting statistics (also known as shot noise) dictates that the error in the quantity of viruses or beads counted is given by $\frac{1}{\sqrt{n}}$ (John and Adkins 2010), where *n* is the number of objects enumerated, and therefore the total error in viral abundance is:

$$\sigma_{\text{total}} = \sqrt{\frac{1}{n_{virus}} + \frac{1}{n_{beads}}} \quad (1)$$

where n_{virus} and n_{beads} are the total number of viruses and beads counted, respectively. When at least 100 of each viruses and beads are enumerated, the maximum error is 14%.

2.3.4 STORAGE CONDITIONS FOR SAMPLES PREPARED USING THE WET-MOUNT METHOD

Storage conditions were assessed using two different lysates concentrated 100× using the flocculation method described above. To assess storage after samples were mounted on slides, triplicate samples (S-SM1 lysate) were prepared and analyzed using the full protocol in Table 2.2, with slides stored vertically at -20°C immediately after enumeration, and recounted 7 days later. Additional triplicate samples (S-WHM1 lysates) were prepared through Step 3 in Table 2.2, with 10 µL of the prepared sample analyzed immediately and the remaining sample (~10 µL) stored in a microcentrifuge tube at -20ºC until analysis 7 days later. When at least 100 of each viruses and beads are enumerated, the maximum error is 14%.

2.4 RESULTS AND DISCUSSION

The wet-mount method resulted in fluorescently stained viruses of similar intensity to those in the filter-mount method (Figure 2.2). While there was typically a lower density of viruses in the images derived from samples prepared using the wet-mount method, this is favorable because viruses are enumerated in larger fields of view with the wet-mount as compared to the filter-mount method. However, images depicting a greater density of viruses and cells can be obtained with more concentrated samples (Figure 2.2I). Viral concentrations obtained using the wet-mount method were strongly correlated (Pearson correlation coefficient 0.986, $p < 0.001$) with those obtained using the filter-mount method for all sample types tested including viral lysates and samples from a variety of oceanic and freshwater regions (Figure 2.3). There was no significant difference in viral concentration obtained when using these methods for the majority of samples (13 of 19 samples; two-tailed t-tests; Table 2.1). For the remaining samples with significantly different viral concentrations, neither method consistently resulted in higher or lower viral concentrations, nor were these differences restricted to a specific range of viral concentration (i.e., high vs. low) or sample type (i.e., freshwater vs. marine, natural sample vs. lysate, low vs. high chlorophyll concentration), indicating stochastic variability inherent to analyzing samples (Figure 2.3, Table 2.3). Furthermore, we consider the low magnitude of the differences in average viral concentration for the few significantly different samples to be acceptable for studies of aquatic viruses.

It is important to note that there is no available standard used in aquatic virus enumeration methods. Previous studies comparing aquatic viral concentrations using different methods (i.e., TEM, filter-mount, and flow cytometry) have shown

discrepancies between methods, with one method usually resulting in consistently higher viral concentrations (Hennes and Suttle 1995; Weinbauer and Suttle 1997; Noble and Fuhrman 1998; Marie et al. 1999; Bettarel et al. 2000). However, we observed no such consistent differences in our comparison of the wet-mount and filter-mount methods. Further, the comparison in this study showed that most of the samples had at least 70% agreement between virus concentrations obtained using the wet-mount and filter-mount methods (Figure 2.3), which is similar to previous comparisons of methods used to enumerate viruses (Noble and Fuhrman 1998; Marie et al. 1999). The wet-mount method also had high precision; standard deviations of the mean for triplicate samples were 2–18 % (average 7±4%) of the mean virus concentration and were not significantly different from those obtained using the filter-mount method (two-tailed t-test; $p=0.531$). Thus, the wet-mount method can be used with equal confidence as the filter-mount method. fixed samples.

When enumerating viruses, it is sometimes advantageous to store prepared samples for enumeration at a later date. For example, samples prepared with the filter-mount method can be stored at -20°C for at least 4 months with no significant change in viral concentrations (Suttle and Fuhrman 2010). For wet-mount samples, we tested -20°C storage of prepared samples both in microcentrifuge tubes and on slides (Figure 2.4). While the calculated virus concentration was higher after storage of the prepared samples using both storage conditions, these differences were not significant (two-tailed t-tests; $p=0.210$ and $p=0.083$, respectively). Thus, samples prepared using the wet-mount method can be stored frozen either before or after mounting the sample on slides with no significant change in calculated virus concentration.

The wet-mount method had one major drawback compared to the filter-mount method, which was the inability to efficiently enumerate samples with viral concentrations less than 1×10^6 viruses mL^{-1}. Attempted analysis of samples with lower viral concentrations (i.e., samples below 300m in the Pacific Ocean depth profile) using the wet-mount method resulted in ≤1 virus per field of view, even after maximum concentration (100-fold) with chemical flocculation. Thus, the wet-mount method is not recommended for samples with viral concentrations $<1\times10^6$ viruses mL^{-1} because the low density of viruses on the slide significantly extends the time to analyze a sample. Although this limitation prevented analysis of the deep-sea samples (>300m) in the Pacific Ocean depth profile in this study, many deep-sea samples have viral concentrations above this limit (e.g., Parada et al. 2007) and thus the wet-mount method should be useful for a wide range of environmental samples.

The available methods to enumerate aquatic viruses each have benefits and limitations that are worth considering when planning research projects. For example, TEM-based analyses of aquatic samples can generate information about the morphological characteristics of viruses (e.g., Wommack and Colwell 2000) in addition to viral abundance (e.g., Bergh et al. 1989) but can potentially underestimate the number of viruses because they may be obscured by debris in the sample (Noble and Fuhrman 1998). Fluorescence-based methods for viral enumeration (i.e., epifluorescence microscopy and flow cytometry) are significantly faster than TEM, but can potentially falsely include gene transfer agents or cell debris as viruses (reviewed by Brum et al. 2013) while excluding ssDNA viruses that have very faint fluorescence (Holmfeldt et al. 2012). One additional advantage of fluorescence-based methods is the ability to

enumerate both viruses and bacteria (if present) using the same prepared sample (22). However, the wet mount method presented here has not yet been evaluated for accuracy in counting bacterial cells. Among the available epifluorescence-based methods, the filter-mount method also provides an opportunity to obtain images with a high density of viruses and cells while the flow cytometry method does not. The viral density in images obtained using the wet-mount method is generally much lower than for filter-mount samples, though the density of viruses and cells increases when more concentrated samples are used. While each of these variables is important when evaluating potential virus enumeration methods for a given project, we offer the wet-mount method as a cost-effective alternative to the widely-used filter-mount epifluorescence method.

A significant advantage of the wet-mount method over the filter-mount method is the lack of a requirement for costly 0.02 μm-pore-size ceramic filters. Currently, these filters are only available from one supplier and are expensive (~$10 US each). Instead, the wet-mount method uses microsphere silica beads that can be purchased from several suppliers at ~500-fold lower cost ($0.02 for 20 μL of 10^8 bead mL^{-1} working solution per sample, calculated based on $150 USD for 15 mL of 10^9 bead mL^{-1} stock solution). Even after accounting for the cost of other reagents and slides, the per-sample materials cost for the wet-mount method is much lower (~$0.10 per sample). Thus, the wet-mount method is recommended as an equivalently accurate and precise, but cheaper alternative for enumerating viruses in field and laboratory samples with viral concentrations $>1\times10^6$ mL^{-1}.

2.5 CONCLUSION

Enumeration of viruses in field and laboratory samples is an important tool for investigating the numerous influences of viruses in aquatic environmental systems. However, the high cost of enumerating viruses in aquatic samples using the established filter-mount epifluorescence microscopy method can be a significant burden in conducting aquatic viral research. In this study we present a new, less-expensive wet-mount method for aquatic virus enumeration that can be used with equivalent accuracy and precision as the filter-mount method for a variety of environmental and laboratory samples.

TABLE 2.1. Reagent preparation for wet-mount virus enumeration protocol.

SYBR Gold Working Stock: Dilute SYBR Gold (Invitrogen; 10,000x stock) into PBS (phosphate buffered saline) to prepare a 1000x solution.
Ascorbic Acid Antifade Solution: Dissolve ascorbic acid into PBS to create a 10% (wt/vol) solution (Patel et al. 2007).
Working Bead Solution: Thoroughly vortex the stock bead solution (Bangs Laboratories, 2.34 μm silica spheres, Cat. # SS04N/4186) and dilute it 10-fold into PBS to obtain a concentration of ~10^8 beads mL^{-1}; store at 4°C.
Iron Chloride Solution: Dissolve $FeCl_3 \cdot 6H_2O$ into ultrapure water to form a solution of 10 g Fe L^{-1}; solution has expired if cloudy precipitate forms (John et al. 2011).
Ascorbate-EDTA Buffer: Combine equal parts of 0.4 M Mg_2EDTA and 0.8 M ascorbic acid, adjust with 10 N NaOH to reach a pH of 6-7; prepare fresh within 48 hours of use (John et al. 2011)[1].

[1]An alternative Ascorbate-EDTA Buffer can be made with $MgCl_2$ and Na_2EDTA if Mg_2EDTA is unavailable (John et al. 2011).

TABLE 2.2. Wet-mount protocol for virus enumeration.

1. If virus concentration is expected to be lower than 5×10^7 mL^{-1}, concentrate the viruses by chemical flocculation as follows. Add 1 µL Iron Chloride Solution to 1 mL sample in a microcentrifuge tube, mix by inversion, and centrifuge 20 min at ~14,000 × *g*. Remove the supernatant and resuspend the pellet in 10 µL Ascorbate-EDTA Buffer.[1]

2. Add 2 µL SYBR Gold Working Stock to the concentrated sample, vortex, and incubate 15 min in the dark. If the sample was not concentrated with chemical flocculation (i.e., is expected to exceed 5×10^7 viruses mL^{-1}), mix 10 µL unconcentrated sample with 2 µL SYBR Gold Working Stock in a microcentrifuge tube.

3. Add 5 µL glycerol, vortex, and add 2 µL Working Bead Solution (thoroughly vortex the Working Bead Solution before addition to the sample to ensure accurate pipetting of the beads). If the sample was not concentrated with chemical flocculation, add 1 µL Ascorbic Acid Antifade Solution as well.

4. Mix the prepared sample thoroughly by pipetting up and down, and then immediately pipette 10 µL onto a glass microscope slide and place a coverslip over the sample (both the glass slide and coverslip should be cleaned with isopropanol). Avoid trapping air under the coverslip.

5. Using an epifluorescence microscope, count the number of viruses in a given area within the microscope reticle under blue (~495 nm) excitation at 1000x magnification. Within the same field of view, count the beads under white light. Continue counting fields of view until at least 100 each of viruses and beads have been counted.

6. Virus concentration is calculated as:

$$c_{virus} = \frac{n_{virus}}{n_{beads}} * \frac{v_{beads}}{v_{sample}} * c_{beads}$$

where c_{virus} is the virus concentration in the sample (viruses mL^{-1}), n_{virus} is the total number of viruses counted, n_{beads} is the total number of beads counted, v_{beads} is the volume of Working Bead Solution added (µL), v_{sample} is the sample volume (µL; the volume prior to concentration if chemical flocculation is used), and c_{beads} is the bead concentration in the Working Bead Solution (beads mL^{-1}).

[1]If a lower concentration factor is desired, the pellet may be resuspended in a larger volume of Ascorbate-EDTA Buffer. In this case, increase the amount of SYBR Gold, glycerol, and silica beads accordingly in subsequent steps.

Table 2.3. Description of samples used for comparison of the wet-mount and filter-mount virus enumeration methods.

Sample	Latitude	Longitude	Depth (m)	Chlorophyll (mg m^{-3})	Prefilter	Storage Conditions	Fe-flocculation concentration factor	Wet-mount (viruses ml^{-1})	Filter-mount (viruses ml^{-1})	t-test (p-value)
Pacific Ocean depth profile	18.92ºN	104.89º W	5	N/A	none	0.5% glutaraldehyde, -80ºC	100x	$1.72 \times 10^7 \pm 2.20 \times 10^5$	$2.39 \times 10^7 \pm 1.67 \times 10^6$	0.013
Pacific Ocean depth profile	18.92ºN	104.89º W	30	N/A	none	0.5% glutaraldehyde, -80ºC	100x	$3.04 \times 10^7 \pm 6.08 \times 10^6$	$2.84 \times 10^7 \pm 1.10 \times 10^6$	0.593
Pacific Ocean depth profile	18.92ºN	104.89º W	60	N/A	none	0.5% glutaraldehyde, -80ºC	100x	$8.03 \times 10^6 \pm 2.46 \times 10^6$	$6.01 \times 10^6 \pm 213 \times 10^5$	0.229
Pacific Ocean depth profile	18.92ºN	104.89º W	85	N/A	none	0.5% glutaraldehyde, -80ºC	100x	$1.09 \times 10^7 \pm 1.05 \times 10^6$	$6.92 \times 10^6 \pm 4.51 \times 10^5$	0.008
Pacific Ocean depth profile	18.92ºN	104.89º W	100	N/A	none	0.5% glutaraldehyde, -80ºC	100x	$7.85 \times 10^6 \pm 2.39 \times 10^6$	$4.94 \times 10^6 \pm 1.51 \times 10^5$	0.103
Pacific Ocean depth profile	18.92ºN	104.89º W	300	N/A	none	0.5% glutaraldehyde, -80ºC	100x	$3.59 \times 10^6 \pm 2.04 \times 10^6$	$1.41 \times 10^6 \pm 3.44 \times 10^4$	0.138
Tara Oceans, Station 96, Pacific Ocean	29.72ºS	101.16º W	5	0.008	0.22 µm	0.5% glutaraldehyde, -80ºC	100x	$2.17 \times 10^6 \pm 4.61 \times 10^5$	$1.04 \times 10^6 \pm 1.22 \times 10^5$	0.048
Tara Oceans, Station 142, Atlantic Ocean	25.51ºN	88.38ºW	5	0.052	0.22 µm	0.5% glutaraldehyde, -80ºC	100x	$4.16 \times 10^6 \pm 5.21 \times 10^5$	$5.71 \times 10^6 \pm 1.28 \times 10^5$	0.007
Tara Oceans, Station 81, Atlantic Ocean	44.53ºS	52.47ºW	5	0.112	0.22 µm	0.5% glutaraldehyde, -80ºC	100x	$5.40 \times 10^6 \pm 6.59 \times 10^5$	$5.84 \times 10^6 \pm 1.20 \times 10^5$	0.434
Tara Oceans, Station 139, Pacific Ocean	6.48ºN	94.96ºW	5	0.226	0.22 µm	0.5% glutaraldehyde, -80ºC	100x	$1.47 \times 10^7 \pm 3.51 \times 10^6$	$1.74 \times 10^7 \pm 1.42 \times 10^6$	0.284

Tara Oceans, Station 90, Pacific Ocean	39.62ºS	76.96ºW	5	1.339	0.22 µm	0.5% glutaraldehyde, -80ºC	100x	$1.42 \times 10^7 \pm 2.07 \times 10^6$	$2.06 \times 10^7 \pm 1.25 \times 10^6$	0.021
Tara Oceans, Station 89, Pacific Ocean	57.73ºS	67.11ºW	5	1.962	0.22 µm	0.5% glutaraldehyde, -80ºC	100x	$4.61 \times 10^6 \pm 1.73 \times 10^6$	$2.20 \times 10^6 \pm 2.81 \times 10^5$	0.191
Tara Oceans, Station 92, Pacific Ocean	33.69ºS	72.00ºW	5	3.142	0.22 µm	0.5% glutaraldehyde, -80ºC	100x	$2.22 \times 10^7 \pm 4.73 \times 10^6$	$3.22 \times 10^7 \pm 1.54 \times 10^6$	0.036
Tara Oceans, Station 87, Southern Ocean	63.85ºS	56.13ºW	5	5.691	0.22 µm	0.5% glutaraldehyde, -80ºC	100x	$7.45 \times 10^6 \pm 2.88 \times 10^6$	$8.25 \times 10^6 \pm 7.36 \times 10^5$	0.667
Lake Murray, South Carolina, USA	34.04 ºN	81.22ºW	1	N/A	0.22 µm	0.5% glutaraldehyde, -80ºC	10x	$6.28 \times 10^6 \pm 2.13 \times 10^5$	$5.98 \times 10^6 \pm 3.86 \times 10^5$	0.295
Lysate SWHM1	N/A	N/A	N/A	N/A	0.22 µm	4ºC	100x	$1.30 \times 10^7 \pm 6.78 \times 10^5$	$1.24 \times 10^7 \pm 1.80 \times 10^6$	0.629
Lysate PHM2	N/A	N/A	N/A	N/A	0.22 µm	4ºC	100x	$7.30 \times 10^6 \pm 4.18 \times 10^5$	$7.82 \times 10^6 \pm 5.37 \times 10^5$	0.257
Lysate S-SM1	N/A	N/A	N/A	N/A	0.22 µm	4ºC	N/A	$7.38 \times 10^7 \pm 1.07 \times 10^7$	$5.72 \times 10^7 \pm 4.13 \times 10^6$	0.067
Lysate S-SM1	N/A	N/A	N/A	N/A	0.22 µm	4ºC	N/A	$1.37 \times 10^8 \pm 1.90 \times 10^7$	$1.20 \times 10^8 \pm 2.18 \times 10^7$	0.434

N/A; not applicable or not available

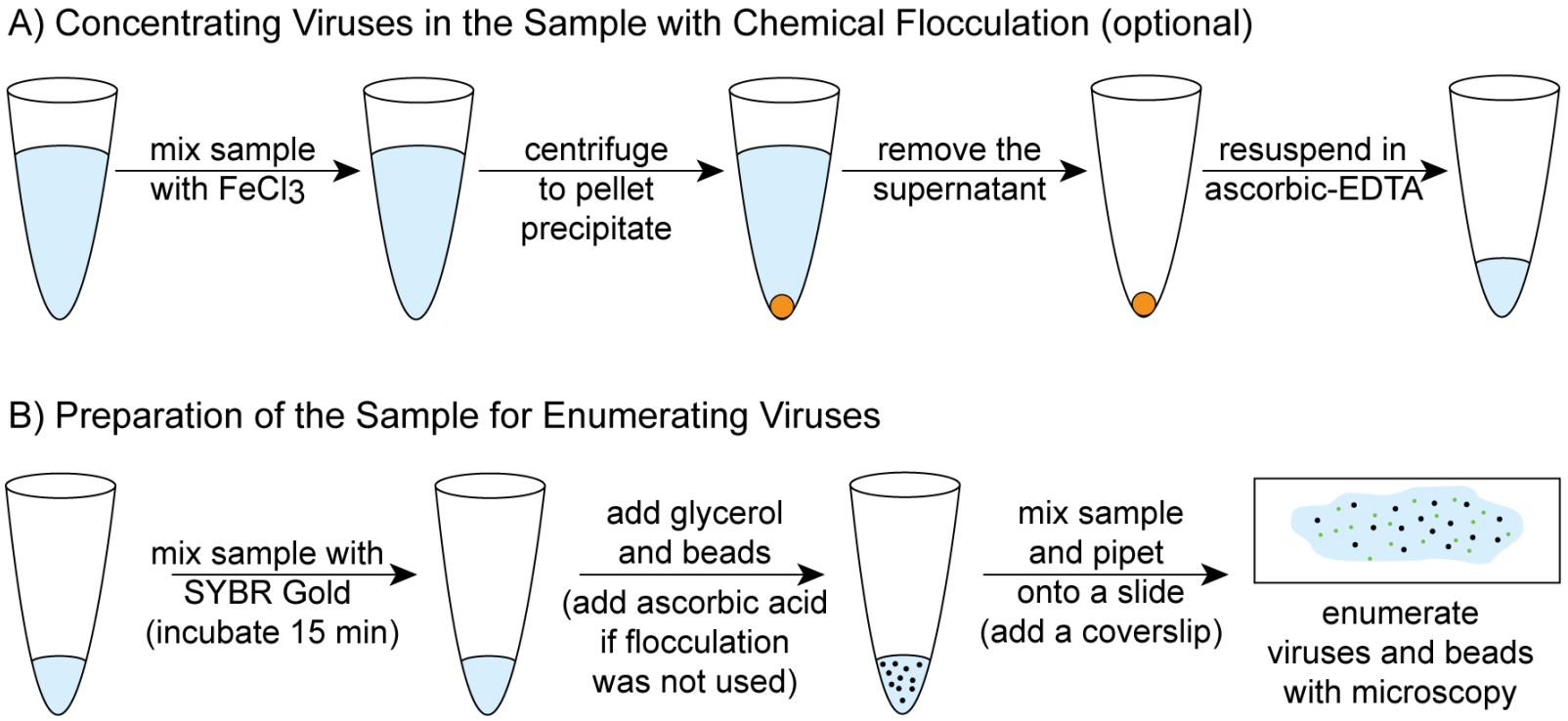

Figure 2.1 Overview of the wet-mount method for enumerating aquatic viruses.

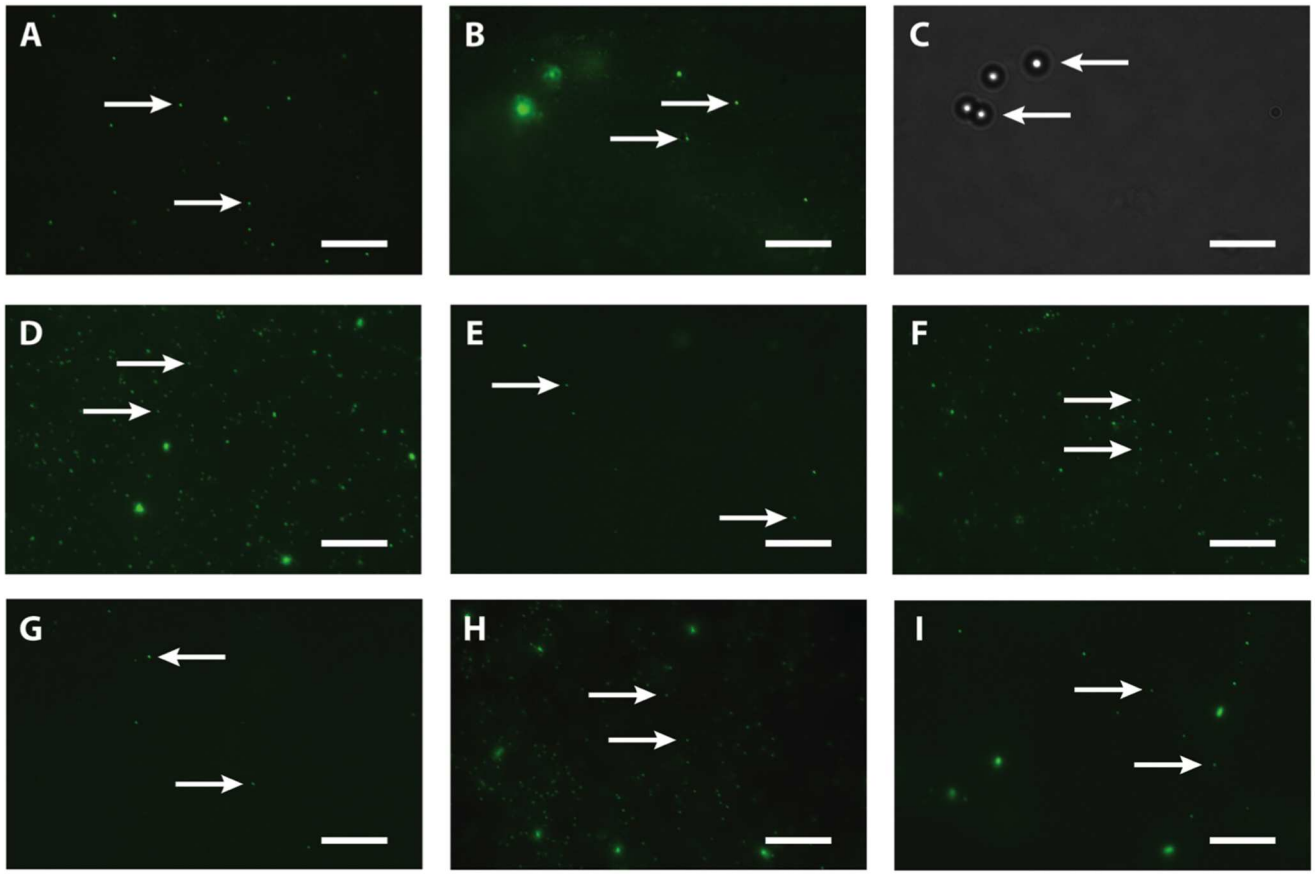

Figure 2.2 Images of samples prepared by use of the filter mount and wet-mount virus enumeration methods. Shown are epifluorescence images of purified S-SM1 lysate obtained by using the filter mount (A) and wet-mount (B) methods, seawater from 30 m in the Pacific Ocean depth profile by using the filter mount (D) and wet-mount (E) methods, freshwater from Lake Murray by using the filter mount (F) and wet-mount (G) methods, and unpurified S-SM1 lysate with *Synechococcus* cells by using the filter mount (H) and wet-mount (I) methods. These epifluorescence images include arrows pointing to two of the viruses in each image. Under white light (C), beads are visible in the same field of view as for the wet-mount sample (B), with arrows pointing to two of the beads in the image. Bar 10 μm.

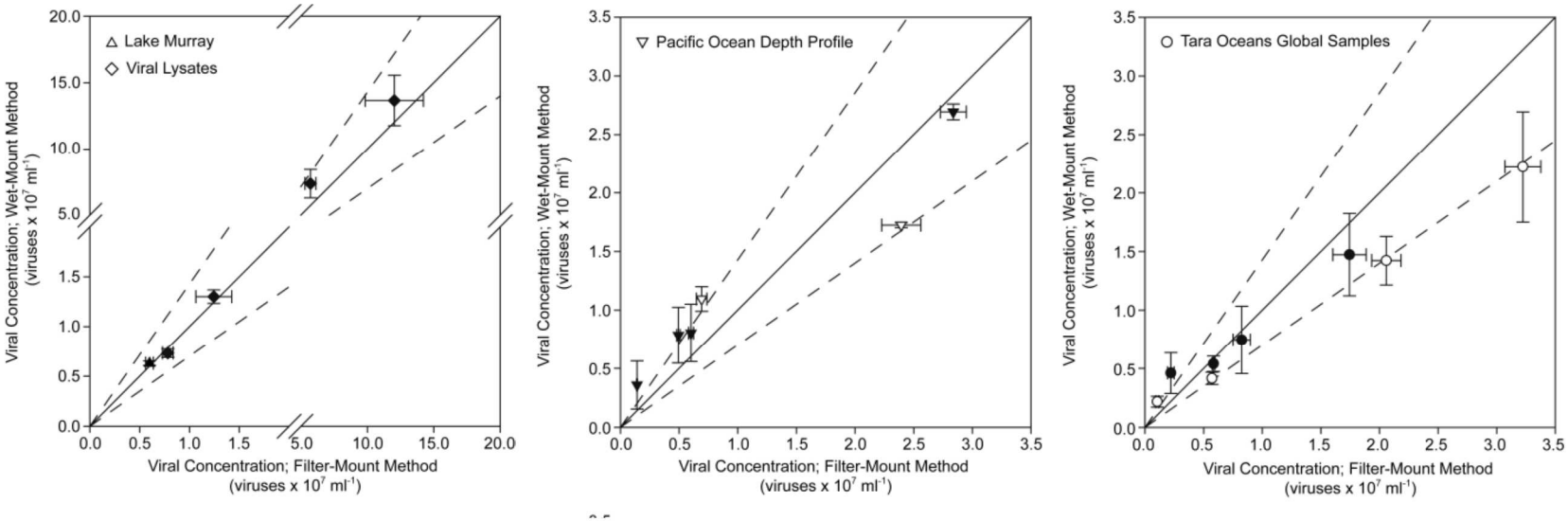

Figure 2.3 Viral concentrations in natural samples and lysates obtained by using the filter mount and wet-mount enumeration methods. Error bars are standard deviations of the means of data from triplicate samples. Closed symbols represent samples in which there was no significant difference in virus concentrations obtained by using the filter mount and wet-mount methods ($P \leq 0.05$ by two-tailed t tests), while open symbols represent samples in which there was a significant difference (see Table 2.S1 in the supplemental material). Average viral concentrations for all samples obtained by using each method were strongly and positively correlated (Pearson correlation coefficient, 0.986; $P \leq 0.001$). The solid lines represent a 1:1 relationship, and dashed lines represent an interval of 70% agreement between methods around the 1:1 relationship to facilitate visual comparison of results.

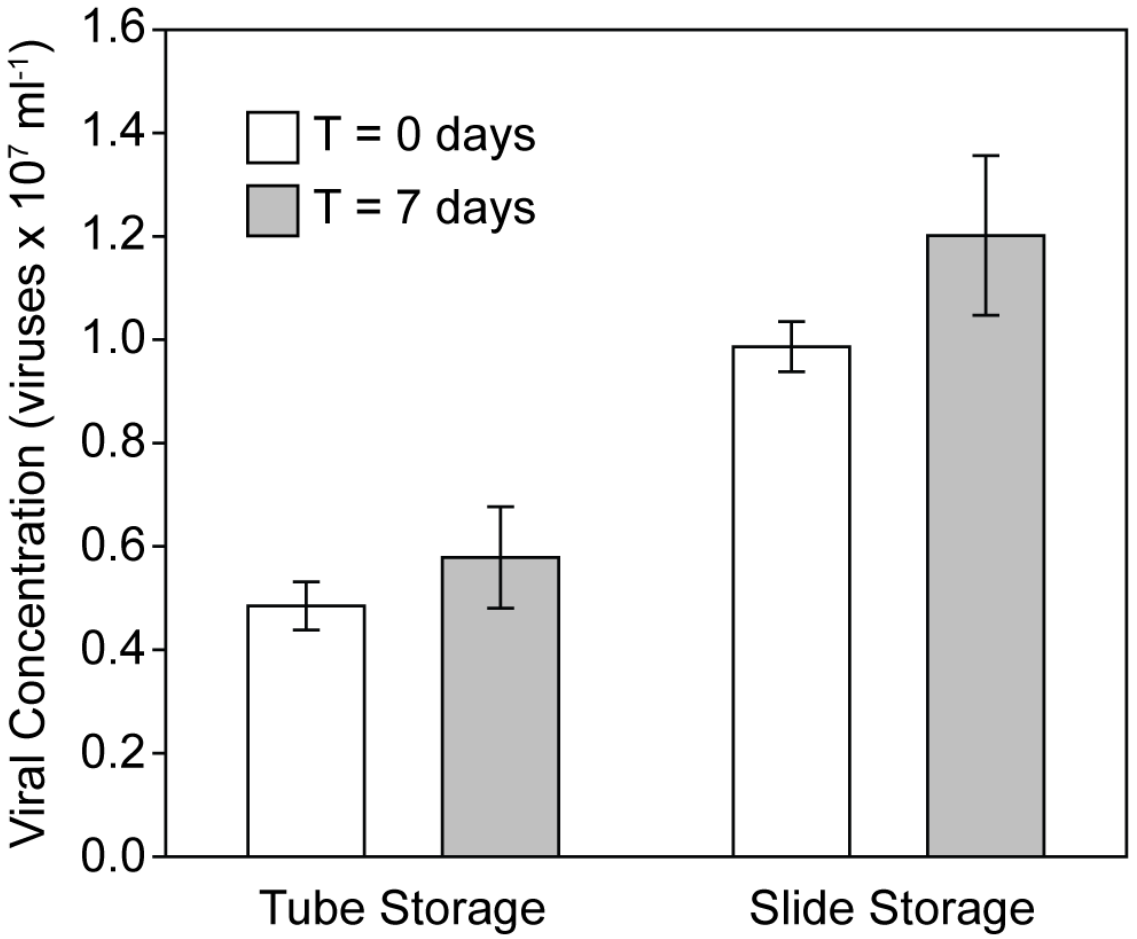

Figure 2.4 Concentration of viruses in triplicate samples (S-SM1 lysate for Tube Storage and S-WHM1 lysate for Slide Storage) prepared according to the wet-mount protocol and stored at -20°C in microcentrifuge tubes (Tube Storage) or wet-mounted on slides (Slide Storage). Viruses were enumerated immediately after preparation (T = 0 days) and after 7 days of storage (T = 7 days). Error bars are standard deviations of the means for triplicate samples.

CHAPTER 3

PHAGE GROWTH KINETICS OF 3 CYANOPHAGES PROPAGATED ON FE-LIMITED HOST *SYNECHOCOCCUS* WH7803

3.1 ABSTRACT

Marine viruses are an extremely important component to the microbial loop and biological pump. They influence biogeochemical cycling, microbial mortality, and metabolic functions through infection and lysis of phytoplankton. During photosynthesis, phytoplankton assimilate nutrients from the surrounding media and grow. Then, they can become prey for either zooplankton, which then transfer nutrients to higher trophic levels, or viruses, which create a shunt and release nutrients back into the media. To further our understanding of marine virus ecology, researchers have conducted experiments observing the viral/phage growth kinetics (e.g. viral burst size and latency period) of a multitude of phages and hosts. However, many of these experiments grow the phytoplankton host in ideal conditions with an abundance of nutrients. These conditions are not typical open-ocean conditions, where nutrient concentrations can be extremely low. Therefore, some experiments have been performed using hosts grown in P-limited media, to mimic certain ocean regions. These experiments have shown decreased viral burst size and increased latency period. Here, we have Fe-limited our hosts to 50% growth rate to determine if decreased viral reproduction is restricted to only P-limitation or is a more general phenomenon when host cells become stressed. We discovered that

Fe-limitation of hosts had no effects on phage growth kinetics for 3 cyanophages (Syn9, S-SM1, S-PM2) individually propagated on nutrient-replete and Fe-limited host *Synechococcus* WH7803. Therefore, if future climate change causes increased Fe-limitation in many ocean regions, we may observe a less efficient microbial loop and biological pump since host cells are growing slower, but producing a similar concentration of viruses. This would cause an increase in viral infection and lysis reducing carbon fixation and sequestration.

3.2 INTRODUCTION

Over the last few decades, researchers have determined that viruses are the most abundant biological entity in the ocean, averaging $3x10^9$ viruses l^{-1} (Suttle 2005). Marine viruses infect many microorganisms and influence microbial ecology, biogeochemical cycling, and gene transfer within the ocean (Breitbart 2012). However, viral replication varies between strains and even among the metabolic status of the host (Weinbauer 2004). For example, it has been shown that viral burst size (the number of viral particles released per infected host cell) of phages can range from ~20 to greater than 200 and viral latency period (time from infection to lysis of a cell) can range from ~1 hour to greater than 9 hours (Wilson et al. 1996; Mann et al. 2003; Brown et al. 2006; Lindell et al. 2007; Stoddard et al. 2007; Wang 2007; Kuznetsov et al. 2010; Raytcheva et al. 2011; Sabehi et al. 2012; Maat et al. 2014).

Even with the current data on viral growth kinetics, the total information is minimal due to the diversity of phages in natural environments. In fact, many of the studies in the literature present viral growth kinetics from hosts growing in favorable conditions with excess nutrients. However, these conditions are not representative of all

areas of the ocean. There are many areas in the ocean where phytoplankton can either by limited of co-limited by available nutrients, influencing growth and metabolism of cells (Moore et al. 2013). One of the first and most commonly studied nutrient limitations is phosphorus (P) limitation. Interestingly, one viral kinetics study analyzed the effects of a phosphate-replete and phosphate-deplete host (WH7803) on viral kinetics of phage S-PM2. It was discovered that under phosphate limitation the viral burst size was reduced by 80% and the latency period increased compared to the host grown in phosphate-replete conditions (Wilson et al. 1996). Other studies on marine eukaryotes have shown similar reduction in viral production under P-limitation (Bratbak et al. 1993, 1998; Maat et al. 2014). However, there was no observed difference in viral growth kinetics when an eukaryotic host was grown in the absence of metals Zn, Cd, or Co, (Gledhill et al. 2012).

In addition to the macronutrients N and P, iron (Fe) is a commonly studied nutrient. Since 1990, when John Martin first published his Fe-fertilization experiments, Fe has been recognized, alongside P, as a limiting nutrient that can influence phytoplankton growth throughout large areas of the ocean (Martin 1990; Martin et al. 1990; Boyd et al. 2007). However, it can be difficult to culture and maintain Fe-limited phytoplankton. Therefore, viral growth kinetics determined from Fe-limited phytoplankton have been minimally researched. Here, we describe the viral growth kinetics of three phages (Syn9, S-SM1, S-PM2) infecting host *Synechococcus* WH7803 grown in nutrient-replete and Fe-limited media. Phages Syn9 and S-SM1 are lytic, while phage S-PM2 is a temperate phage that can switch between lytic and lysogenic replication depending on host metabolism (Weinbauer 2004). Originally, we

hypothesized that Fe-limitation of hosts would illicit a similar response in phage growth kinetics to P-limitation, where phage production decreases and latency period increases.

3.3 MATERIALS AND METHODS

The strain *Synechococcus* WH7803 (CCMP 1334) used as a host throughout this study was routinely grown in 1 L trace metal cleaned polycarbonate bottles with constant bubbling from air pushed through a 0.2 μm filter. These cultures were grown under a 14:10 light:dark cycle at 40 μEinsteins at 23° C in trace metal ion buffered artificial sweater (ASW) (Sunda et al. 2005) with the addition of nutrients to create SN media (Waterbury et al. 1986). ASW contained 409 mM NaCl, 53 mM $MgCl_2$ * $6H_2O$, 28 mM Na_2SO_4, 10 mM $CaCl_2$ * $2H_2O$, 9 mM KCl, 2.7 mM $NaHCO_3$, 824 μM KBr, 420 μM H_3BO_3, 90 μM $SrCl_2$ * $6H_2O$, 71 μM NaF. To create SN media in a 1 L polycarbonate bottle, 750 mL ASW was combined with 236 mL ultrapure water (UPW) with the following addition of nutrients and trace metals to achieve final concentrations of 9 mM $NaNO_3$, 99 μM K_2HPO_4, 15 μM Na_2EDTA * $2H_2O$, 100 μM Na_2CO_3, 738 pM cyanocobalomin, 32.5 μM citric acid * H_2O, 23 μM ferric ammonium citrate, 7.08 μM $MnCl_2$ * $2H_2O$, 772 nM $ZnSO_4$ * $7H_2O$, 85.9 nM $Co(NO_3)_2$ * $6H_2O$. For Fe-limited SN media, the ferric ammonium citrate was reduced 100-fold to 230 nM, while all other nutrient concentrations remained the same. Also, since EDTA is a metal chelator in the media, free Fe (Fe') concentrations can be calculated using equations from Sunda (Sunda et al. 2005) equaling 100 nM Fe' and 1 nM Fe' in the nutrient-replete and Fe-limited media, respectively.

3.3.1 PREPARATION OF PHAGE STOCK

Phage stocks ranged in concentration from 2.1 to $8.7x10^8$ virus mL^{-1} and were generated by adding an aliquot of phage lysate to an exponentially growing 1 L Fe-replete culture. The infected culture was kept at 23° C under 14:10 light:dark illumination at 40 μEinsteins. Phage was harvested when cell lysis was observed by flow cytometry in the infected culture. Harvested phage was filtered through a 0.2 μm filter to remove cellular debris. To increase total phage concentration, the 0.2 μm filtered lysate was concentrated from 1 L to ~50 mL using a 100kDa Sartoris 50R.

3.3.2 DETERMINATION OF PHAGE TITER

Phage titer was determined by most probably number (MPN) assay (Cochran 1950). Briefly, this assay combines exponentially growing WH7803 with a serial dilution of phage in a 96-well plate. The plate is kept in the incubator and visually inspected daily for cell lysis. If lysis occurs in a well, the phage dilution previously recorded assumes that there are at least that many infective phage particles in solution. For example, if lysis occurs in a well with phage stock diluted 10^{-6}, and not in 10^{-7} phage dilution well, then there are at least 10^6 infective phages mL^{-1}. Phage titer in these experiments was 10^7 for Syn9, S-SM1, and S-PM2.

3.3.3 GROWTH CURVES OF WH7803

Growth curves of *Synechococcus* WH7803 grown in nutrient-replete and Fe-deplete media were tracked daily ~4 hours after lights on via cell count and fluorescence. Growth rates were determined by cell count, which was performed using a Guava HPL flow cytometer, while fluorescence, used as a rough proxy for cellular stress, was performed using a Turner Trilogy.

3.3.4 CONCENTRATION OF HOST CELLS

Exponentially growing *Synechococcus* WH7803 in both nutrient-replete and Fe-limited SN media were harvested when concentrations reached 10^7 cells mL^{-1} as determined by flow cytometry. The cells were transferred in to trace metal clean 50 mL centrifuge tubes and centrifuged at 5000 x g for 10 minutes at room temperature. The supernatant was removed and the cells were resuspended in ~5 mL of nutrient-replete or Fe-limited SN media to achieve 10^8 cell mL^{-1}.

3.3.5 PHAGE GROWTH KINETICS

Growth kinetics for each phage strain was determined by one-step growth curves. In triplicate, 1 mL of host cells at a concentration of 10^8 mL^{-1} were combined with 1 mL of infective phage at a concentration of 10^7 mL^{-1} in 15 mL trace metal clean tubes (adsorption tube) to create a multiplicity of infection (MOI) of 0.1. The adsorption tubes were placed in the incubator for 15 minutes at 23° C in 40 μEinsteins to allow phage to adsorb to the host. After 15 minutes, the adsorption tubes were removed and 0.5 mL from each adsorption tube were transferred into 49.5 mL nutrient-replete or Fe-deplete SN media, creating a 100-fold dilution tubes (DIL tubes). The tubes were placed back in the incubator until sampling. Beginning with T0 and extending up to T27, depending on the phage, 1 mL was twice sampled and then 0.2 μm filtered from each DIL tube. The first of the filtered sample was placed in a freezer at -20° C until exterior phage concentration analysis, while the sample was placed in the fridge until MPN analysis. Host cells were also sampled to determine host concentration over the course of the experiment. Unfiltered, 100 μL samples from each DIL tube was pipetted into a 96-well plate, diluted 10-fold in triplicate and then run immediately on a flow cytometer. Exterior phage and

host cell concentrations were then used to determine burst size of the phage by dividing the number of newly produced phages by the number of lysed host cells (Maat et al. 2014).

3.3.6 QUANTITY OF EXTERIOR PHAGE

The quantities of exterior phages produced over time were determined by quantitative real-time polymerase chain reaction (qPCR). Primers for Syn9, S-SM1, and S-PM2 was designed using Primer3 software with an ideal primer size of 18-22bp and a product size of ~120bp. The primer sequences for each phage are as follows: Syn9 forward AGCGATTAAAGCAGTCAACC, Syn9 reverse AGGGAGATTACCAACGTCAA, S-SM1 forward GTCCAGAAGAACTGCGTGGT, S-SM1 reverse GCAATTTTCATGCCCTGATT (Zeng and Chisholm 2012), S-PM2 forward CTACACTTCCAGGCGGTCAG, and S-PM2 reverse TCGAAGGATCTCCGTGGACT (this study).

To perform qPCR, phage standards were created by serially diluting phage in ASW from 10^8 to 10^4 phage mL^{-1}, where phage concentration was determined by wet-mount enumeration of stock lysate (Cunningham et al. 2015). The standards and one-step growth curve lysates were further diluted 50X in 10 mM Tris. The quantification of phages was performed by combining 10 µL lysate, 12.5 µL of master mix (iTaq Universal SYBER Green Supermix), and 1.25 µL of both primers in a 96-well PCR plate for a final volume of 25 µL per well. The thermal cycle and measurement of SYBR Green fluorescence were performed on a Bio-Rad CFX96 Real-Time PCR Detection System using the following program: pre-incubation at 95°C for 10 min; amplification for 39 cycles consisting of denaturation at 95°C for 15 s, annealing at 56°C for 15 s, and

extension at 72°C for 30 s; melting curve analysis heated to 95°C for 10 s, annealing at 65°C for 5 s, and extension at 95°C for 5 s.

3.4 RESULTS AND DISCUSSION

3.4.1 RESPONSE OF HOST CELLS TO FE-LIMITATION

Synechococcus WH7803 host cells grown in nutrient-replete and Fe-limited media were measured by cell count and fluorescence to analyze cell growth and stress. Host cell population doublings per day were on average 0.8 ± 0.1 in nutrient-replete media and 0.39 ± 0.1 in Fe-limited media, while fluorescence also showed a decrease by ~1/3 between nutrient-replete and Fe-limited media (Table 3.1). Both measurements show that the growth rate between cells in Fe-limited media is at least halved allowing us to believe that these cells are Fe-limited.

3.4.2 PHAGE GROWTH KINETICS

Phage growth kinetics were determine using one-step growth curves for 3 phage strains: Syn9, S-SM1, and S-PM2. Syn9 one-step growth curve reveals no difference between phage production or latency period of host cells grown in nutrient-replete vs. Fe-limited media (Figure 3.1). Syn9 phage latent period lasts 18 hours and has a burst size of 42 in host cells grown in both medias. S-SM1 phage latent period lasts 1.5 hours and has a burst size of 39 in Fe-replete media and 31.6 Fe-deplete media. S-PM2 phage latent period lasts 6 hours and has a burst size of 59 in Fe-replete and 63 in Fe-deplete media (Table 3.1). It should be noted that the use of qPCR to determine phage number calculates total phage and does not directly reveal phage infectivity.

3.4.3 COMPARISON OF PHAGE GROWTH KINETICS

Here, we intended to model our experiments after a set of experiments performed by Wilson et al. (Wilson et al. 1996) using the same host and phage. However, instead of P-limiting the host we instead grew the host under Fe-limitation and performed phage kinetics on three phages, including the phage used in the original experiments. Wilson et al. (Wilson et al. 1996) found that phage S-PM2 propagated on P-deplete host WH7803 showed a delayed latency period of 18 hours and a decreased burst size of 80% when compared to S-PM2 propagated on the P-replete host. Our results showed no change in latency period or significant difference in burst size for all three phages when propagated on host WH7803 under nutrient-replete and Fe-deplete conditions.

However, there are several methodological differences that may account for differences in phage growth kinetics observed between this study and the Wilson et al. (Wilson et al. 1996) study. First, in this study we used qPCR to determine total exterior phage quantity, while Wilson et al. used plaque assays to determine total infective exterior phage. Total infective phage can vary from a few percent to 100% of the total phage population (Suttle and Chan 1994; Bratbak et al. 1998). Therefore, it may have been possible that our study did not observed a delayed latency period or reduced burst size in Fe-limited host cells since we were calculating total phage and not infective phage. To check this assumption, we used MPN assays to determine infectivity of the total phage for each phage growth kinetic experiment. The assays revealed no difference in latency period or total infective exterior phage produced between phages propagated on nutrient-replete and Fe-deplete WH7803 host cells.

Another difference between experiments is host cellular growth conditions. For our study, host growth rate was determined by cell count, while Wilson et al. host growth rate was determined by absorbance. The difference in methodologies makes host growth rates difficult to directly compare, but our study observed a 50% average decrease in host growth rate from nutrient-replete to Fe-deplete cells, while Wilson et al. observed a 40% decrease. The reduction in growth rates between the studies is similar, but difference in experimental methodologies occurs when nutrient-limiting the host cells. To Fe-limit our host cells, we transfer nutrient-replete WH7803 into Fe-deplete media and grow these cells over multiple generations in low Fe conditions. In the Wilson et al. study, nutrient-replete host cells are transferred to P-deplete media and immediately used in phage growth kinetic experiments. It is possible that our host cells grown in Fe-limited conditions over successive generations have adapted their cellular machinery to low Fe conditions for optimal performance. On the other hand, the host cells in the Wilson et al. study may be "shocked" when first transferred into P-deplete media and may respond by slowing down cellular machinery, thereby increasing the time to lysis and producing less phage during infection.

Finally, we induced a decreased growth rate of host cells through Fe-limitation instead of P-limitation. Unlike Fe, P is a major nutrient required for DNA replication for the host and virus (Cohen 1948). This may be why we do not observe a change in phage growth kinetics. A similar experiment found no change in viral growth kinetics when the host was growth limited by other trace metals (Gledhill et al. 2012). Also, it may be possible that even though we decreased host growth rate by half, we may not have sufficiently stressed the cell to potentially see a change in phage growth kinetics. The

host *Synechococcus* WH7803 is an oceanic strain that is adapted for low Fe conditions, but does not elicit a typical response to Fe-limitation. Unlike other cyanobacteria, this strain does not produce siderophores to capture Fe nor does it synthesize the flavodoxin protein, a protein that replaces ferrodoxin during periods of low Fe availability (Chadd et al. 1996; Roche et al. 1996). Instead, this strain produces the IdiA protein, which is predicted to function in Fe transport and photosystem II protection during Fe stress (Fulda et al. 2000; Tölle et al. 2002). Interestingly, when WH7803 was cultured and Fe-limited, IdiA, which can be used as an indicator of Fe-stress, was only significantly detected when Fe was completely removed from the media (Webb et al. 2001; Rivers et al. 2009). Since our media still contained 230 nM Fe, it may be possible extreme Fe-stress was not induced in our cultures. Finally, a recent study of Fe-limited oceanic *Synechococcus* suggests that Fe-limitation does not depend on Fe alone, but also depends on the availability of Fe, N, and P (Mackey et al. 2015a).

3.5 CONCLUSION

We have produced one of the first sets of phage growth kinetic data sets propagated on a Fe-limited cyanobacterial host, *Synechococcus* WH7803. Our data shows that under Fe-limitation, unlike P-limitation, viral production would not be reduced, but cellular growth rate would be reduced. In this scenario it is possible that the combination of decreased cellular growth rate and no change in viral reproduction, we may observe faster cycling of the microbial loop leading to increased nutrient input from viral lysate.

Table 3.1. Physiological measurements of host and phage production.

Phage	Media	Cell count Growth Rate (day^{-1})	Fluorescence Growth Rate (day^{-1})	Latent Period (hours)	Burst Size
Syn9	Nutrient-replete	0.72	0.26	15-18	42.1
	Fe-limited	0.33	0.13	15-18	41.8
S-SM1	Nutrient-replete	0.76	0.34	1.5-2	39
	Fe-limited	0.34	0.11	1.5-2	31.6
S-PM2	Nutrient-replete	0.93	0.36	6-9	57.8
	Fe-limited	0.51	0.18	6-9	62.9

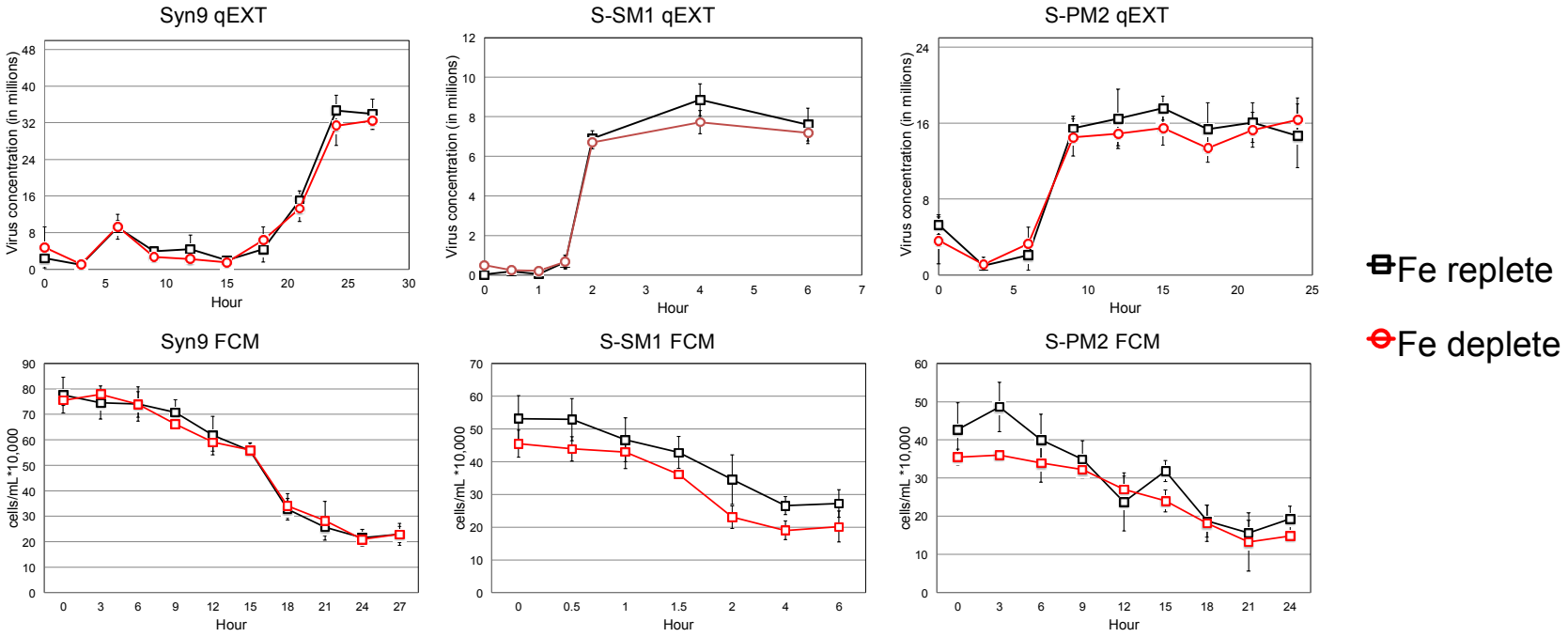

Figure 3.1. Comparison of external virus production (viruses mL^{-1}) and cell counts (cells mL^{-1}) throughout infection. The top row of graphs display external virus production, while the bottom row displays cell number. Black squares represent virus/cell number of Fe-replete host, while red squares represent virus/cell number of Fe-deplete host.

CHAPTER 4

CHANGES IN ELEMENTAL STOICHIOMETRY OF PICOPHYTOPLANKTON GROWN UNDER FE-LIMITATION AND INFECTION

4.1 ABSTRACT

Phytoplankton elemental stoichiometry reveals the utilization and availability of nutrients in media surrounding the cell. This information provides oceanographers with an in depth look into how individual species are interacting and influencing the surrounding environment. However, outside of canonical Redfield Ratio of 106C:16N:1P, there is limited information regarding the extended elemental stoichiometry of metal concentrations in phytoplankton cells. Metal concentrations can vary greatly throughout the ocean and in some instances can even be low enough to cause growth-limitation of phytoplankton cells. One of the metals most commonly attributed to phytoplankton growth limitation is Fe. Fe is found in low concentrations throughout large areas of the ocean, but in particular, large areas of the subtropical open ocean can experience Fe-limited conditions. These areas are dominated by cyanobacteria and picoeukaryotic phytoplankton, also known as picophytoplankton. Current literature has not focused on the extended elemental stoichiometry of these phytoplankton and instead have either used large eukaryotic phytoplankton species or methods that do not directly reveal C and N stoichiometry. Here, we examine how Fe-limitation influences the extended elemental

stoichiometry of two cyanobacteria and one picoeukaryotic phytoplankton species. We find the average elemental composition of the nutrient-replete cells to be $(C_{80}N_{18.5}P_1Mg_6Ca_2)_{1000}Fe_{20.5}Mn_{1.68}Zn_{1.1}Cu_{0.5}Ni_{0.3}Co_{0.04}Cd_{0.002}$, while Fe-limited cells average is $(C_{123}N_{30}P_1Mg_{11}Ca_{1.7})_{1000}Fe_{9.32}Mn_{2.7}Zn_{1.4}Cu_{0.6}Ni_{0.66}Co_{0.11}Cd_{0.0033}$. We also examined how viral infection can influence the extended elemental stoichiometry of an Fe-limited cyanobacteria host. Our data show that viral infection leads to an increase P concentration in the cell. This increase in P is accompanied by increases in Zn, Mg, and Ca that could indicate production of the alkaline phosphatase and 5' nucleotidase enzymes. By analyzing the data from extended elemental stoichiometry of Fe-limited picophytoplankton, we may be able to determine how impending climate change and variation in nutrient availability may impact phytoplankton growth and utilization of nutrients.

4.2 INTRODUCTION

Alfred Redfield was one of the first oceanographers to study the composition of plankton in seawater, discovering an almost constant ratio of 106 carbon (C) to 16 nitrogen (N) to 1 phosphorus (P) in plankton biomass and dissolved nutrients in seawater (Redfield 1934, 1958). This ratio is commonly referred to as the Redfield Ratio and has been vital to understanding phytoplankton growth and biogeochemical cycling in the ocean. The Redfield Ratio describes a tight correlation between the ratio of N atoms per atoms of P in phytoplankton cells and dissolved nutrients in seawater (Anderson and Sarmiento 1994). This relationship between N and P in seawater is typically considered to be a critical threshold between N- and P-limitation influencing phytoplankton photosynthesis, growth, and therefore carbon sequestration (Broecker 1982; Codispoti 1989). Originally,

it was believed that if the 16:1 ratio in seawater were altered, phytoplankton would experience N-limitation (ratios below 16:1) or P-limitation (ratios above 16:1). However, recently is has been discovered that N:P composition of some phytoplankton communities can range by over an order of magnitude (Geider and La Roche 2002). This range in N:P ratios are due to the regional variation in the phytoplankton community species composition and typically range from 12:1 in polar oceans to 20:1 in sub-Antarctic oceans These findings lead to the idea that the average dissolved nutrient concentration of 16:1 is controlled by global ocean circulation patterns that distribute dissolved N:P ratios derived from variation in particulate ratios (Weber and Deutsch 2010, 2012).

There are several proposed explanations for the regional variation observed in the Redfield Ratio for various phytoplankton species (Martiny et al. 2013). The first explanation is that differences among phytoplankton taxonomic composition may alter the Redfield Ratio. For example, researchers have discovered that diatoms typically have lower C:P and N:P ratios compared to that of cyanobacteria (Arrigo 1999; Bertilsson et al. 2003; Twining et al. 2004; Price 2005). Therefore, seasonal and regional variations could alter phytoplankton community structure, influencing the Redfield Ratio. The second explanation is that detrital material and dead cells are also collected while harvesting phytoplankton cells. Detrital material and dead cells are already partially decomposed, altering the nutrient concentrations, and influencing the observed elemental stoichiometry of live cells (Martiny et al. 2013). The third explanation is phytoplankton cells can allocate resources differently for varying growth strategies. This explanation asserts that if competitive equilibrium favors low-P resource allocation, then N:P will be

high, but if it favors exponential growth, then N:P will be low (Elser et al. 2003; Klausmeier et al. 2004). The fourth explanation is the alteration of cellular elemental stoichiometry due to availability of nutrients in the surrounding media. This is commonly observed in laboratory cultures where phytoplankton can exhibit varying elemental stoichiometry by altering nutrient concentration in situ (Rhee 1978; Bertilsson et al. 2003).

Among these explanations, one of the most important to climate change and trophic food web dynamics is determining how the variation in nutrient availability alters cellular elemental stoichiometry. Several studies have analyzed changes in elemental stoichiometry in laboratory cultures of nutrient-limited phytoplankton (Hutchins et al. 1999; Lynn et al. 2000; Sañudo-Wilhelmy et al. 2001; Bertilsson et al. 2003; Ho et al. 2003), but very few studies have analyzed the effects of Fe-limitation on the Redfield Ratio or the extended elemental stoichiometry (Price 2005; Hoffmann et al. 2007). Analyzing the extended elemental stoichiometry of nutrient-replete and nutrient-limited phytoplankton in laboratory cultures can reveal differences between uptake of micro- and macronutrients that can be extrapolated to oceanic populations. These differences could help understand how climate change will influence particulate nutrient concentration in surface seawater.

To gain a greater understanding of differences among phytoplankton extended elemental stoichiometry, more information should be obtained regarding the abundant, cosmopolitan phytoplankton species, the cyanobacteria and picoeukaryotic phytoplankton. These phytoplankton are ubiquitous in the subtropical open ocean and live in a wide range of environments throughout the euphotic zone (Johnson et al. 2006).

However, there exists little research determining the extended elemental stoichiometry of these phytoplankton species in Fe-limited conditions. Available research has used synchrotron X-ray fluorescence microscopy (SXRF) to determine P:element ratios in field samples of cyanobacteria cells (Twining et al. 2010; Twining and Baines 2013). This work is extremely important in that it is some of the first research to determine P:element ratios of cyanobacteria. However, SXRF cannot directly determine C and N concentrations. Determining these macronutrient concentrations, in conjunction with other elements, would provide further information to make conclusions about extended elemental stoichiometry of picophytoplankton.

Our research analyzes the extended elemental stoichiometry, including C and N, of laboratory cultures of oceanic strains of cyanobacteria and picoeukaryotic phytoplankton. We axenically grew two strains of cyanobacteria (*Synechococcus* WH7803 and *Prochlorococcus* MED4) and one strain of picoeukaryotic phytoplankton (*Ostreococcus lucimarinus*) in nutrient-replete and Fe-limited media. Here, we report the first full comparison of extended elemental stoichiometry of laboratory grown nutrient-replete and Fe-limited picophytoplankton. We find significant differences between average element:P ratios of C, N, Co, Fe, Mn, and Cd between nutrient-replete and Fe-limited picophytoplankton cells. Also, when we separate the elemental stoichiometry ratios based on species, we find interesting patterns possibly relating to production of stress-reducing enzymes. To gain a fuller understanding of how trophic food web dynamics influence picophytoplantkon elemental stoichiometry, we also examined the effects of viral infection on the extended elemental stoichiometry of Fe-limited *Synechococcus* WH7803 cells. We found several interesting trends, including a

significant increase in P concentration (moles cell^{-1}) in the treatments containing active virus compared to uninfected treatments.

4.3 MATERIALS AND METHODS

4.3.1 GROWTH OF LABORATORY CULTURES

Three strains of picophytoplankton (*Synechococcus* WH7803, *Prochlorococcus* MED4, *Ostreococcus lucimarinus*) were axenically grown in nutrient-replete and Fe-deplete media. Each culture was routinely grown in 1 L trace metal cleaned polycarbonate bottles with constant bubbling from air pushed through a 0.2 μm filter. These cultures were grown under a 14:10 light:dark cycle at 40 μEinsteins at 23° C. Cell concentrations were tracked daily using a Guava easyCyte HPL flow cytometer. We observed significant decreases in growth rate between cells grown in nutrient-replete and Fe-limited cultures (Table 4.1).

To promote sustained growth in culture, each strain was cultured in a slightly different media. *Synechococcus* WH7803 was grown in SN media, *Prochlorococcus* MED4 was grown in PRO99 media, and *Ostreococcus lucimarinus* was grown in Aquil media. Each media was previously formulated to promote optimal culture growth for each individual species (Sunda et al. 2005; Moore et al. 2007). Therefore, the medias vary slightly in macronutrient concentration, but tend to have similar free metal concentrations since each media uses EDTA to buffer the free metal concentrations. In particular, each EDTA-buffered media allowed us to alter the total Fe concentrations within the medias to establish a similar free Fe (Fe') concentration for both nutrient-replete and Fe-deplete conditions. From this, we were able to promote similar decreases

in growth rates between nutrient-replete and Fe-deplete conditions for each species. Below we further describe the recipes for each media.

The strain *Synechococcus* WH7803 (CCMP1334) was grown in trace metal ion buffered artificial sweater (ASW) (Sunda et al. 2005) with the addition of nutrients to create SN media (Waterbury et al. 1986). ASW contained final concentrations of 409 mM NaCl, 53 mM $MgCl_2$ * $6H_2O$, 28 mM Na_2SO_4, 10 mM $CaCl_2$ * $2H_2O$, 9 mM KCl, 2.7 mM $NaHCO_3$, 824 μM KBr, 420 μM H_3BO_3, 90 μM $SrCl_2$ * $6H_2O$, 71 μM NaF. To create SN media in a 1 L polycarbonate bottle, 750 mL ASW was combined with 236 mL ultrapure water (UPW) with the following addition of nutrients and trace metals to achieve final concentrations of 9 mM $NaNO_3$, 99 μM K_2HPO_4, 15 μM Na_2EDTA * $2H_2O$, 100 μM Na_2CO_3, 738 pM cyanocobalamin, 32.5 μM citric acid * H_2O, 23 μM ferric ammonium citrate, 7.08 μM $MnCl_2$ * $2H_2O$, 772 nM $ZnSO_4$ * $7H_2O$, 85.9 nM $Co(NO_3)_2$ * $6H_2O$. For Fe-limited SN media, the ferric ammonium citrate was reduced 100-fold to 230 nM, while all other nutrient concentrations remained the same.

The strain *Prochlorococcus* MED4 (CCMP1986) was grown in low-nutrient, 0.2 μm filtered and microwave sterilized seawater with the addition of nutrients to create PRO99 media (Moore et al. 2007). The seawater was combined macronutrients to achieve final concentrations of 50 μM NaH_2PO4 * H_2O, 800 μM NH_4Cl, and trace element mixture. The trace element mixture was filter sterilized, added at a concentration of 1 mL L^{-1} of PRO99 media, and contained final nutrient concentrations of 1.17 μM Na_2EDTA * $2H_2O$, 1.17 μM $FeCl_3$ * $6H_2O$, 8 nM $ZnSO_4$ * $7H_2O$, 5 nM $CoCl_2$ * $6H_2O$, 90 nM $MnCl_2$ * $4H_2O$, 3 nM $NaMoO_4$ * $2H_2O$, 10 nM Na_2SeO_3, 10 nM $NiSO_4$ * $6H_2O$.

For Fe-limited PRO99 media, the $FeCl_3$ * $6H_2O$ was reduced 100-fold to 11.7 nM, while all other nutrient concentrations remained the same.

The strain *Ostreococcus lucimarinus* was grown in trace metal ion buffered ASW with the addition of nutrients to create Aquil media (Sunda et al. 2005). ASW contained the same salt concentrations described in the above paragraph creating SN media. To create Aquil the following addition of nutrients, trace metals, and vitamins were added to achieve final concentrations of 10 μM NaH_2PO_4 * H_2O, 100 μM $NaNO_3$, 100 μM Na_2SiO_3 * $9H_2O$, 100 μM Na_2EDTA * $2H_2O$, 1 μM $FeCl_3$ * $6H_2O$, 79.7 nM $ZnSO_4$ * $7H_2O$, 50.3 nM $CoCl_2$ * $6H_2O$, 121 nM $MnCl_2$ * $4H_2O$, 100 nM $NaMoO_4$ * $2H_2O$, 10 nM Na_2SeO_3, 19.6 nM $CuSO_4$ * $5H_2O$, 297 nM thiamine, 2.25 nM biotin, 370 pM cyanocobalamin.

4.3.2 PROPAGATION OF VIRUS

The virus was propagated on WH7803 host cells grown in Fe-limited conditions to reduce Fe-contamination when infecting Fe-limited cultures. The infected culture was kept at 23° C under 14:10 light:dark illumination at 40 μEinsteins. Virus was harvested when cell lysis was observed by flow cytometry in the infected culture. Harvested virus was filtered through a 0.2 μm filter to remove cellular debris. To increase total virus concentration, the 0.2 μm filtered lysate was concentrated from 1 L to ~50 mL using a 100kDa Sartoris 50R. The final virus concentration totaled $8.7x10^9$ virus mL^{-1}.

4.3.3 INFECTION OF FE-LIMITED CELLS

To assess the effect of infection on picophytoplankton extended elemental stoichiometry, four replicates of *Synechococcus* WH7803 cells were grown in Fe-limited SN media, infected in duplicate with either active virus (AV, containing cyanophage Syn9) or heat

killed virus (HK, Syn9 removed) media, and tracked over the course of the infection by flow cytometry. Initially, exponentially-growing Fe-limited WH7803 cells were transferred into four separate 4 L trace metal cleaned polycarbonate bottles, each containing 2 L of Fe-limited SN media. Each bottle was aerated with constant bubbling from air pushed through a 0.2 μm filter. These cultures were grown under a 14:10 light:dark cycle at 40 μEinsteins at 23° C. Once cells reached early exponential growth (~$5x10^6$ cells mL^{-1}), 5 mLs of either AV or HK media was added to separate duplicate cultures. The AV media contained ~10^8 infective Syn9 virus particles, creating a multiplicity of infection (MOI) of 0.05. The HK media was used as a control for the addition of nutrients when AV/HK media was transferred to each culture. Since the virus were propagated on Fe-deplete media and addition of AV/HK media is only 0.25% of the total culture media, any nutrient-addition effect should be negligible. After the addition of AV/HK media, cultures were tracked and harvested for elemental concentration at T0 (time of infection), T24, T48, T72 hours past infection. The procedures outlining harvesting of cells and extended elemental stoichiometry measurements are described below.

4.3.3 PARTICULATE CARBON AND NITROGREN MEASUREMENTS

Measurements of particulate carbon and nitrogen were completed by vacuum filtering 25 mL of individual culture onto precombusted 25-mm GF/F filters. Filtrations were performed in triplicate for each culture. Filters were then dried and combusted using a GV Instruments Isoprime IRMS at the Marine Sediments Research Lab at University of South Carolina to determine carbon and nitrogen concentration (ppb).

4.3.4 TRACE ELEMENT MEASUREMENTS

To analyze trace elements concentration of cells, the cells were harvested, processed, and run on an Element 2 ICP-MS to determine cellular elemental concentration. Briefly, cells were harvested when they achieved mid-log phase growth. Initially, cells were washed in 60 mL oxalate solution per 1 L culture to remove any metals that had precipitated onto the outside of the cells. This solution has been shown to remove surface adsorbed Fe and other metals from phytoplankton cells (Tovar-Sanchez et al. 2003; Sanudo-Wilhelmy et al. 2004). Then, cultures were inverted and incubated at room temperature for 30 minutes. After incubation, 100 mL of culture was vacuum-filtered onto trace-metal cleaned 47-mm 0.2 μm polycarbonate filters. Filtrations were performed in triplicate for each culture. Once filtration was complete, the filter rig was washed 3X with 5 mL of UPW to rinse remaining cells off the filter rig wall. Filters were then cleanly removed and placed in individual acid cleaned Teflon pots. A 10-pbb-indium standard was added to the filters to control for metals retained on the filters during the leaching process. Then, 1 mL each of concentrated ultrapure quartz distilled HCl and HNO_3 were combined in the Teflon pots, forming Aqua regia, to leach the metals from the filters. The pots were allowed to sit overnight, venting, as the Aqua regia reaction took place. Filters were then cleanly removed from the pots with acid-rinsed tefzel tweezers. The filters were then rinsed twice with UPW into the Teflon pots to ensure that the filtrate were washed from filters and then the filters were discarded. The pots were placed on a drying plate to evaporate to dryness overnight and then the evaporite is redissolved in 500 μL of 0.1 N HNO_3. Samples were then run on a Thermo Element 2 ICP-MS at the Center for

Elemental Mass Spectrometry at the University of South Carolina with a 10-pbb multi-element standard to determine extended elemental stoichiometry.

4.3.5 DATA ANALYSIS

Statistical comparison of elemental composition of phytoplankton cells obtained throughout the experiments was performed using two-tailed t-tests and Kolmogorov-Smirnov tests for normality (SPSS Statistics v23.0, IBM Corporation).

4.4 RESULTS AND DISCUSSION

4.4.1 ELEMENTAL STOICHIOMETRY OF PICOPHYTOPLANKTON

We average the extended elemental stoichiometry data of two prokaryotes and one eukaryote grown in laboratory cultures. We find significant ($p<0.05$) element:P quota (moles cell^{-1}) increases in C , N, Mn, Co, and Cd and a decrease in Fe between cells grown in nutrient-replete compared to Fe-limited media (Table 4.2). Overall, the average elemental composition of the nutrient-replete cells is $(C_{80}N_{18.5}P_1Mg_6Ca_2)_{1000}Fe_{20.5}Mn_{1.68}Zn_{1.1}Cu_{0.5}Ni_{0.3}Co_{0.04}Cd_{0.002}$, while Fe-limited cells average $(C_{123}N_{30}P_1Mg_{11}Ca_{1.7})_{1000}Fe_{9.32}Mn_{2.7}Zn_{1.4}Cu_{0.6}Ni_{0.66}Co_{0.11}Cd_{0.0033}$.

4.4.1.1 MACRONUTRIENT CONCENTRATIONS

The increase in the C:P and N:P concentrations for our Fe-limited phytoplankton cells was unexpected. A prior study researching the effect of Fe-limitation on diatom elemental stoichiometry observed the opposite effect. This study shows a decline in C:P and N:P ratios. They attributed the decline in ratios to a 1.5X increase in cellular P content (Price 2005). This finding has implications for both present day and paleoceanography. For present day oceanography, this shows that Fe-limitation of diatom cells can alter assimilation rates of C, N, and P in areas where diatoms are prevalent. For

paleoceanography, this research has implications when interpreting Cd:P ratios. Within seawater, Cd and P exhibit similar distributions, which are controlled by phytoplankton biological uptake and remineralization (Boyle et al. 1976; de Baar et al. 1994). Since, cellular P concentrations influence cellular Cd concentrations, Cd deposits in ocean cores can be used as a proxy for biological P uptake. Therefore, this helps researchers better understand phytoplankton growth and ocean nutrient regimes during various times throughout geological history (Cullen et al. 1999; Lane et al. 2009).

However, in our research, we observe an increase in C:P and N:P ratios when picophytoplankton cells were grown in Fe-limited media. The increase in macronutrient ratios is driven by an average 1.5X decrease in cellular P concentration of our cells (Figure 4.1), with *Synechococcus* cellular P concentration reducing the most with a 2.1X decrease from nutrient-replete to Fe-limited media, followed by *Prochlorococcus* cells reducing 1.5X, and then *Ostreococcus* cells reducing the least with a 1.03X decrease. The opposing findings between our study and the Price (2005) study are driven by two main, interrelated factors that are important when determining and interpreting regional differences in phytoplankton macronutrient assimilation. First, the Price (2005) study used a different phytoplankton class than our study. The Price experiments were completed using a diatom species. This diatom species is faster growing and larger on average (15 μm compared to ~1 μm) than our picophytoplankton cells. It has previously been shown that nutrient-replete diatoms tend to exhibit lower N:P ratios than smaller, slow-growing phytoplankton (Mills and Arrigo 2010; Weber and Deutsch 2012). Second, diatoms tend to be more abundant in different habitats (coastal and polar compared to subtropical open ocean) than the picophytoplankton (Armbrust 1990; Lomas and Gilbert

2000). These habitats exhibit varying nutrient concentrations, which influence phytoplankton community composition. Together, this information shows that increase in cellular P concentration of Fe-limited diatoms in the Price (2005) study may not phytoplankton response observed for all phytoplankton, but may only be applicable to certain ocean regions. Our data shows that Fe-limited smaller species of phytoplankton, native to different habitats actually have reduced cellular P concentrations, potentially influencing local biogeochemical cycling in certain ocean regions differently than that of diatoms.

Interestingly, our results match results from other studies of elemental stoichiometry of P-limited picophytoplankton of cyanobacteria cells (Sañudo-Wilhelmy et al. 2001; Bertilsson et al. 2003; Ji and Sherrell 2008). These studies show that under P-limitation, phytoplankton cellular P concentrations decrease, causing N:P ratios to increase. The P-limited phytoplankton N:P ratios varied substantially based on species and ranged from an average of 21:1 for *Trichodesmium* (Sañudo-Wilhelmy et al. 2001) to 57:1 for picoeukaryotes (Ji and Sherrell 2008) to 109:1 for *Synechococcus* and *Prochlorococcus* cells (Bertilsson et al. 2003). Under P-limitation, it would be expected that cellular P concentrations would decrease in response to reduced amounts of dissolved P in the surrounding media. However, a decrease in cellular P concentration when only dissolved Fe concentrations are reduced and dissolved P concentrations remain unaltered is fascinating. Under Fe-limitation we observe increased N:P ratios ranging from 25:1 for *Ostreococcus* to 29:1 for *Prochlorococcus* to 32:1 for *Synechococcus* (Table 4.3). Coincidentally, we also observe a reduction in cellular growth rates by 42% for *Ostreococcus*, 24% for *Prochlorococcus*, and 38% for

Synechococcus (Table 4.1). These findings may suggest that for Fe-limited picophytoplankton, dissolved P uptake is not regulated by ambient P concentration, but instead by bulk cellular growth rate. The reduction in cellular P concentration leading to the increase in cellular N:P ratios under Fe-limitation indicate that phytoplankton metal-limitation and cellular metal concentration may be extremely important in interpreting particulate cellular and dissolved oceanic macronutrient concentrations.

Our particulate phytoplankton findings also match modeled data of dissolved N:P variations due to changes in oceanic Fe concentrations and denitrification (Weber and Deutsch 2012). The model predicts that with increasing ocean Fe-limitation and decreasing denitrification, subtropical ocean regions will exhibit larger dissolved N:P ratios than the common 16:1 Redfield ratio (Weber and Deutsch 2012). This modeling data matches data from our study where we observe an increase in particulate N:P ratios from an average of 18.5 in replete media to an average of 28.5 in Fe-limited media (Table 4.3). As described earlier, particulate and dissolved stoichiometric ratios are tightly correlated. Phytoplankton growth corresponds to the available concentrations of dissolved nutrients in the surrounding media. When phytoplankton die, the decomposition of the cells remineralize and the nutrients are redistributed back into the dissolved phase. Typically, in regions where high particulate N:P content is observed, competition among phytoplankton for dissolved N is high. This competition limits the amount of available N, causing phytoplankton growth limitation. Under this scenario, N_2 fixing cyanobacteria (diazotrophs) have a competitive advantage since they can fix their own N. This ability provides diazoptrophs with an abundant source of the needed macronutrient. However, diazotrophs do not grow well under all conditions. When

nutrients are abundant, for instance under bloom conditions, diazotrophs are usually growth-limited due to their requirement for large concentrations of Fe to fix N_2 and photosynthesize. Non-N_2-fixing phytoplankton can prosper under these conditions since their major Fe requirement is used solely for photosynthesis. However, under Fe-limitation, unlike N-limitation, diazotrophs lose their competitive growth advantage. It has been shown that under Fe-limitation, diazotrophs conserve Fe by selectively sacrificing N_2 fixation to ensure photosynthetic efficiency (Berman-Frank et al. 2001; Moore et al. 2002; Moore and Doney 2007; Shi et al. 2007). A reduction or termination of diazotroph N_2 fixation would cause effects throughout the phytoplankton community. Typically, it is assumed that diazotrophs are responsible for high N:P signals in particulate ocean samples (Sohm et al. 2011; Weber and Deutsch 2012). As described earlier, particulate stoichiometric ratios are tightly correlated with dissolved ratios. Since large portions of the global ocean, including vast areas of the Pacific Ocean and Southern Atlantic Ocean, are considered Fe-limited (Sohm et al. 2011), it may be possible that Fe-limited picophytoplankton, not diazotrophs, are driving the high N:P signals observed in the subtropical open oceans. Again, our data shows that cultured Fe-limited picophytoplankton have larger N:P ratios than picophytoplankton grown in replete conditions.

Most stoichiometric studies of picophytoplankton have directed their focus on cellular macronutrient concentrations. While macronutrients are very important to understanding global biogeochemical cycling, there have been few studies that have analyzed the trace metal and micronutrient extended elemental stoichiometry of picophytoplankton. These elemental stoichiometry studies have either focused on cells

grown in P-limitation or used equipment (SXRF) that can only measure metal:P ratios and do not directly measure C:N:P ratios (Bertilsson et al. 2003; Twining and Baines 2013). On the other hand, the studies that have examined extended elemental stoichiometry of picophytoplankton were performed using SXRF on field samples that could only determined metal elemental composition of phytoplankton in low-nutrient habitats (Twining et al. 2004, 2010; Twining and Baines 2013). Our study differs in that we are able to determine the entire elemental stoichiometry spectrum, including C and N, while comparing laboratory cultured phytoplankton grown in Fe-limited media to nutrient-replete media (Table 4.3).

4.4.1.2 Fe, Zn, Co, Cd CONCENTRATIONS

On average, the trace metal composition of cells grown in nutrient-replete media do not vary more than a factor of 4 from cells grown in Fe-limited media. The metal concentrations follow the order Fe>Mn>Zn>Cu>Ni>Co>Cd in nutrient-replete and Fe>Mn>Zn>Cu≈Ni>Co>Cd in Fe-limited cell cultures (Table 4.2). As stated earlier, we observe significant increases in cellular concentrations of Mn, Co, and Cd and a significant decrease in Fe when picophytoplankton are grown in Fe-limited compared to nutrient-replete media. Interestingly, there are also certain inter-species variations that we observe when the element:P quotas are plotted by species and culture media (Figure 4.2, Table 4.3). When individually comparing the prokaryotes (*Synechococcus* and *Prochlorococcus*) to the eukaryote (*Ostreococcus*) we observe higher concentrations of Fe in the prokaryotes compared to the eukaryote when grown in either nutrient-replete or Fe-limited media (Figure 4.2). This finding is similar to other culture studies that have shown that prokaryotes have higher cellular Fe concentrations and requirements than

eukaryotes (Brand 1991; Wilhelm et al. 1996; Twining and Baines 2013). It was observed that when cyanobacteria cells and eukaryotic phytoplankton were grown under the same conditions, cyanobacteria cells appeared to be Fe-limited, while the eukaryotic phytoplankton growth was not impaired (Brand 1991). Another study shows that unlike eukaryotic phytoplankton, certain strains of cyanobacteria can produce siderophores to assimilate previously unavailable Fe from the surrounding media (Wilhelm et al. 1996). Overall, it seems that a potential reason for the difference in Fe concentrations and requirements between prokaryotes and eukaryotes is due to the absence of carbon-rich structures in prokaryotes (Twining and Baines 2013).

In particular, our data shows that *Synechococcus* WH7803 cells seem to have an order of magnitude higher Fe concentration when grown in nutrient-replete media compared to Fe-deplete media (Figure 4.3). These results match recent data that shows luxury Fe uptake by cultured strains of *Synechococcus* (Mackey et al. 2015b). In this study, the authors compare Fe acquisition abilities of a coastal (WH8020) and oceanic (WH8102) *Synechococcus* strain and find that the coastal strain tends to be better adapted to Fe-limited conditions and is better able to maintain a more stable growth rate when compared to the oceanic strain. The authors attribute the growth rate stability in the coastal strain to the cells ability to alter Fe acquisition through changes in storage, photosynthetic proteins, and photophysiology. Conversely, the oceanic strain seems to have few acclimation responses to Fe-limitation, but is well suited to ocean areas with high dust input, leading to greater Fe acclimation capacity. Aeolian dust deposition is a major source of Fe for certain areas of the open ocean (Gao et al. 2001). Our results support the Mackey et al. (2015) findings in that our *Synechococcus* strain (WH7803) is

an oceanic strain (Carr and Mann 2004) and tends to acquire large amounts of Fe when increased dissolved Fe concentrations are available.

The observed increases in cellular P and Fe concentration should not be due to any excess cellular adsorbtion of P or Fe particles. The oxalate-EDTA wash was used to rinse the cells of any extracellular material prior to cell processing (Tovar-Sanchez et al. 2003). In fact, the phytoplankton (WH7803) that exhibited the greatest change in P and Fe concentration between medias also seems to exhibit a large change in cell size. Our flow cytometry measurements show a size difference between WH7803 cells grown in nutrient-replete and Fe-limited media, which is not apparent in measurements of our other cells. When WH7803 is grown on nutrient-replete media, we see larger on average cell size by forward scatter compared to Fe-limited media. This pattern is not observed in cultures of Fe-limited or nutrient-replete cultures of *Prochlorococcus* MED4 or *Ostreococcous lucimarinus* (Figure 4.4). This size difference could potentially account for the increased cellular P and Fe due to production of a larger cellular body leading to a larger cell surface area that facilitates increased nutrient uptake.

Finally, we also found lower cellular Zn concentrations among prokaryotes compared to the eukaryote when the strains are grown in nutrient-replete media (Figure 4.2). This finding is similar to other studies where prokaryotes contain lower cellular Zn concentrations than eukaryotes (Sunda and Huntsman 1995; Saito and Moffett 2002; Dupont et al. 2010). However, when the cells are stressed by Fe-limitation, we see an increase in cellular Zn concentrations in the prokaryotes, but a decrease in the eukaryote. Other studies have observed similar increases in Zn content when both eukaryotic and prokaryotic phytoplankton are grown in P-limitation (Ji and Sherrell 2008; Twining et al.

2010). It is possible that we observe a decrease in cellular Zn concentration in the Fe-limited eukaryote because Co and Cd can substitute for Zn when cells become stressed, which is supported by the observed significant increase in cellular Co and Cd concentrations when cells are Fe-limited or P-limited (Price and Morel 1990; Ji and Sherrell 2008).

4.4.1.3 Mn, Ni, Cu CONCENTRATIONS

The remaining metals in our study, Mn, Ni, and Cu are important metal cofactors in oxidative-stress relieving enzymes. When aerobic cells become stressed, destructive reactive oxygen species (ROS) are produced intra- and extracellularly (Asada et al. 1999; Apel and Hirt 2004). In phytoplankton, ROS is produced during photosynthesis and in order to prevent damage from ROS species, phytoplankton form superoxide dismutase (SODS). SODS are an enzyme that catalyze and destroy ROS to protect the cell (Wolfe-Simon et al. 2005). SODS come in four metalloforms and each isoform contains a different metal center cofactor, Fe, Mn, CuZn, or Ni. In our study the prokaryotes are both cyanobacteria, which have been shown to contain combinations of Fe, CuZn and NiSODS metalloforms, while the eukaryote is a prasinophyte, which contains CuZnSODS (Chadd et al. 1996; Eitinger 2004; Wolfe-Simon et al. 2005, 2006; Dupont et al. 2008; Kanematsu et al. 2010). Our data shows interspecies variations among the three SODS metalloforms. We observe decreases in Fe across all three species presumably due to the cells grown in Fe-limited media. Cu and Zn exhibit inverse relationships where the concentration of one will increase, while the other will decrease in Fe-limited media. Since the Cu and Zn are connected in their SODS metalloform, the production of the CuZnSODS should show a similar increase across both elements. Finally, we observe a

slight increase in Ni for *Prochlorococcus* MED4 potentially indicating the production of NiSODS (Figure 4.5). Overall, we do not observe many trends across all three species grown in Fe-limited media. However, we do observe a significant increase in Ni in *Prochlorococcus* MED4 that may indicate NiSODS are being formed in the MED4 cell in response to Fe stress.

4.4.2 ELEMENTAL STOICHIOMETRY DURING INFECTION

We are unaware of any other studies attempting to determine the elemental stoichiometry of infected phytoplankton cells. However, research has shown that viral infection can influence host cellular metabolism through regulation of host gene expression (Breitbart 2012; Zeng and Chisholm 2012). In this study, researchers found up-regulation of host phosphate-binding protein gene (*pstS*) and alkaline phosphatase gene (*phoA*) when viruses infected P starved cyanobacteria hosts compared to P-replete control hosts. This is the first finding to show regulation of genes by viral infection during host nutrient limitation. In addition, other studies have analyzed the elemental composition of viral particles and found that C per virus particle can range from 0.055-0.2 fg C depending on variability across virus particles (Wilhelm and Suttle 1999; Steward et al. 2007; Jover et al. 2014). Using that information, further exploration of virus stoichiometry also used virus genomic sequence information and stoichiometry of structural viral proteins to model virus C:N:P ratios (Jover et al. 2014). This study found that a stoichiometric mismatch exists between virus and host. Under this model, virus particles would exhibit an average C:N:P ratio of 17.2:5.9:1. They concluded that the cellular material released during lysis (material not bound to viruses) would be P-deplete relative to C and N, providing differential DOM cycling between host and virus through the viral shunt.

Overall, this shows that viral particles could be an important component to dissolved organic phosphorus (DOP) in surface seawaters.

It should be noted that there is a possibility that the trends we observe are not due to infected cellular uptake, but instead due to collection of cellular debris from viral lysis. Earlier, we mentioned that this scenario is one of the possible reasons for the variations are observed in phytoplankton elemental stoichiometry is due to the collection of dead cells and detrital material onto the filter (Martiny et al. 2013). Though, even if the trends we observe are due to cellular lysis, we are still observing a change in particulate (>0.2 μm) nutrient concentration. Studies have shown that viral lysate can produce nutrients that are more bioavailable than other nutrients in the surrounding media (Gobler et al. 1997; Poorvin et al. 2011). This change in nutrient bioavailability is also suggested to impact DOM cycling (Jover et al. 2014). On the other hand, we are not observing patterns of increasing concentration in all elements in the AV treatment. We are only observing increases in certain elements that can potentially be explained as a function of viral infection. One way to possibly ensure that P and Zn concentrations are actually increasing in the AV treatment would be to analyze the cells using SXRF. Unfortunately, that is outside the scope of our laboratory.

Overall, we find several significant changes in cell number and cellular nutrient concentrations of Fe-limited *Synechococcus* cells over the course of the sampling period between treatments containing either active virus (AV) or heat killed/filtered virus (HK) treatments. Prior to infection, the AV treatments had an average growth rate of 0.521 ± 0.011 d^{-1}, while the HK treatments had a similar growth rate of 0.515 ± 0.015 d^{-1}. Post-infection, we observe a sharp decline in cell number in the AV treatment just after the

T24 sampling (Figure 4.6). The P concentration (moles $cell^{-1}$) declined throughout the sampling in the HK treatment, but increased in the AV treatment. Furthermore, at T72, P concentration was over an order of magnitude higher in the AV treatment ($2.98x10^{-15}$ moles $cell^{-1}$) compared to the HK treatment ($1.06x10^{-16}$ moles $cell^{-1}$) (Figure 4.7). Since viruses can influence host cellular metabolism, as described above, it is not surprising that the average P concentration $cell^{-1}$ increases in the AV treatment due to the importance of P for viral reproduction within the hosts (Bratbak et al. 1993). It is possible that the virus is forcing the cell to use cellular machinery, perhaps an up-regulation in alkaline phosphatase production, to cleave inorganic P from organically bound P in the surrounding media for viral production (Zeng and Chisholm 2012). Also, Zn is the main cofactor in alkaline phosphatase and we observe a 7-fold and 3-fold increases in Zn:P ratios at T48 and T72, respectively, in the AV compared to the HK treatment. This enzyme also require Mg^{2+} and Ca^{2+}, which we also observe increasing in the AV treatment at T48 and T72 (Figure 4.8) (Shaked et al. 2006).

Changes also occur in other macronutrients and trace elements throughout sampling (Table 4.4). The macronutrients, C and N, display slight variation. At T0, we observe the ratio of N:P to be almost 1.5X higher in the AV treatment. Ideally, both treatments should have similar C:P and N:P ratios at T0. At T24 and T48 the C:P ratio is larger in the HK treatment possibly indicating early stages of cellular P-limitation due to increasing cell number and use of available P in the media. At T72, we once again see N:P ratio almost 1.5X higher in the AV treatment, similar to T0 which may be biological variation between cultures (Figure 4.9). The trace elements Mn and Cu also exhibit variation. Mn increases in the AV treatment from T0 to T72. This increase could be the

development of MnSODS as described earlier. Cu fluctuates throughout sampling and may also be biological variation. Finally, the trace elements Fe, Co, and Ni exhibit slight variation between AV and HK treatments, but produce no discernable pattern (Figure 4.10).

4.5 CONCLUSION

Our evaluation of bottom-up and top-down effects on picophytoplankton elemental stoichiometry can provide greater insight into marine biogeochemical cycles. It appears that Fe-limitation of picophytoplankton cells elicits a similar macronutrient uptake response to P-limitation without being grown in P-limited media. We observe a reduction in cellular P concentration, leading to an increase in C:P and N:P ratios. The reduction in cellular P uptake combined with low levels of Fe may alleviate some P-limited ocean regions. However, the top-down effect of viral infection could lead to greater nutrient limitation through infected cellular uptake of P and Zn causing slower phytoplankton growth, reducing C sequestration. This effect may not have long lasting impact on marine biogeochemistry, but this dichotomy of bottom-up and top-down effects on picophytoplankton extended elemental stoichiometry should be further evaluated.

Table 4.1. Average growth rates (day^{-1}) of picophytoplankton cells grown in nutrient-replete and Fe-limited media before harvest.

	Avg. nutrient-replete media growth rate (day^{-1})	Avg. Fe-limited media growth rate (day^{-1})
Synechococcus WH7803	0.72 ± 0.04	0.52 ± 0.03
Prochlorococcus MED4	0.98 ± 0.07	0.75 ± 0.03
Ostreococcus lucimarinus	0.76 ± 0.06	0.52 ± 0.05

Table 4.2. Comparison of the combined average elemental stoichiometry of nutrient-replete and Fe-limited cells. P-values in red indicate statistically significant difference between treatments.

	mols/cell P ± 1 S.E.										
	C	**N**	**Mg**	**Ca**	**Fe***	**Mn***	**Zn***	**Cu***	**Ni***	**Co***	**Cd***
Replete Avg	80 ± 5.2	18.5 ± 0.91	5.7 ± 0.77	1.96 ± 0.95	20.5 ± 4.2	1.68 ± 0.36	1.11 ± 0.26	0.49 ± 0.068	0.3 ± 0.12	0.04 ± 0.017	0.0016 ± 0.00026
Fe-limited Avg	123 ± 20	29 ± 1.9	11 ± 1.9	1.65 ± 0.48	9.32 ± 2.6	2.75 ± 0.82	1.42 ± 0.34	0.58 ± 0.13	0.66 ± 0.35	0.11 ± 0.037	0.0033 ± 0.00043
P-value	0.044	0.002	0.008	0.605	0.028^{T}	0.046^{T}	0.379	0.355	0.463	0.032	0.006

*mmols/cell P ± 1 S.E.

Table 4.3. Comparison of the average elemental stoichiometry for each species grown in nutrient-replete and Fe-limited cells.

	mols/cell P ± 1 S.E.										
	C	**N**	**Mg**	**Ca**	**Fe***	**Mn***	**Zn***	**Cu***	**Ni***	**Co***	**Cd***
Rep WH7803	65 ± 3.9	20 ± 1.2	3.4 ± 0.12	0.25 ± 0.011	78 ± 0.24	2.8 ± 0.028	1.4 ± 0.15	0.37 ± 0.019	0.61 ± 0.39	0.088 ± 0.023	0.0023 ± 0.0003
FeLim WH7803	73 ± 8.8	32 ± 4.4	6.4 ± 0.15	0.48 ± 0.046	17 ± 4.06	5.2 ± 0.15	2.4 ± 0.021	0.21 ± 0.018	0.31 ± 0.016	0.21 ± 0.044	0.0042 ± 0.00027
Rep MED4	89± 1.7	17 ± 0.17	7.4 ± 0.19	4.5 ± 2.1	26 ± 1.9	1 ± 0.41	0.3 ± 0.15	0.42 ± 0.17	0.2 ± 0.041	0.0059 ± 0.0027	0.0015 ± 0.00051
FeLim MED4	169 ± 17	29 ± 1.8	16 ± 7.6	2.9 ± 2.2	7 ± 5.3	1.2 ± 0.41	0.98 ± 0.72	0.62 ± 0.21	0.4 ± 0.16	0.014 ± 0.0079	0.0035 ± 0.0016
Rep O. luci	86 ± 8.9	18 ± 3.6	6.3 ± 0.69	1 ± 0.093	7.2 ± 0.38	1.2 ± 0.014	1.6 ± 0.079	0.67 ± 0.052	0.086 ± 0.0024	0.025 ± 0.0019	0.0011 ± 0.00019
FeLim O. luci	120 ± 19	25 ± 4.2	12 ± 5.1	1.8 ± 0.78	4.2 ± 0.1	1.7 ± 0.26	0.91 ± 0.11	0.94 ± 0.23	0.17 ± 0.11	0.11 ± 0.065	0.0024 ± 0.0013

*mmols/cell P ± 1 S.E.

Table 4.4. Time course comparison of the average elemental stoichiometry for Fe-limited *Synechococcus* WH7803 inoculated with active virus (AV) or heat killed media (HK).

	mols/cell P ± 1 S.E.									
	C	**N**	**Mg**	**Ca**	**Fe***	**Zn***	**Mn***	**Cu***	**Ni***	**Co***
T0 AV	79 ± 2.9	39 ± 4.4	19 ± 4.1	1.9 ± 0.42	8.7 ± 0.58	34 ± 4	1.5 ± 1.3	0.35 ± 0.13	0.11 ± 0.023	0.091 ± 0.01
T0 HK	71± 1.6	27 ± 1.1	14 ± 3	1.4 ± 0.35	8.3 ± 2	50 ± 3.7	3.3 ± 2.1	0.21 ± 0.062	0.1 ± 0.031	0.11 ± 0.043
T24 AV	75 ± 9	30 ± 11	14 ± 4.8	1.4 ± 0.53	9.6 ± 4	4 ± 0.36	2.5 ± 1	0.19 ± 0.071	0.13 ± 0.037	0.095 ± 0.054
T24 HK	102 ± 12	34 ± 6	12 ± 2	1.3 ± 0.46	7 ± 1.3	6 ± 0.77	1.9 ± 0.12	0.1 ± 0.023	0.1 ± 0.013	0.065 ± 0.004
T48 AV	85 ± 21	37 ± 10	17 ± 3.4	2.0 ± 0.90	7.5 ± 0.2	37 ± 4	3.1 ± 1.1	0.26 ± 0.21	0.15 ± 0.006	0.089 ± 0.02
T48 HK	113 ± 20	32 ± 7.5	8 ± 2	1.2 ± 0.57	6.9 ± 1.8	5.1 ± 0.44	1.5 ± 0.38	0.09 ± 0.035	0.11 ± 0.021	0.06 ± 0.011
T72 AV	149 ± 26	52 ± 14	25 ± 2	2.8 ± 0.84	7.4 ± 1.7	6.2 ± 0.24	3.7 ± 0.13	0.14 ± 0.021	0.13 ± 0.032	0.1 ± 0.016
T72 HK	137 ± 13	34 ± 2	5 ± 0.6	1.7 ± 0.54	8.2 ± 1.2	2.1 ± 0.032	1.3 ± 0.08	0.12 ± 0.005	0.19 ± 0.026	0.077 ± 0.001

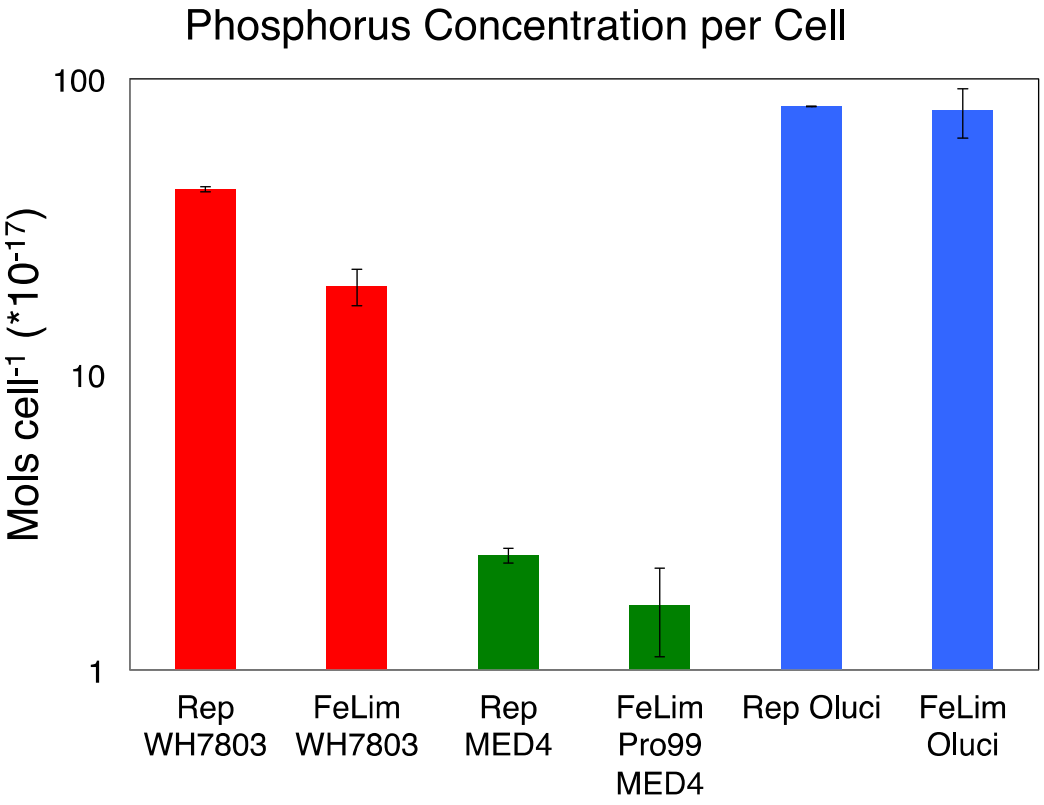

Figure 4.1. Average cellular P concentration per cell for *Synechococcus* WH7803 (red bars), *Prochlorococcus* MED4 (green bars), and *Ostreococcus lucimarinus* (blue bars) grown in either nutrient-replete (Rep) or Fe-limited (FeLim) media. Error bars represent 1 SE.

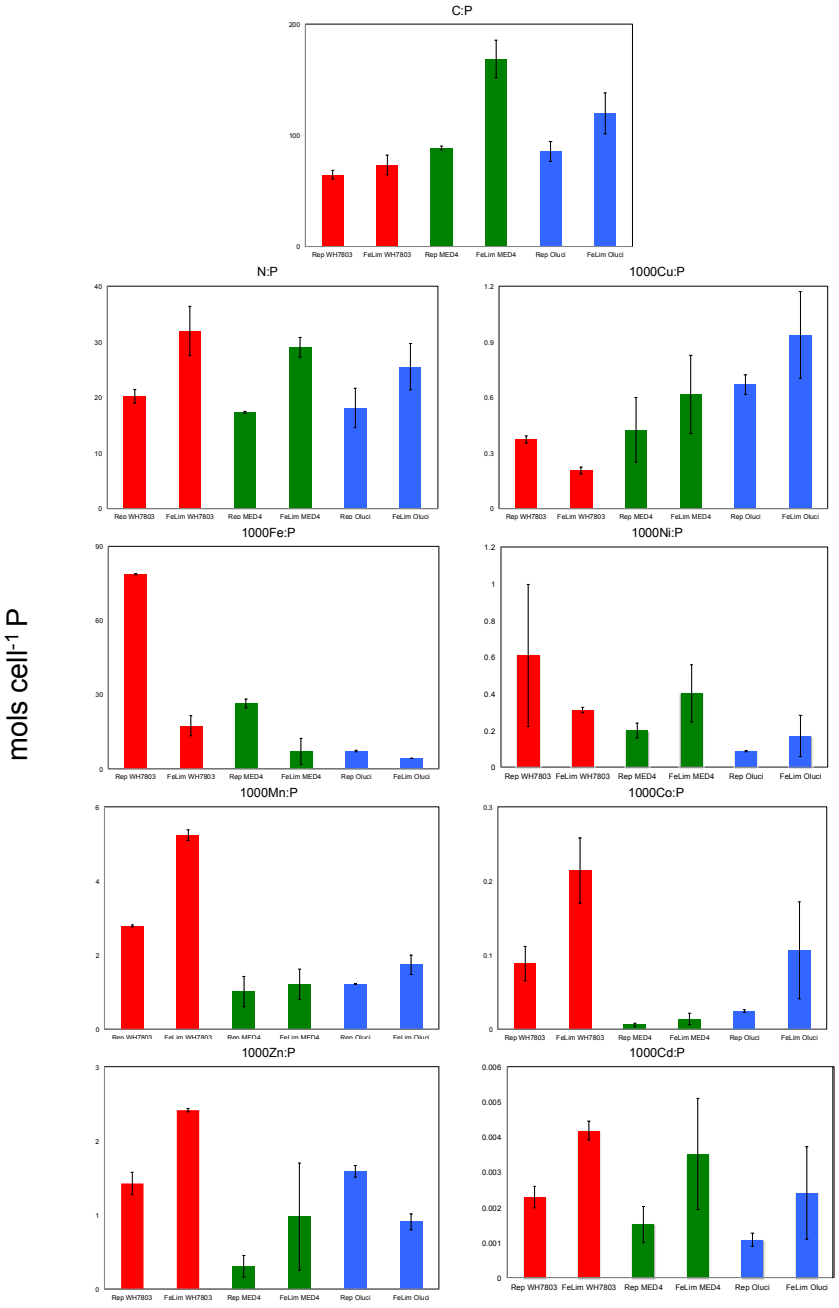

Figure 4.2. Comparison of average elemental quotas of *Synechococcus* WH7803 (red bars), *Prochlorococcus* MED4 (green bars), and *Ostreococcus lucimarinus* (blue bars) grown in either nutrient-replete (Rep) or Fe-limited (FeLim) media. All elements are normalized to P

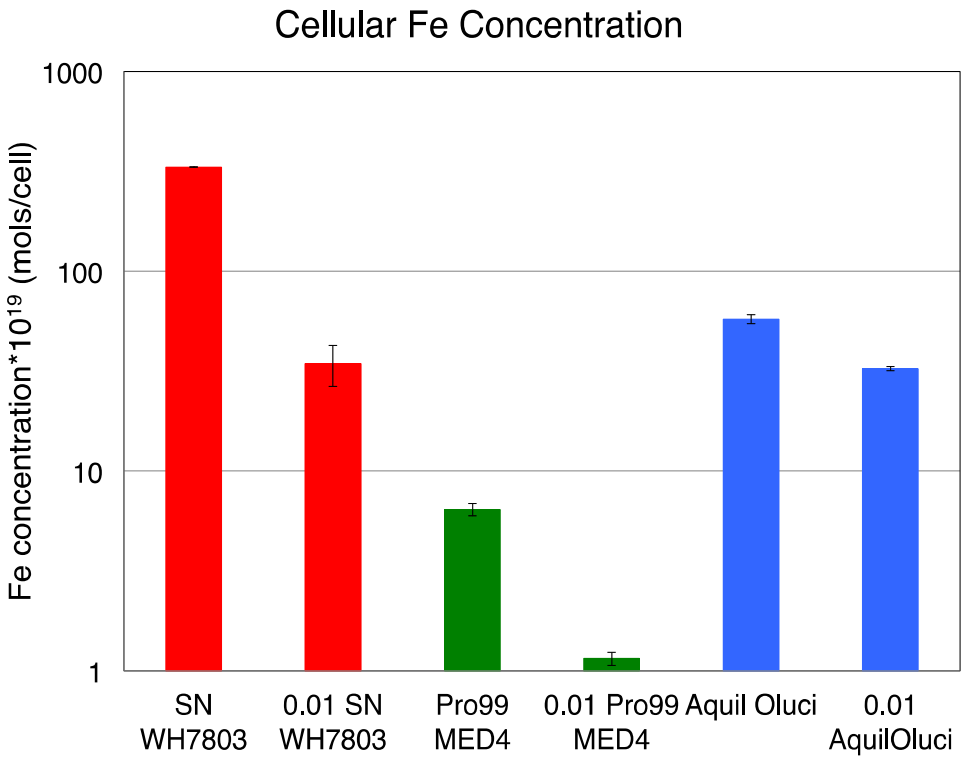

Figure 4.3. Average cellular Fe concentration per cell for *Synechococcus* WH7803 (red bars), *Prochlorococcus* MED4 (green bars), and *Ostreococcus lucimarinus* (blue bars) grown in either nutrient-replete (Rep) or Fe-limited (FeLim) media. Error bars represent 1 SE.

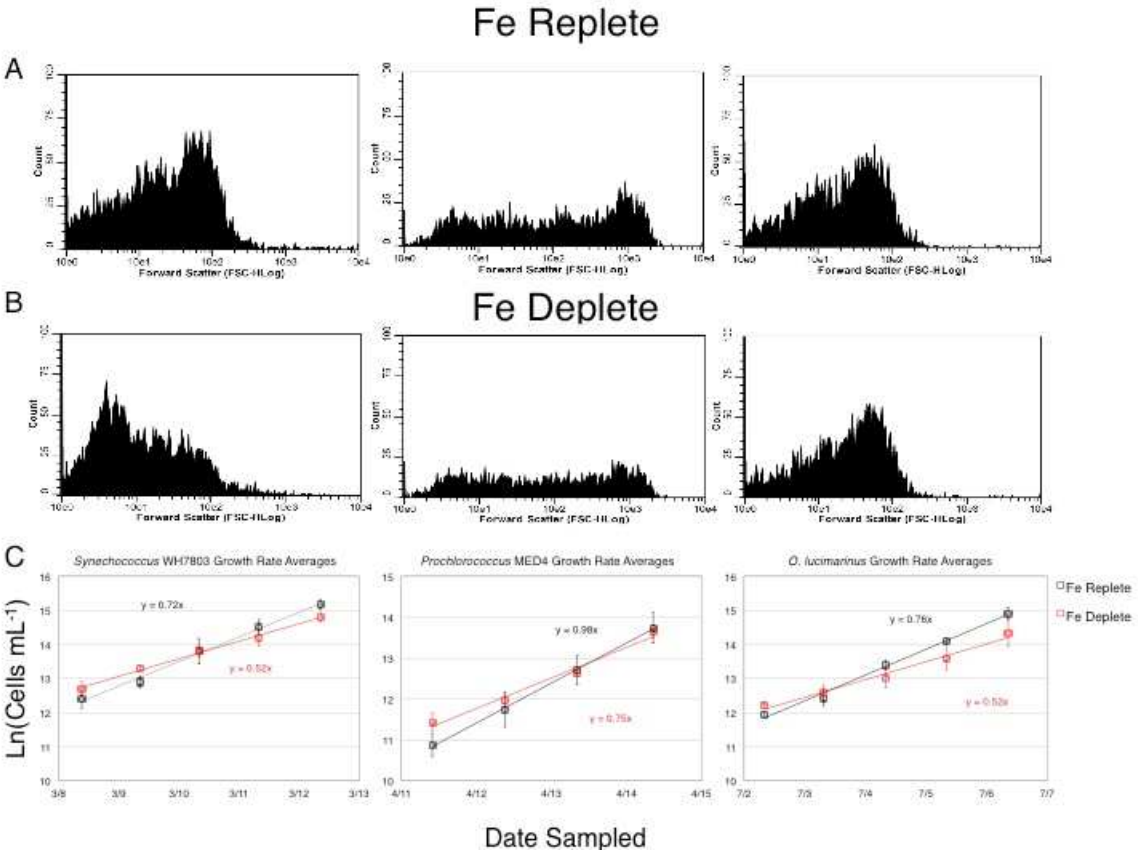

Figure 4.4. Comparison of flow cytometry data between *Synechococcus* WH7803, *Prochlorococcus* MED4, and *Ostreococcus lucimarinus* cells grown in nutrient-replete (A) and Fe-limited (B) media. Histograms in rows A and B plot forward scatter vs. total number of cells. The larger the forward scatter, the larger the cell. Graphs in row C compare growth rates over time for each species in either nutrient-replete (black squares) or Fe-limited (red squares) media.

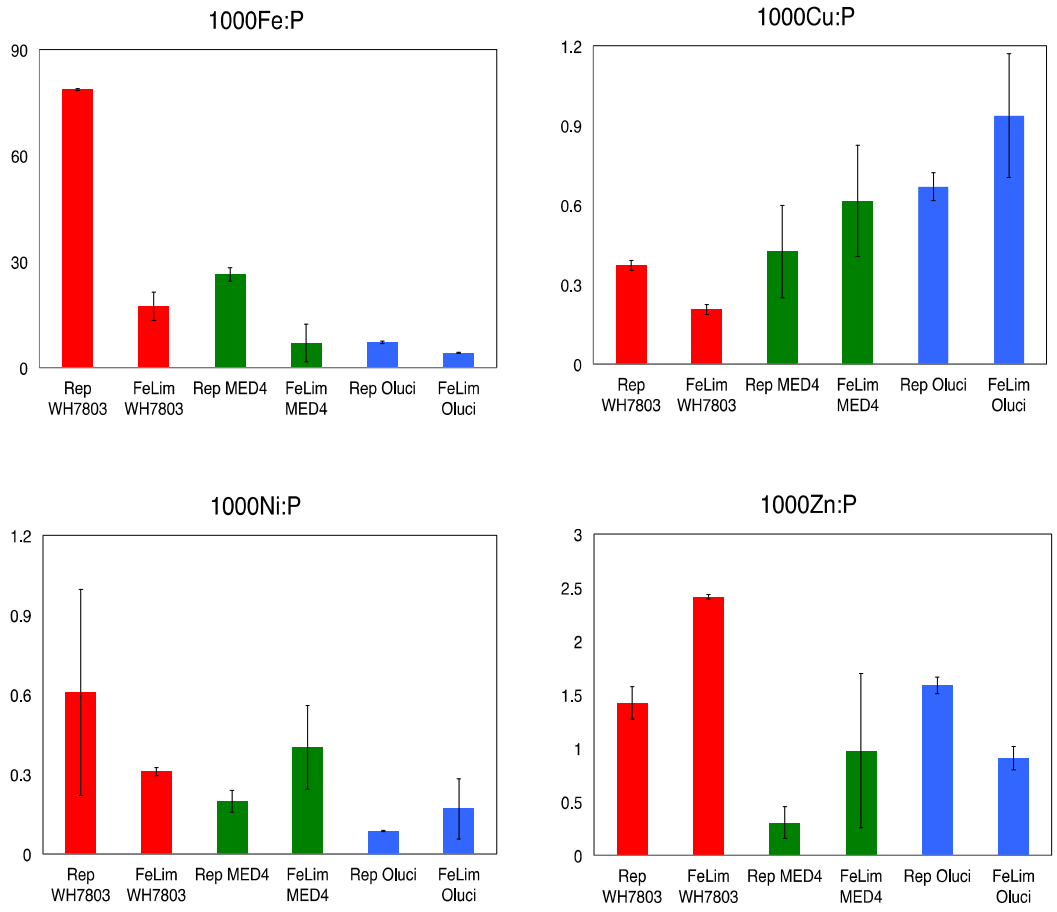

Figure 4.5. Comparison of average elemental quotas of metal cofactors in SODS for *Synechococcus* WH7803 (red bars), *Prochlorococcus* MED4 (green bars), and *Ostreococcus lucimarinus* (blue bars) grown in either nutrient-replete (Rep) or Fe-limited (FeLim) media. All elements are normalized to P (mol/mol or mmol/mol). Error bars represent 1 SE.

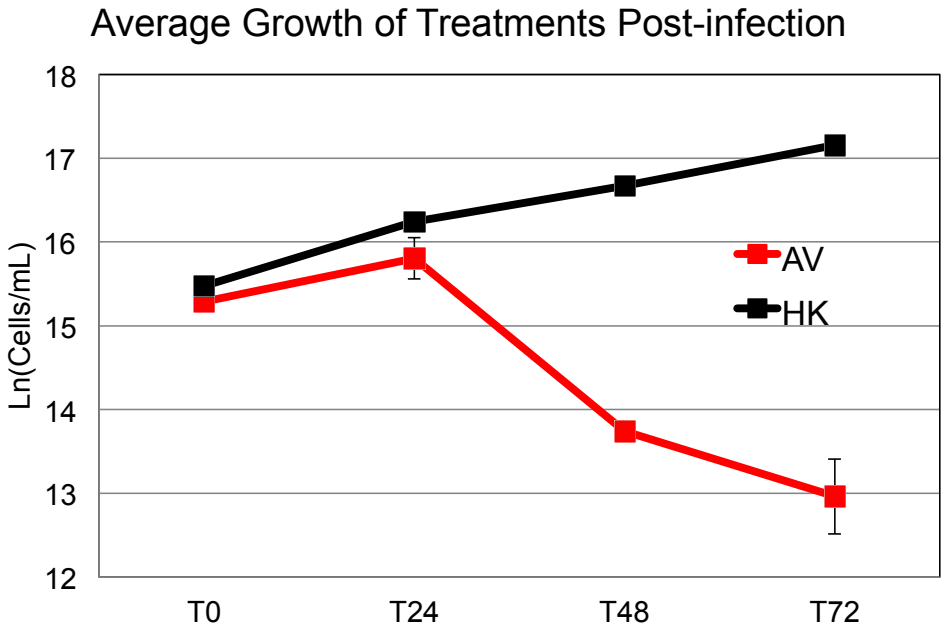

Figure 4.6. Average growth rate of *Synechococcus* WH7803 cells post-inoculation with active virus (AV, red squares) or heat-killed/filtered virus (HK, black squares). T0 indicates time of first inoculation. Error bars represent 1 SE.

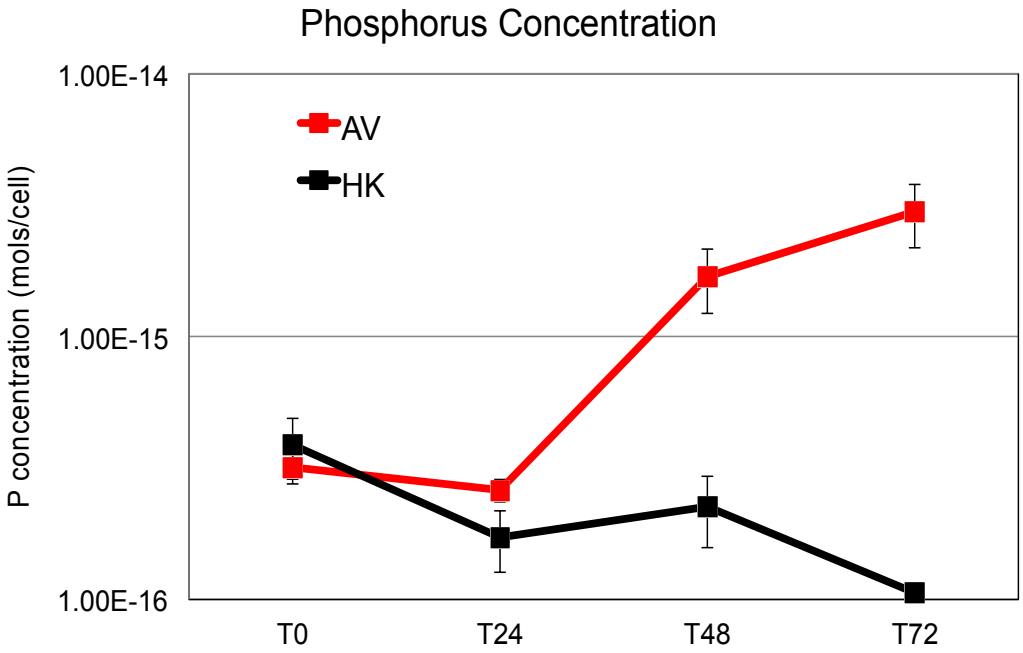

Figure 4.7. Changes in P cellular concentration in mols/cell of *Synechococcus* WH7803 cells post-inoculation with active virus (AV, red squares) or heat-killed/filtered virus (HK, black squares). T0 indicates time of first inoculation. Error bars represent 1 SE.

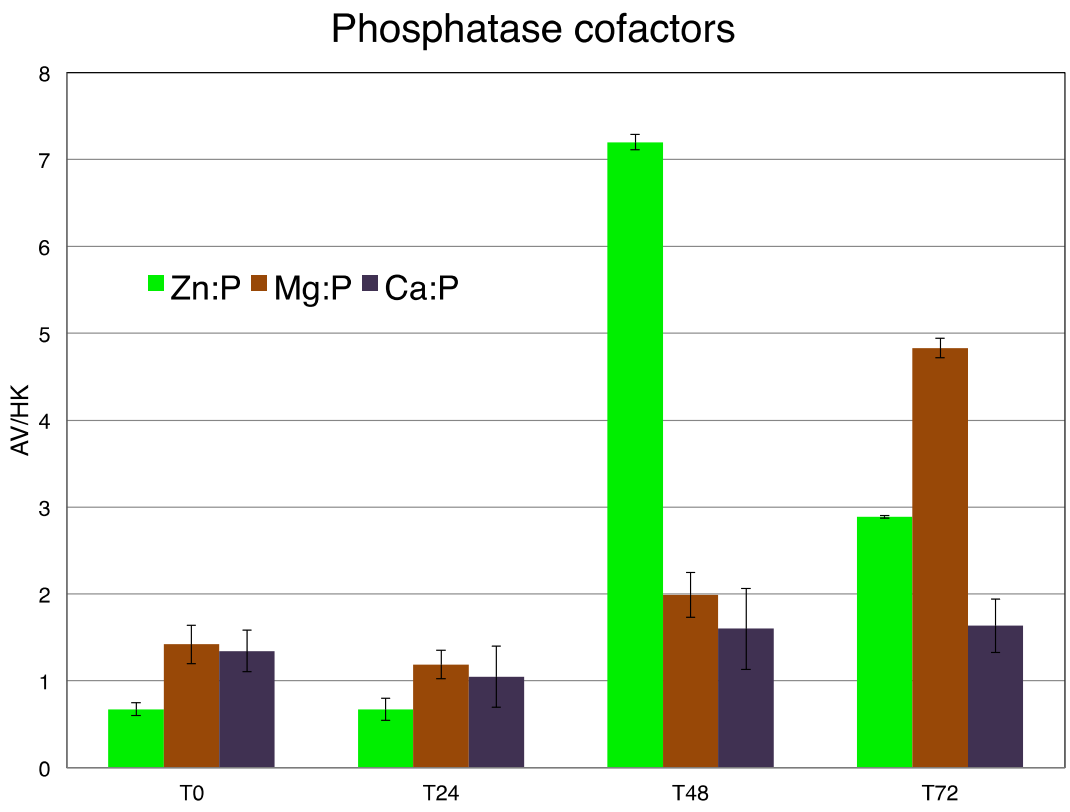

Figure 4.8. Changes in average elemental quotas of alkaline phosphatase cofactors zinc (green), magnesium (brown), and calcium (purple) in *Synechococcus* WH7803 cells over time post-inoculation. The vertical axis is shows active virus (AV) treatments divided by heat-killed/filtered virus (HK) treatment. Bars >1 indicate a higher elemental quota in the AV treatment. T0 indicates time of first inoculation. Error bars represent 1 SE.

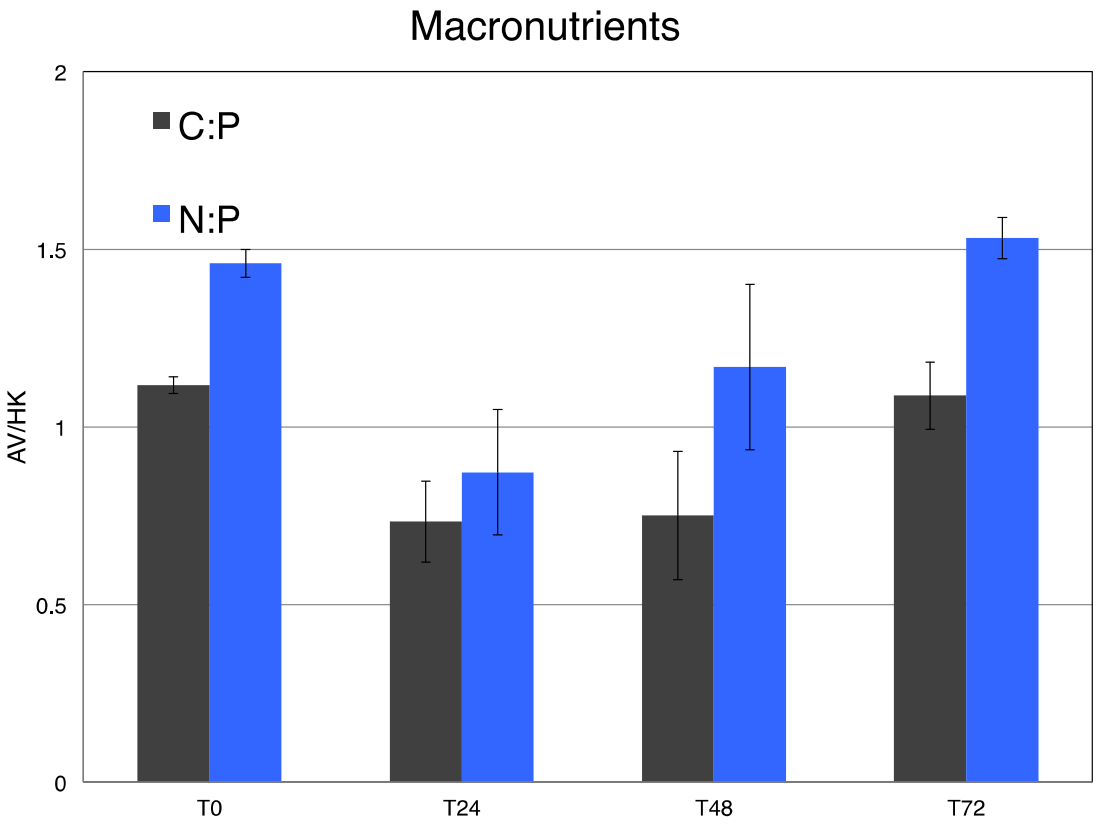

Figure 4.9. Changes in average elemental quotas of macronutrients, carbon (grey) and nitrogen (blue) in *Synechococcus* WH7803 cells over time post-inoculation. The vertical axis is shows active virus (AV) treatments divided by heat-killed/filtered virus (HK) treatment. Bars >1 indicate a higher elemental quota in the AV treatment. T0 indicates time of first inoculation. Error bars represent 1 SE.

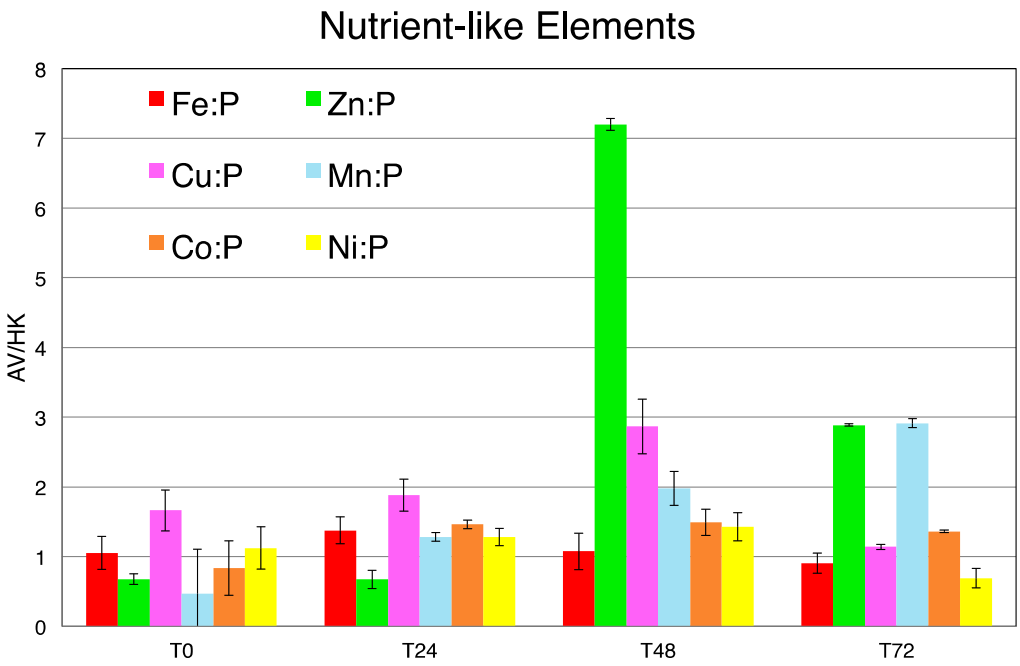

Figure 4.10. Changes in average elemental quotas of nutrient-like elements, iron (red), copper (pink), cobalt (orange), zinc (green), manganese (blue), and nickel (yellow) in *Synechococcus* WH7803 cells over time post-inoculation. The vertical axis is shows active virus (AV) treatments divided by heat-killed/filtered virus (HK) treatment. Bars >1 indicate a higher elemental quota in the AV treatment. T0 indicates time of first inoculation. Error bars represent 1 SE.

CHAPTER 5

CONCLUSIONS AND CLIMATE CHANGE

The goal of this dissertation is to explore the top-down and bottom-up effects of viral infection and trace metals on picophytoplankton growth. This work builds on previous physiological and chemical studies describing the effects of nutrient-limitation on phage growth kinetics and phytoplankton elemental stoichiometry. This final chapter provides a summary of the findings in this dissertation as well as an extrapolation of these findings to provide a more complete understanding of the potential effects of climate change on ocean nutrient cycles.

5.1 FE-LIMITATION DURING CLIMATE CHANGE

Throughout the upcoming century, we will observe increasing effects of anthropogenic induced climate change including decreasing oceanic pH, increasing sea surface temperature (SST), and changing global precipitation and wind patterns (Sarmiento et al. 1998; Boyd et al. 2010; Hoffmann et al. 2012). Satellite data has shown that low nutrient areas of the subtropical open oceans, typical habitat for picophytoplankton, are expanding at a rate of 0.8 to 4.3%/yr. The expansion is due to ocean warming causing increased vertical stratification, which decreases nutrient upwelling (Polovina et al. 2008). However, it should be noted that satellite time series of ~40 years are needed to distinguish global climate change from natural variability (Henson et al. 2010). Since these areas are expanding, it is important to understand how decreasing nutrient fluxes will influence future picophytoplankton growth and elemental stoichiometry. As stated

earlier, Fe is one of the most common growth-limiting nutrients. In fact, some studies show that the effects of reduced Fe bioavailability can potentially have a stronger influence on ocean biota than N- or P-limitation due to increased vertical stratification during climate change, preventing remineralized Fe from reaching the surface ocean (Sarmiento et al. 1998; Behrenfeld et al. 2006).

Currently, it is unclear how future climate change will influence biogeochemical cycling and Fe bioavailability for picophytoplankton species (Boyd and Ellwood 2010). A recent modeling study suggests that due to ocean stratification, macronutrients will become more limiting to phytoplankton growth actually alleviating Fe stress in some regions. The model suggests that in the North Atlantic Ocean and other high-latitude regions there will be a significant increase in surface Fe concentrations. This increase will be due to a steady input of Fe dust deposition combined with a reduced Fe requirement when phytoplankton are macronutrient growth limited (Boyd et al. 2015). However, the South Atlantic and the South Pacific Ocean will experience a decline in surface Fe leading to increased Fe stress (Yool et al. 2013). The combination of research from these studies seems to indicate that future Fe bioavailability may only influence certain areas of the ocean.

Within the South Atlantic and South Pacific Ocean, Fe bioavailability may not only be influenced by ocean stratification, but also by ocean acidification. Ocean acidification occurs as atmospheric carbon dioxide (CO_2) increases and more CO_2 is absorbed into the ocean. Increasing oceanic CO_2 leads to predictable changes in ocean chemistry causing a decrease in ocean pH and carbonate ion concentration [CO_3^{2-}]. The decreasing pH causes a change in Fe speciation and solubility. Under normal conditions

with seawater at pH 8, soluble Fe rapidly precipitates setting up a competition between adsorption to particulates in the water column, hydroxide ions, biological uptake, and organic ligand complexation (de Baar and de Jong 2001; Jickells et al. 2005). However, decreasing ocean pH decreases the concentration of hydroxide ions, which decreases Fe solubility and causes organic ligands to bind more Fe. Overall, these effects lead to a decrease in Fe-bioavailability for marine phytoplankton causing increased Fe stress and growth limitation in some ocean regions (Shi et al. 2010).

Since increasing ocean acidification and ocean stratification will lead to increased Fe-limitation in some ocean regions, we can then use the data presented in this manuscript to make an informed prediction on the impact of climate change on picophytoplankton cellular extended elemental stoichiometry and viral infection. As discussed earlier, the combination of these bottom-up and top-down trophic effects can have major influences on ocean biogeochemistry (Millero et al. 2005; Shi et al. 2010; Danovaro et al. 2010; Hoffmann et al. 2012). Our data show that Fe-limitation seems to affect picophytoplankton C and N concentrations in a manner similar to that of P-limitation. We observe slower growth rates and significant increases in C:P and N:P cellular quotas when growing cells in Fe-limited media. The higher C:P and N:P cellular quotas are due to a decreased cellular P concentration combined with a constant C and N concentration. The slower Fe-limited cellular growth rate combined with decreased uptake of P into the cells could increase extracellular P concentrations in P-limited ocean regions. These conditions could select for picoeukaryotic phytoplankton growth since they require less Fe than prokaryotes and have a larger genome, necessitating a greater

need for P during DNA replication (Brand 1991; Wilhelm et al. 1996; Palenik et al. 2007; Twining and Baines 2013; Zubkov 2014).

5.2 CLIMATE CHANGE AND VIRAL INFECTION OF FE-LIMITED CYANOBACTERIA

In our experiments, we observed a decreased growth rate in our Fe-limited *Synechococcus* host cultures, but no change in phage growth kinetics between nutrient-replete and Fe-limited hosts. Therefore, with a decreased host growth rate, it's possible we would observe a decreased uptake in carbon (C), but similar viral reproduction, possibly causing a faster cycling of the microbial loop. Interestingly, it has been shown that Fe produced from viral lysate is more bioavailable than Fe bound to bacterially-produced siderophores (Poorvin et al. 2011). This more bioavailable Fe may benefit uninfected cells in Fe-limited regions resulting in a negative feedback loop, but it has not been shown how ocean acidification will influence Fe bioavailability from viral lysate. On the other hand, a potential decrease in Fe bioavailability under conditions of increased ligand binding could cause a positive feedback loop increasing Fe-limitation for ocean surface microbiota during climate change.

Viral infection during Fe-limitation may not only affect Fe, but it may affect the availability of other nutrients as well. Ocean P concentration is extremely important to cellular growth and photosynthesis during viral infection and replication. Our results show that infected Fe-limited cyanobacteria cells contain much higher concentrations of P and Zn relative to Fe-limited uninfected cells over the course of infection. The combination of infection and a reduction in cellular growth rate would lead to slower C uptake, reducing C sequestration, but a potential for increased cellular P and Zn uptake.

The increased uptake of P and Zn could further nutrient-limit a region that already causes slow phytoplankton growth. The combination of all these factors would cause a further reduction in C sequestration leading to a positive feed back cycle where phytoplankton cells lack sufficient nutrients to grow. Overall, the reduction in C uptake and sequestration would decrease the removal of carbon from the atmosphere, leading to increased warming from the green house effect.

5.3 CLIMATE CHANGE AND EXTENDED ELEMENTAL STOICHIOMETRY OF FE-LIMITED PICOPHYTOPLANKTON

Due to the abundance of picophytoplankton in the subtropical open oceans, their photosynthesis and growth are extremely important to C sequestration and biogeochemical cycling. Our data show that Fe-limitation seems to affect phytoplankton C and N concentrations similar of that of P-limitation. We observe slower growth rates and significant increases in C:P and N:P cellular quotas when growing cells in Fe-limited media. The higher C and N cellular quotas are due to a decreased cellular P concentration with a constant C and N concentration. The slower Fe-limited cellular growth rate combined with decreased uptake of P into the cells could increase P concentrations in ocean regions. These conditions would select for picoeukaryotic phytoplankton growth since they require less Fe than prokaryotes and have a larger genome, necessitating a greater need for P during DNA replication (Brand 1991; Wilhelm et al. 1996; Palenik et al. 2007; Twining and Baines 2013; Zubkov 2014).

Another potential, but major, effect of increased Fe-limitation is the reduced role of diazotrophs fixing N_2 and increased regional N-limitation. Under macronutrient limitation, diazotrophs tend to have a competitive growth advantage over other

phytoplankton species due to their ability to fix their own N (Weber and Deutsch 2012). However, that advantage comes at a cost. Diazotrophs have higher Fe requirements than other phytoplankton in order to sustain photosynthesis and N_2 fixation. Under Fe-limitation, diazotrophs can conserve Fe by selectively sacrificing N_2 fixation to ensure photosynthetic efficiency (Berman-Frank et al. 2001; Moore et al. 2002; Moore and Doney 2007; Shi et al. 2007). If subtropical open ocean regions become increasingly Fe-limited due to ocean acidification, we may see a reduction in diazotroph N_2 fixation. This reduction accompanied by the high N:P cellular quotas of Fe-limited picophytoplankton could cause more wide-spread N-limitation, further reducing cellular growth and photosynthesis of picophytoplankton. This reduction may ultimately influence the C cycle as growth-limited phytoplankton take up less C, reducing C sequestration. This could potentially lead to increasing atmospheric C, causing a positive feedback loop further exacerbating climate change.

5.4 FUTURE DIRECTIONS

This chapter describes some of the possible ramifications of climate change in relation to the data presented. The changes in macronutrient concentrations of Fe-limited picophytoplankton cells raise interesting questions. What happens when cyanobacteria and picoeukaryotes are grown in co-culture under Fe-limitation? As described earlier, it is possible that the picoeukaroytes have an advantage due to their smaller requirement for Fe. However, does infection of cyanobacteria reduce available P and Zn for the picoeukaryote? This could potentially create a dynamic where the picoeukaryote is still unable to compete with the cyanobacteria. Finally, what happens when diazotrophs are co-cultured with cyanobacteria in Fe-limited media? Earlier, I suggest that under Fe-

limitation, the diazotroph will reduce or cease N_2 fixation due to the large Fe needs, causing N-limitation within culture. Before we are able to fully understand how aspects of climate change influence picophytoplankton extended elemental stoichiometry, it is necessary to understand the greater ecological interactions between cells and viruses.

REFERENCES

Anderson, L. A., and J. L. Sarmiento. 1994. Redfield ratios of remineralization determined by nutrient data analysis. Global Biogeochem. Cycles **8**: 65–80.

Apel, K., and H. Hirt. 2004. Reactive oxygen species: metabolism, oxidative stress, and signal transduction. Annu. Rev. Plant Biol. **55**: 373–399.

Armbrust, E. V. 1990. The Life Cycle of the Centric Diatom Thalassiosira weissflogii: Control of Gametogenesis and Cell Size. Massachusetts Institute of Technology.

Arrigo, K. R. 1999. Phytoplankton Community Structure and the Drawdown of Nutrients and CO2 in the Southern Ocean. Science (80-.). **283**: 365–367.

Asada, S., K. Fukuda, M. Oh, C. Hamanishi, and S. Tanaka. 1999. Effect of hydrogen peroxide on the metabolism of articular chondrocytes. Inflamm. Res. **48**: 399–403.

Azam, F. 1998. Microbial Control of Oceanic Carbon Flux: The Plot Thickens. Science (80-.). **280**: 694–696.

Azam, F., T. Fenchel, J. G. Field, J. S. Gray, L. A. Meyer-Reil, and F. Thingstad. 1983. The Ecological Role of Water-Column Microbes in the Sea. Mar. Ecol. Prog. Ser. **10**: 257–263.

de Baar, H. J. W., and J. T. M. de Jong. 2001. Distributions, sources and sinks of iron in seawater, p. 123–253. *In* The Biogeochemistry of Iron in Seawater. IUPAC Series on Analytical and Physical Chemistry of Environmental Systems.

de Baar, H. J. W., P. M. Saager, R. F. Nolting, and J. van der Meer. 1994. Cadmium versus phosphate in the world ocean. Mar. Chem. **46**: 261–281.

Behrenfeld, M., R. O'Malley, D. Siegel, C. McClain, J. Sarmiento, G. Feldman, A. Milligan, P. Falkowski, R. Letelier, and E. Boss. 2006. Climate-driven trends in contemporary ocean productivity. Nature **444**: 752–755.

Bergh, O., K. Borsheim, G. Bratbak, and M. Heldal. 1989. High abundance of viruses found in aquatic environments. Nature **340**: 467–468.

Berman-Frank, I., J. T. Cullen, Y. Shaked, R. M. Sherrell, and P. G. Falkowski. 2001.

Iron availability, cellular iron quotas, and nitrogen fixation in Trichodesmium. Limnol. Oceanogr. **46**: 1249–1260.

Bertilsson, S., O. Berglund, D. M. Karl, and S. W. Chisholm. 2003. Elemental composition of marine Prochlorococcus and Synechococcus: Implications for the ecological stoichiometry of the sea. Limnol. Oceanogr. **48**: 1721–1731.

Bettarel, Y., T. Sime-Ngando, C. Amblard, and H. Laveran. 2000. A comparison of methods for counting viruses in aquatic systems. Appl. Environ. Microbiol. **66**: 2283–2289.

Bouvy, M., Y. Bettarel, C. Bouvier, I. Domaizon, S. Jacquet, E. Le Floc'h, H. Montanié, B. Mostajir, T. Sime-Ngando, J. P. Torréton, F. Vidussi, and T. Bouvier. 2011. Trophic interactions between viruses, bacteria and nanoflagellates under various nutrient conditions and simulated climate change. Environ. Microbiol. **13**: 1842–57.

Bouvy, M., M. Troussellier, P. Got, and R. Arfi. 2004. Bacterioplankton responses to bottom-up and top-down controls in a West African reservoir (Sélingué, Mali). Aquat. Microb. Ecol. **35**: 301–307.

Boyd, P. W., and M. J. Ellwood. 2010. The biogeochemical cycle of iron in the ocean. Nat. Geosci. **3**: 675–682.

Boyd, P. W., T. Jickells, C. S. Law, S. Blain, E. A. Boyle, K. O. Buesseler, K. H. Coale, J. J. Cullen, H. J. W. de Baar, M. Follows, M. Harvey, C. Lancelot, M. Levasseur, N. P. J. Owens, R. Pollard, R. B. Rivkin, J. Sarmiento, V. Schoemann, V. Smetacek, S. Takeda, A. Tsuda, S. Turner, and A. J. Watson. 2007. Mesoscale iron enrichment experiments 1993-2005: synthesis and future directions. Science **315**: 612–7.

Boyd, P. W., S. T. Lennartz, D. M. Glover, and S. C. Doney. 2015. Biological ramifications of climate-change-mediated oceanic multi-stressors. Nat. Clim. Chang. **5**: 71–79.

Boyd, P. W., R. Strzepek, F. Fu, and D. a. Hutchins. 2010. Environmental control of open-ocean phytoplankton groups: Now and in the future. Limnol. Oceanogr. **55**: 1353–1376.

Boyd, P. W., A. J. Watson, C. S. Law, E. R. Abraham, T. Trull, R. Murdoch, D. C. Bakker, A. R. Bowie, K. O. Buesseler, H. Chang, M. Charette, P. Croot, K. Downing, R. Frew, M. Gall, M. Hadfield, J. Hall, M. Harvey, G. Jameson, J. LaRoche, M. Liddicoat, R. Ling, M. T. Maldonado, R. M. McKay, S. Nodder, S. Pickmere, R. Pridmore, S. Rintoul, K. Safi, P. Sutton, R. Strzepek, K. Tanneberger, S. Turner, A. Waite, and J. Zeldis. 2000. A mesoscale phytoplankton bloom in the polar Southern Ocean stimulated by iron fertilization. Nature **407**: 695–702.

Boyle, E., F. Sclater, and J. Edmond. 1976. On the marine geochemistry of cadmium. Nature **263**: 42–44.

Brand, L. E. 1991. Minimum iron requirements of marine plhytoplankton and the implications for the biogeochemical control of new production. Limnol. Oceanogr. **36**: 1756–1771.

Bratbak, G., J. Egge, and M. Heldal. 1993. Viral mortality of the marine alga Emiliania huxleyi (Haptophyceae) and termination of algal blooms. Mar. Ecol. Prog. Ser. **93**: 39–48.

Bratbak, G., A. Jacobsen, M. Heldal, K. Nagasaki, and F. Thingstad. 1998. Virus production in Phaeocystis pouchetii and its relation to host cell growth and nutrition. Aquat. Microb. **16**: 1–9.

Breitbart, M. 2012. Marine Viruses: Truth or Dare. Ann. Rev. Mar. Sci. **4**: 425–448.

Broecker, W. S. 1982. Ocean chemistry during glacial time. Geochim. Cosmochim. Acta **47**: 1539–1540.

Brown, C. M., J. E. Lawrence, and D. A. Campbell. 2006. Are phytoplankton population density maxima predictable through analysis of host and viral genomic DNA content? J. Mar. Biol. Assoc. UK **86**: 491.

Brum, J. R., R. O. Schenck, and M. B. Sullivan. 2013. Global morphological analysis of marine viruses shows minimal regional variation and dominance of non-tailed viruses. ISME J. **7**: 1738–1751.

Brussaard, C., J. Payet, C. Winter, and M. Weinbauer. 2010. Quantification of aquatic viruses by flow cytometry, p. 102–109. *In* S.W. Wilhelm, M.G. Weinbauer, and C.A. Suttle [eds.], Manual of Aquatic Viral Ecology. ASLO.

Carr, N. G., and N. H. Mann. 2004. The Oceanic Cyanobacterial Picoplankton, p. 27–48. *In* The Molecular Biology of Cyanobacteria.

Chadd, H. E., I. R. Joint, N. H. Mann, and N. G. Carr. 1996. The marine picoplankter Synechococcus sp. WH 7803 exhibits an adaptive response to restricted iron availability. FEMS Microbiol. Ecol. **21**: 69–76.

Chisholm, S. W. 1992. Phytoplankton Size, p. 213–237. *In* Primary Productivity and Biogeochemical Cycles in the Sea.

Chisholm, S. W., and F. M. M. Morel. 1991. What controls phytoplankton production in nutrient-rich areas of the open sea? Limonology Oceanogr. **36**: U1507–U1511.

Coale, K., K. Johnson, S. Fitzwater, R. Gordon, S. Tanner, F. Chavez, L. Ferioli, C.

Sakamoto, P. Rogers, F. Millero, P. Steinberg, P. Nightingale, D. Cooper, W. Cochlan, M. Landry, J. Constantinou, G. Rollwagen, A. Trasvina, and R. Kudela. 1996. A massive phytoplankton bloom induced by an ecosystem-scale iron fertilization experiment in the equatorial Pacific Ocean. Nature **383**: 495–501.

Cochran, W. G. 1950. Estimation of bacterial densities by means of the "most probable number". Biometrics **6**: 105–116.

Codispoti, L. A. 1989. Phosphorus vs Nitrogen limitation of new and export production., p. 377–394. *In* Productivity of the oceans: Present and past.

Cohen, S. S. 1948. THE SYNTHESIS OF BACTERIAL VIRUSES II. THE ORIGIN OF PHOSPHORUS FOUND IN DESOXYRIBONUCLEIC ACIDS OF THE T2 AND T4 BACTERIOPHAGES. J. Biol. Chem. **174**: 295–303.

Cullen, J., T. Lane, F. Morel, and R. Sherrell. 1999. Modulation of cadmium uptake in phytoplankton by seawater CO2 concentration. Nature **402**: 165–167.

Cunningham, B. R., J. R. Brum, S. M. Schwenck, M. B. Sullivan, and S. G. John. 2015. An inexpensive, accurate and precise wet-mount method for enumerating aquatic viruses. Appl. Environ. Microbiol. **81**: 2995–3000.

Danovaro, R., C. Corinaldesi, A. Dell'anno, J. A. Fuhrman, J. J. Middelburg, R. T. Noble, and C. A. Suttle. 2010. Marine viruses and global climate change. FEMS Microbiol. Rev. **35**: 993–1034.

Deng, L., A. Gregory, S. Yilmaz, B. Poulos, P. Hugenholtz, and M. B. Sullivan. 2013. Contrasting Life Strategies of Viruses that Infect Photo-and Heterotrophic Bacteria, as Revealed by Viral Tagging. MBio **3**: 1–8.

Dupont, C. L., A. Butcher, R. E. Valas, P. E. Bourne, and G. Caetano-Anollés. 2010. History of biological metal utilization inferred through phylogenomic analysis of protein structures. Proc. Natl. Acad. Sci. U. S. A. **107**: 10567–10572.

Dupont, C. L., K. Neupane, J. Shearer, and B. Palenik. 2008. Diversity, function and evolution of genes coding for putative Ni-containing superoxide dismutases. Environ. Microbiol. **10**: 1831–1843.

Eitinger, T. 2004. In vivo production of active nickel superoxide dismutase from Prochlorococcus marinus MIT9313 is dependent on its cognate peptidase. J. Bacteriol. **186**: 7821–7825.

Elser, J. J., K. Acharya, M. Kyle, J. Cotner, W. Makino, T. Markow, T. Watts, S. Hobbie, W. Fagan, J. Schade, J. Hood, and R. W. Sterner. 2003. Growth rate-stoichiometry couplings in diverse biota. Ecol. Lett. **6**: 936–943.

Falkowski, P. G., R. Barber, and V. Smetacek. 1998. Biogeochemical Controls and Feedbacks on Ocean Primary Production. Science (80-.). **281**: 200–206.

Field, C. B., M. J. Behrenfeld, J. T. Randerson, and P. Falkowski. 1998. Primary Production of the Biosphere: Integrating Terrestrial and Oceanic Components. Science (80-.). **281**: 237–240.

Fuhrman, J. A. 1999. Marine viruses and their biogeochemical and ecological effects. Nature **399**: 541–8.

Fulda, S., F. Huang, F. Nilsson, M. Hagemann, and B. Norling. 2000. Proteomics of Synechocysits sp. strain PCC 6803. Eur. J. Biochem. **267**: 5900–5907.

Gao, Y., Y. J. Kaufman, D. Tanré, D. Kolber, and P. G. Falkowski. 2001. Seasonal distributions of Aeolian iron fluxes to the global ocean. Geophys. Res. Lett. **28**: 29–32.

Geider, R., and J. La Roche. 2002. Redfield revisited: variability of C:N:P in marine microalgae and its biochemical basis. Eur. J. Phycol. **37**: 1–17.

Gledhill, M., A. Devez, A. Highfield, C. Singleton, E. P. Achterberg, and D. Schroeder. 2012. Effect of Metals on the Lytic Cycle of the Coccolithovirus, EhV86. Front. Microbiol. **3**: 155.

Gobler, C. J., D. a. Hutchins, N. S. Fisher, E. M. Cosper, and S. Saøudo-Wilhelmy. 1997. Release and bioavailability of C, N, P Se, and Fe following viral lysis of a marine chrysophyte. Limnol. Oceanogr. **42**: 1492–1504.

Hecky, R., and P. Kilham. 1988. Nutrient limitation of phytoplankton in freshwater and marine environments : A review of recent evidence on the effects of enrichment. Limnol. Oceanogr. **33**: 796–822.

Hennes, K. P., and C. A. Suttle. 1995. Direct counts of viruses in natural waters and laboratory cultures by epifluorescence microscopy. Limnol. Oceanogr. **40**: 1050–1055.

Henson, S. A., J. L. Sarmiento, J. P. Dunne, L. Bopp, I. Lima, S. C. Doney, J. John, and C. Beaulieu. 2010. Detection of anthropogenic climate change in satellite records of ocean chlorophyll and productivity. Biogeosciences 621–640.

Ho, T., A. Quigg, Z. Finkel, A. Milligan, K. Wyman, P. Falkowski, and F. Morel. 2003. The elemental composition of some marine phytoplankton. J. Phycol. **1159**: 1145–1159.

Hoffmann, L., E. Breitbarth, P. Boyd, and K. Hunter. 2012. Influence of ocean warming and acidification on trace metal biogeochemistry. Mar. Ecol. Prog. Ser. **470**: 191–

205.

Hoffmann, L. J., I. Peeken, and K. Lochte. 2007. Effects of iron on the elemental stoichiometry during EIFEX and in the diatoms Fragilariopsis kerguelensis and Chaetoceros dichaeta. Biogeosciences **4**: 569–579.

Holmfeldt, K., D. Odić, M. B. Sullivan, M. Middelboe, and L. Riemann. 2012. Cultivated single-stranded DNA phages that infect marine Bacteroidetes prove difficult to detect with DNA-binding stains. Appl. Environ. Microbiol. **78**: 892–894.

Hutchins, D., A. Witter, A. Butler, and G. Luther III. 1999. Competition among marine phytoplankton for different chelated iron species. Nature **400**: 858–61.

Ji, Y., and R. M. Sherrell. 2008. Differential effects of phosphorus limitation on cellular metals in Chlorella and Microcystis. Limnol. Oceanogr. **53**: 1790–1804.

Jickells, T. D., Z. S. An, K. K. Andersen, A. R. Baker, G. Bergametti, N. Brooks, J. J. Cao, P. W. Boyd, R. A. Duce, K. A. Hunter, H. Kawahata, N. Kubilay, J. LaRoche, P. S. Liss, N. Mahowald, J. M. Prospero, A. J. Ridgwell, I. Tegen, and R. Torres. 2005. Global iron connections between desert dust, ocean biogeochemistry, and climate. Science **308**: 67–71.

John, S. G., and J. F. Adkins. 2010. Analysis of dissolved iron isotopes in seawater. Mar. Chem. **119**: 65–76.

John, S. G., C. B. Mendez, L. Deng, B. Poulos, A. K. M. Kauffman, S. Kern, J. Brum, M. F. Polz, E. A. Boyle, and M. B. Sullivan. 2011. A simple and efficient method for concentration of ocean viruses by chemical flocculation. Environ. Microbiol. Rep. **3**: 195–202.

Johnson, Z. I., E. R. Zinser, A. Coe, N. P. McNulty, E. M. S. Woodward, and S. W. Chisholm. 2006. Niche partitioning among Prochlorococcus ecotypes along ocean-scale environmental gradients. Science (80-.). **311**: 1737–1740.

Jover, L. F., T. C. Effler, A. Buchan, S. W. Wilhelm, and J. S. Weitz. 2014. The elemental composition of virus particles: implications for marine biogeochemical cycles. Nat. Rev. Microbiol. **12**: 519–28.

Kanematsu, S., N. Iriguchi, and A. Ienaga. 2010. Characterization of CuZn-superoxide dismutase gene from the green alga Spirogyra sp . (Streptophyta): Evolutionary implications for the origin of the chloroplastic and cytosolic isoforms. Bull. Minamikyushu Univ. **40A**: 65–77.

Karsenti, E., S. G. Acinas, P. Bork, C. Bowler, C. De Vargas, J. Raes, M. B. Sullivan, D. Arendt, F. Benzoni, J.-M. Claverie, M. Follows, G. Gorsky, P. Hingamp, D.

Iudicone, O. Jaillon, S. Kandels-Lewis, U. Krzic, F. Not, H. Ogata, S. Pesant, E. G. Reynaud, C. Sardet, M. E. Sieracki, S. Speich, D. Velayoudon, J. Weissenbach, and P. Wincker. 2011. A holistic approach to marine eco-systems biology. PLoS Biol. **9**: e1001177.

Klausmeier, C. A., E. Litchman, T. Daufresne, and S. A. Levin. 2004. Optimal nitrogen-to-phosphorus stoichiometry of phytoplankton. Nature **429**: 171–174.

Kuznetsov, Y. G., J. B. H. Martiny, and A. McPherson. 2010. Structural analysis of a Synechococcus myovirus S-CAM4 and infected cells by atomic force microscopy. J. Gen. Virol. **91**: 3095–104.

Lane, E. S., D. M. Semeniuk, R. F. Strzepek, J. T. Cullen, and M. T. Maldonado. 2009. Effects of iron limitation on intracellular cadmium of cultured phytoplankton: Implications for surface dissolved cadmium to phosphate ratios. Mar. Chem. **115**: 155–162.

Lindell, D., J. D. Jaffe, M. L. Coleman, M. E. Futschik, I. M. Axmann, T. Rector, G. Kettler, M. B. Sullivan, R. Steen, W. R. Hess, G. M. Church, and S. W. Chisholm. 2007. Genome-wide expression dynamics of a marine virus and host reveal features of co-evolution. Nature **449**: 83–86.

Lomas, M. W., and P. M. Gilbert. 2000. Comparisons of nitrate uptake, storage, and reduction in marine diatoms and flagellates. J. Phycol. **36**: 903–913.

Lynch, M., and J. Shapiro. 1981. Predation, enrichment, and phytoplankton community structure. Limnol. Oceanogr. **26**: 86–102.

Lynn, S. G., S. S. Kilham, D. a. Kreeger, and S. J. Interlandi. 2000. Effect of nutrient availability on the biochemical and elemental stoichiometry in the freshwater diatom Stephanodiscus minutulus (Bacillariophyceae). J. Phycol. **36**: 510–522.

Maat, D. S., K. J. Crawfurd, K. R. Timmermans, and C. P. D. Brussaard. 2014. Elevated CO2 and phosphate limitation favor micromonas pusilla through stimulated growth and reduced viral impact. Appl. Environ. Microbiol. **80**: 3119–3127.

Mackey, K. R. M., A. F. Post, M. R. McIlvin, G. A. Cutter, S. G. John, and M. A. Saito. 2015a. Divergent responses of Atlantic coastal and oceanic Synechococcus to iron limitation. Proc. Natl. Acad. Sci. 201509448.

Mackey, K. R. M., A. F. Post, M. R. McIlvin, G. A. Cutter, S. G. John, and M. A. Saito. 2015b. Divergent responses of Atlantic coastal and oceanic Synechococcus to iron limitation. Proc. Natl. Acad. Sci. **112**: 201509448.

Maldonado, M., P. Boyd, J. LaRoche, R. Strzepek, A. Waite, A. Bowie, P. Croot, R.

Frew, and N. Price. 2001. Iron uptake and physiological response of phytoplankton during a mesoscale Southern Ocean iron enrichment. Limnol. Oceanogr. **46**: 1802–1808.

Mann, N., A. Cook, A. Millard, and S. Bailey. 2003. Bacterial photosynthesis genes in a virus. Nature **424**: 741–742.

Maranon, E., P. M. Holligan, R. Barciela, N. Gonzalez, B. Mourino, M. Pazo, and M. Varela. 2001. Patterns of phytoplankton size structure and productivity in contrasting open-ocean environments. Mar. Ecol. Prog. Ser. **216**: 43–56.

Marie, D., C. Brussaard, R. Thyrhaug, G. Bratbak, and D. Vaulot. 1999. Enumeration of marine viruses in culture and natural samples by flow cytometry. Appl. Environ. Microbiol. **65**: 45–52.

Martin, J. 1990. Glacial-interglacial CO2 change: The iron hypothesis. Paleoceanography **5**: 1–13.

Martin, J., K. Coale, K. Johnson, S. Fitzwater, R. Gordon, S. Tanner, C. Hunter, V. Elrod, J. Nowickli, T. Coley, R. Barber, S. Lindley, A. Watson, K. Van Scoy, C. Law, M. Liddicoat, R. Ling, T. Stanton, J. Stockel, C. Collins, A. Anderson, R. Bidigare, M. Ondrusek, M. Latasa, F. MIllero, K. Lee, W. Yao, J. Zhang, G. Friederich, C. Sakamoto, F. Chavez, K. Buck, Z. Kolber, R. Greene, P. Falkowski, S. Chisholm, F. Hoge, R. Swift, J. Yungel, S. Turner, P. Nightingale, A. Hatton, P. Liss, and N. Tindale. 1994. Testing the iron hypothesis in ecosystems of the equatorial Pacific Ocean. Nature **371**: 123–129.

Martin, J., R. Gordon, and S. Fitzwater. 1990. Iron in Antarctic waters. Nature **345**: 156–8.

Martiny, A., C. Pham, F. Primeau, J. Vrugt, J. Moore, S. Levin, and M. W. Lomas. 2013. Strong latitudinal patterns in the elemental ratios of marine plankton and organic matter. Nat. Geosci. **6**: 1–5.

McCauley, E., and F. Briand. 1979. Hypothesis Zooplankton grazing and phytoplankton species richness : Field tests of the predation hypothesis. Limnol. Oceanogr. **24**: 243–252.

Menzel, D. W., and J. H. Ryther. 1961. Nutrients limiting the production of phytoplankton in the Sargasso sea, with special reference to iron. Deep Sea Res. **7**: 276–281.

Millard, A., M. R. J. Clokie, D. A. Shub, and N. H. Mann. 2004. Genetic organization of the psbAD region in phages infecting marine Synechococcus strains. Proc. Natl. Acad. Sci. U. S. A. **101**: 11007–11012.

Millero, F. J., R. Woosley, B. Ditrolio, and J. Waters. 2005. Effect of Ocean acidification on the Speciation of Metals in Seawater. Oceanography **22**: 72–85.

Mills, M. M., and K. R. Arrigo. 2010. Magnitude of oceanic nitrogen fixation influenced by the nutrient uptake ratio of phytoplankton. Nat. Geosci. **3**: 412–416.

Moore, C. M., M. M. Mills, K. Arrigo, I. Berman-Frank, L. Bopp, P. W. Boyd, E. D. Galbraith, R. J. Geider, C. Guieu, S. L. Jaccard, T. D. Jickells, J. La Roche, T. M. Lenton, N. M. Mahowald, E. Marañón, I. Marinov, J. K. Moore, T. Nakatsuka, A. Oschlies, M. A. Saito, T. F. Thingstad, A. Tsuda, and O. Ulloa. 2013. Processes and patterns of oceanic nutrient limitation. Nat. Geosci. 1–10.

Moore, J. K., and S. C. Doney. 2007. Iron availability limits the ocean nitrogen inventory stabilizing feedbacks between marine denitrification and nitrogen fixation. Global Biogeochem. Cycles **21**: 1–12.

Moore, J. K., S. C. Doney, D. M. Glover, and I. Y. Fung. 2002. Iron cycling and nutrient-limitation patterns in surface waters of the world ocean. Deep. Res. Part II Top. Stud. Oceanogr. **49**: 463–507.

Moore, L. R., A. Coe, E. R. Zinser, M. a. Saito, M. B. Sullivan, D. Lindell, K. Frois-Moniz, J. Waterbury, and S. W. Chisholm. 2007. Culturing the marine cyanobacterium Prochlorococcus. Limnol. Oceanogr. Methods **5**: 353–362.

Morel, F., R. Hudson, and N. M. Price. 1991. Limitation of productivity by trace metals in the sea. Limnol. Oceanogr. **36**: 1742–1755.

Noble, R., and J. Fuhrman. 1998. Use of SYBR Green I for rapid epifluorescence counts of marine viruses and bacteria. Aquat. Microb. Ecol. **14**: 113–118.

Palenik, B., J. Grimwood, A. Aerts, P. Rouzé, A. Salamov, N. Putnam, C. Dupont, R. Jorgensen, E. Derelle, S. Rombauts, K. Zhou, R. Otillar, S. S. Merchant, S. Podell, T. Gaasterland, C. Napoli, K. Gendler, A. Manuell, V. Tai, O. Vallon, G. Piganeau, S. Jancek, M. Heijde, K. Jabbari, C. Bowler, M. Lohr, S. Robbens, G. Werner, I. Dubchak, G. J. Pazour, Q. Ren, I. Paulsen, C. Delwiche, J. Schmutz, D. Rokhsar, Y. Van de Peer, H. Moreau, and I. V Grigoriev. 2007. The tiny eukaryote Ostreococcus provides genomic insights into the paradox of plankton speciation. Proc. Natl. Acad. Sci. U. S. A. **104**: 7705–7710.

Parada, V., E. Sintes, H. M. van Aken, M. G. Weinbauer, and G. J. Herndl. 2007. Viral abundance, decay, and diversity in the meso- and bathypelagic waters of the north atlantic. Appl. Environ. Microbiol. **73**: 4429–38.

Patel, A., R. T. Noble, J. A. Steele, M. S. Schwalbach, I. Hewson, and J. A. Fuhrman. 2007. Virus and prokaryote enumeration from planktonic aquatic environments by

epifluorescence microscopy with SYBR Green I. Nat. Protoc. **2**: 269–276.

Polovina, J. J., E. A. Howell, and M. Abecassis. 2008. Ocean's least productive waters are expanding. Geophys. Res. Lett. **35**: L03618.

Poorvin, L., S. G. Sander, I. Velasquez, E. Ibisanmi, G. R. LeCleir, and S. W. Wilhelm. 2011. A comparison of Fe bioavailability and binding of a catecholate siderophore with virus-mediated lysates from the marine bacterium Vibrio alginolyticus PWH3a. J. Exp. Mar. Bio. Ecol. **399**: 43–47.

Price, N. M. 2005. The elemental stoichiometry and composition of an iron-limited diatom. Limnol. Oceanogr. **50**: 1159–1171.

Price, N., and F. M. M. Morel. 1990. Cadmium and cobalt substitution for zinc in a marine diatom. Nature **344**: 658–60.

Proctor, L., and J. A. Fuhrman. 1990. Viral mortality of marine bacteria and cyanobacteria. Nature **343**: 60–62.

Rachel T Nobel, J. A. F. 1998. Use of SYBR Green I for rapid epifluorescense counts of marine viruses and bacteria. Aquat. Microb. Ecol. **14**: 113–118.

Raytcheva, D. A., C. Haase-Pettingell, J. M. Piret, and J. A. King. 2011. Intracellular assembly of cyanophage Syn5 proceeds through a scaffold-containing procapsid. J. Virol. **85**: 2406–2415.

Redfield, A. 1934. On the proportions of organic derivatives in sea water and their relation to the composition of plankton, p. 177–192. *In* D. RJ [ed.], James Johnstone Memorial Volume. University Press of Liverpool.

Redfield, A. C. 1958. The biological control of chemical factors in the environment. Am. Sci. **46**: 205–221.

Rhee, G.-Y. 1978. Effects of N:P atomic ratios nitrate limitation on algal growth, cell composition, nitrate uptake. Limnol. Oceanogr. **23**: 10–25.

Rivers, A. R., R. W. Jakuba, and E. A. Webb. 2009. Iron stress genes in marine Synechococcus and the development of a flow cytometric iron stress assay. Environ. Microbiol. **11**: 382–96.

Roche, J. La, P. Boyd, R. McKay, and R. Geider. 1996. Flavodoxin as an in situ marker for iron stress in phytoplankton. Nature

Sabehi, G., L. Shaulov, D. H. Silver, I. Yanai, A. Harel, and D. Lindell. 2012. A novel lineage of myoviruses infecting cyanobacteria is widespread in the oceans. Proc. Natl. Acad. Sci. **109**: 2037–2042.

Saito, M. A., and J. W. Moffett. 2002. Temporal and spatial variability of cobalt in the Atlantic Ocean. Geochim. Cosmochim. Acta **66**: 1943–1953.

Sañudo-Wilhelmy, S. A., A. B. Kustka, C. J. Gobler, D. A. Hutchins, M. Yang, K. Lwiza, J. Burns, D. G. Capone, J. A. Raven, and E. J. Carpenter. 2001. Phosphorus limitation of nitrogen fixation by Trichodesmium in the central Atlantic Ocean. Nature **411**: 66–69.

Sanudo-Wilhelmy, S. A., A. Tovar-Sanchez, F.-X. Fu, D. G. Capone, E. J. Carpenter, and D. A. Hutchins. 2004. The impact of surface-adsorbed phosphorus on phytoplankton Redfield stoichiometry. Nature **432**: 897–901.

Sarmiento, J., T. Hughes, R. Stouffer, and S. Manabe. 1998. Simulated response of the ocean carbon cycle to anthropogenic climate warming. Nature **393**: 245–249.

Scharek, R., M. Van Leeuwe, and H. De Baar. 1997. Responses of Southern Ocean phytoplankton to the addition of trace metals. Deep Sea Res. Part II **44**: 209–227.

Shaked, Y., Y. Xu, K. Leblanc, and F. M. M. Morel. 2006. Zinc availability and alkaline phosphatase activity in Emiliania huxleyi: Implications for Zn-P co-limitation in the ocean. Limnol. Oceanogr. **51**: 299–309.

Shi, D., Y. Xu, B. M. Hopkinson, and F. M. M. Morel. 2010. Effect of ocean acidification on iron availability to marine phytoplankton. Science **327**: 676–9.

Shi, T., Y. Sun, and P. G. Falkowski. 2007. Effects of iron limitation on the expression of metabolic genes in the marine cyanobacterium Trichodesmium erythraeum IMS101. Environ. Microbiol. **9**: 2945–2956.

Sohm, J. A., E. A. Webb, and D. G. Capone. 2011. Emerging patterns of marine nitrogen fixation. Nat. Rev. Microbiol. **9**: 499–508.

Steward, G. F., L. B. Fandino, J. T. Hollibaugh, T. E. Whitledge, and F. Azam. 2007. Microbial biomass and viral infections of heterotrophic prokaryotes in the sub-surface layer of the central Arctic Ocean. Deep. Res. Part I Oceanogr. Res. Pap. **54**: 1744–1757.

Stoddard, L. I., J. B. H. Martiny, and M. F. Marston. 2007. Selection and characterization of cyanophage resistance in marine Synechococcus strains. Appl. Environ. Microbiol. **73**: 5516–5522.

Sullivan, M. B., K. H. Huang, J. C. Ignacio-Espinoza, A. M. Berlin, L. Kelly, P. R. Weigele, A. S. DeFrancesco, S. E. Kern, L. R. Thompson, S. Young, C. Yandava, R. Fu, B. Krastins, M. Chase, D. Sarracino, M. S. Osburne, M. R. Henn, and S. W. Chisholm. 2010. Genomic analysis of oceanic cyanobacterial myoviruses compared

with T4-like myoviruses from diverse hosts and environments. Environ. Microbiol. **12**: 3035–3056.

Sullivan, M. B., J. B. Waterbury, and S. W. Chisholm. 2003. Cyanophages infecting the oceanic cyanobacterium Prochlorococcus. Nature **424**: 1047–1051.

Sunda, W. G., and S. A. Huntsman. 1995. Cobalt and zinc interreplacement in marine phytoplankton: Biological and geochemical implications. Limnol. Oceanogr. **40**: 1404–1417.

Sunda, W., N. Price, and F. Morel. 2005. Trace metal ion buffers and their use in culture studies, p. 35. *In* Algal culturing techinques.

Suttle, C. A. 2005. Viruses in the sea. Nature **437**: 356–361.

Suttle, C. A., and A. Chan. 1994. Dynamics and Distribution of Cyanophages and Their Effect on Marine Synechococcus spp. Appl. Environ. Microbiol. **60**: 3167–74.

Suttle, C. A., and J. Fuhrman. 2010. Enumeration of virus particles in aquatic or sediment samples by epifluorescence microscopy, p. 145–153. *In* S.W. Wilhelm, M.G. Weinbauer, and C.A. Suttle [eds.], Manual of Aquatic Viral Ecology. ASLO.

Tilman, D., S. Kilham, and P. Kilham. 1982. Phytoplankton community ecology: the role of limiting nutrients. Annu. Rev. Ecol. Syst. **13**: 349–372.

Tölle, J., K.-P. Michel, J. Kruip, U. Kahmann, A. Preisfeld, and E. K. Pistorius. 2002. Localization and function of the IdiA homologue Slr1295 in the cyanobacterium Synechocystis sp. strain PCC 6803. Microbiology **148**: 3293–3305.

Tovar-Sanchez, A., S. a. Sanudo-Wilhelmy, M. Garcia-Vargas, R. S. Weaver, L. C. Popels, and D. A. Hutchins. 2003. A trace metal clean reagent to remove surface-bound iron from marine phytoplankton. Mar. Chem. **85**: 91–99.

Twining, B. S., and S. B. Baines. 2013. The Trace Metal Composition of Marine Phytoplankton. Ann. Rev. Mar. Sci. **5**: 191–215.

Twining, B. S., S. B. Baines, and N. S. Fisher. 2004. Element stoichiometries of individual plankton cells collected during the Southern Ocean Iron Experiment (SOFeX). Limnol. Oceanogr. **49**: 2115–2128.

Twining, B. S., D. Nuñez-Milland, S. Vogt, R. S. Johnson, and P. N. Sedwick. 2010. Variations in Synechococcus cell quotas of phosphorus, sulfur, manganese, iron, nickel, and zinc within mesoscale eddies in the Sargasso Sea. Limnol. Oceanogr. **55**: 492–506.

Wang, K. 2007. Biology and ecology of Synechococcus and their viruses in the

Chesapeake Bay.

Waterbury, J., S. Watson, F. Valois, and D. Franks. 1986. Biological and ecological characterization of the marine unicellular cyanobacterium Synechococcus, p. 71–. *In* T. Platt and W. Li [eds.], Photosynthetic Picoplankton.

Webb, E. A., J. W. Moffett, and J. B. Waterbury. 2001. Iron Stress in Open-Ocean Cyanobacteria (Synechococcus, Trichodesmium, and Crocosphaera spp.): Identification of the IdiA Protein. Appl. Environ. Microbiol. **67**: 5444–5452.

Weber, T., and C. Deutsch. 2012. Oceanic nitrogen reservoir regulated by plankton diversity and ocean circulation. Nature **489**: 419–422.

Weber, T. S., and C. Deutsch. 2010. Ocean nutrient ratios governed by plankton biogeography. Nature **467**: 550–554.

Weinbauer, M. G. 2004. Ecology of prokaryotic viruses. FEMS Microbiol. Rev. **28**: 127–181.

Weinbauer, M. G., and C. A. Suttle. 1997. Comparison of epifluorescence and transmission electron microscopy for counting viruses in natural marine waters. Aquat. Microb. Ecol. **13**: 225–232.

Wilhelm, S. W., D. P. Maxwell, and C. G. Trick. 1996. Growth, iron requirements, and siderophore production in iron-limited Synechococcus PCC 7002. Limnol. Oceanogr. **41**: 89–97.

Wilhelm, S. W., and C. A. Suttle. 1999. Viruses and Nutrient Cycles in the Sea - Viruses play critical roles in the structure and function of aquatic food webs. Bioscience **49**: 781–788.

Wilson, W. H., N. G. Carr, and N. H. Mann. 1996. The effect of phosphate status on the kinetics of cyanophage infection in the oceanic cyanobacterium Synechococcus Sp. WH7803. J. Phycol. **23**: 506–516.

Wolfe-Simon, F., D. Grzebyk, O. Schofield, and P. G. Falkowski. 2005. The role and evolution of superoxide dismutases in algae. J. Phycol. **41**: 453–465.

Wolfe-Simon, F., V. Starovoytov, J. R. Reinfelder, O. Schofield, and P. G. Falkowski. 2006. Localization and role of manganese superoxide dismutase in a marine diatom. Plant Physiol. **142**: 1701–1709.

Wommack, K. E., and R. R. Colwell. 2000. Virioplankton: viruses in aquatic ecosystems. Microbiol. Mol. Biol. Rev. **64**: 69–114.

Yool, A., E. E. Popova, A. C. Coward, D. Bernie, and T. R. Anderson. 2013. Climate

change and ocean acidification impacts on lower trophic levels and the export of organic carbon to the deep ocean. Biogeosciences **10**: 5831–5854.

Zeng, Q., and S. W. Chisholm. 2012. Marine Viruses Exploit Their Host's Two-Component Regulatory System in Response to Resource Limitation. Curr. Biol. **22**: 124–8.

Zubkov, M. V. 2014. Faster growth of the major prokaryotic versus eukaryotic CO2 fixers in the oligotrophic ocean. Nat. Commun. **5**: 3776.

APPENDIX A – PERMISSION TO REPRINT

Authors in ASM journals retain the right to republish discrete portions of his/her article in any other publication (including print, CD-ROM, and other electronic formats) of which he or she is author or editor, provided that proper credit is given to the original ASM publication. ASM authors also retain the right to reuse the full article in his/her dissertation or thesis.

http://journals.asm.org/site/misc/ASM_Author_Statement.xhtml

Copyright Clearance Center RightsLink®

Home | Create Account | Help | Live Chat

AMERICAN SOCIETY FOR MICROBIOLOGY

Title: An Inexpensive, Accurate, and Precise Wet-Mount Method for Enumerating Aquatic Viruses

Author: Brady R. Cunningham, Jennifer R. Brum, Sarah M. Schwenck et al.

Publication: Applied and Environmental Microbiology

Publisher: American Society for Microbiology

Date: May 1, 2015

Copyright © 2015, American Society for Microbiology

LOGIN

If you're a copyright.com user, you can login to RightsLink using your copyright.com credentials. Already **a RightsLink user** or want to learn more?

Permissions Request

Authors in ASM journals retain the right to republish discrete portions of his/her article in any other publication (including print, CD-ROM, and other electronic formats) of which he or she is author or editor, provided that proper credit is given to the original ASM publication. ASM authors also retain the right to reuse the full article in his/her dissertation or thesis. For a full list of author rights, please see: http://journals.asm.org/site/misc/ASM_Author_Statement.xhtml

BACK | CLOSE WINDOW

Copyright © 2015 Copyright Clearance Center, Inc. All Rights Reserved. Privacy statement. Terms and Conditions.
Comments? We would like to hear from you. E-mail us at customercare@copyright.com